arXiv:1004.1142v1 [astro-ph.GA] 7 Apr 2010

# THE SAGE-SPEC SPITZER LEGACY PROGRAM: THE LIFE-CYCLE OF DUST AND GAS IN THE LARGE MAGELLANIC CLOUD

F. Kemper[1], Paul M. Woods[1], V. Antoniou[2], J.-P. Bernard[3], R. D. Blum[4], M. L. Boyer[5], J. Chan[6], C.-H. R. Chen[7], M. Cohen[8], C. Dijkstra[9], C. Engelbracht[10], M. Galametz[11], F. Galliano[11], C. Gielen[12], Karl D. Gordon[5], V. Gorjian[13], J. Harris[10], S. Hony[11], J. L. Hora[14], R. Indebetouw[7,15], O. Jones[1], A. Kawamura[16], E. Lagadec[17,1], B. Lawton[5], J. M. Leisenring[7], S. C. Madden[11], M. Marengo[2,14], M. Matsuura[18,19], I. McDonald[1], C. McGuire[1], M. Meixner[5], A. J. Mulia[6], B. O'Halloran[20], J. M. Oliveira[21], R. Paladini[22], D. Paradis[22], W. T. Reach[22], D. Rubin[11], K. Sandstrom[8,23], B. A. Sargent[5], M. Sewilo[5], B. Shiao[5], G. C. Sloan[24], A. K. Speck[6], S. Srinivasan[25,26], R. Szczerba[27], A. G. G. M. Tielens[28], E. van Aarle[12], S. D. Van Dyk[22], J. Th. van Loon[21], H. Van Winckel[12], Uma P. Vijh[29], K. Volk[5], B. A. Whitney[30], A. N. Wilkins[24], A. A. Zijlstra[1]

*Draft version April 8, 2010*

## ABSTRACT

The *SAGE-Spec Spitzer* Legacy program is a spectroscopic follow-up to the *SAGE-LMC* photometric survey of the Large Magellanic Cloud carried out with the *Spitzer Space Telescope*. We present an overview of SAGE-Spec and some of its first results. The *SAGE-Spec* program aims to study the life cycle of gas and dust in the Large Magellanic Cloud, and to provide information essential to the classification of the point sources observed in the earlier *SAGE-LMC* photometric survey. We acquired 224.6 hours of observations using the *InfraRed Spectrograph* and the SED mode of the *Multiband Imaging Photometer for Spitzer*. The *SAGE-Spec* data, along with archival *Spitzer* spectroscopy of objects in the Large Magellanic Cloud, are reduced and delivered to the community. We discuss the observing strategy, the specific data reduction pipelines applied and the dissemination of data products to the scientific community. Initial science results include the first detection of an extragalactic "21 $\mu$m" feature towards an evolved star and elucidation of the nature of disks around RV Tauri stars in the Large Magellanic Cloud. Towards some young stars, ice features are observed in absorption. We also serendipitously observed a background quasar, at a redshift of $z \approx 0.14$, which appears to be host-less.

*Subject headings:* surveys – Magellanic Clouds – infrared: ISM – infrared: stars – infrared: galaxies – techniques: spectroscopic

[1] Jodrell Bank Centre for Astrophysics, Alan Turing Building, School of Physics and Astronomy, The University of Manchester, Oxford Road, Manchester, M13 9PL, UK

[2] Department of Physics and Astronomy, Iowa State University, Ames, IA 50011

[3] Centre d'Étude Spatiale des Rayonnements, 9 Av. du Colonel Roche, BP 44346, 31028 Toulouse cedex 4, France

[4] NOAO, 950 North Cherry Avenue, Tucson, AZ 85719

[5] Space Telescope Science Institute, 3700 San Martin Drive, Baltimore, MD 21218

[6] Physics & Astronomy Department, University of Missouri, Columbia, MO 65211

[7] Department of Astronomy, University of Virginia, P.O. Box 400325, Charlottesville, VA 22904

[8] Radio Astronomy Laboratory, University of California at Berkeley, 601 Campbell Hall, Berkeley, CA 94720-3411

[9] Passiebloemweg 31, 1338 TT Almere, The Netherlands

[10] Steward Observatory, University of Arizona, 933 North Cherry Avenue, Tucson, AZ 85721

[11] Laboratoire AIM, CEA/DSM - CNRS - Université Paris Diderot DAPNIA/Service d'Astrophysique Bât. 709, CEA-Saclay F-91191 Gif-sur-Yvette Cédex, France

[12] Instituut Voor Sterrenkunde, KULeuven, Celestijnenlaan 200D, 3001 Leuven (Heverlee), Belgium

[13] JPL/Caltech, MS 169-506, 4800 Oak grove Dr., Pasadena, CA 91109

[14] Harvard-Smithsonian Center for Astrophysics, 60 Garden Street, MS 65, Cambridge, MA 02138-1516

[15] National Radio Astronomy Observatory, 520 Edgemont Road, Charlottesville, VA 22903

[16] Department of Astrophysics, Nagoya University, Chikusa-Ku, Nagoya 464-01, Japan

[17] ESO Headquarters Garching, Karl-Schwarzschild-Str. 2, D-85748 Garching bei Muenchen, Germany

[18] Institute of Origins, Department of Physics and Astronomy,

University College London, Gower Street, London WC1E 6BT, UK

[19] Institute of Origins, Mullard Space Science Laboratory, University College London, Holmbury St. Mary, Dorking, Surrey RH5 6NT, UK

[20] Astrophysics Group, Imperial College London, Blackett Laboratory, Prince Consort Road, London, SW7 2AZ,UK

[21] School of Physical & Geographical Sciences, Lennard-Jones Laboratories, Keele University, Staffordshire ST5 5BG, UK

[22] Spitzer Science Center, California Institute of Technology, MS 220-6, Pasadena, CA 91125

[23] Max-Planck-Institut für Astronomie, D-69117 Heidelberg, Germany

[24] Department of Astronomy, Cornell University, Ithaca, NY 14853-6801

[25] Department of Physics and Astronomy, Johns Hopkins University, Homewood Campus, Baltimore, MD 21218

[26] Institut d'Astrophysique de Paris, 98 bis, Boulevard Arago, Paris 75014, France

[27] N. Copernicus Astronomical Center, Rabianska 8, 87-100 Torun, Poland

[28] Leiden Observatory, P.O. Box 9513, NL-2300 RA Leiden, The Netherlands

[29] Ritter Astrophysical Research Center, University of Toledo, Toledo OH 43606

[30] Space Science Institute, 4750 Walnut Street, Suite 205, Boulder, CO 80301

## 1. INTRODUCTION

A photometric survey in the infrared of the Large Magellanic Cloud (LMC) was performed by the *Spitzer* Legacy Program *Surveying the Agents of Galaxy Evolution* (SAGE-LMC; Meixner et al. 2006), which charts the budget of gas and dust contributing to the cycle of star formation and stellar death in the Magellanic Clouds. Here we discuss *SAGE-Spec*, a spectroscopic follow-up to *SAGE-LMC*, which is also a *Spitzer* Legacy Program. For *SAGE-Spec* we observed a variety of circumstellar and interstellar environments with the *Infrared Spectrograph* (IRS; Houck et al. 2004) aboard *Spitzer* (Werner et al. 2004), as well as the SED mode available on the *Multiband Imaging Photometer for Spitzer* (MIPS; Rieke et al. 2004). The *SAGE-Spec* dataset is exceptionally suited to address the following issues: First, it allows us to trace the lifecycle of dust and molecular gas on its journey through the galaxy, from dust production sites (AGB stars, red supergiants, post-AGB-objects, planetary nebulae), to the ISM (atomic and molecular clouds) to star forming regions (H II regions, young stellar objects); and, second, it allows us to develop a photometric color-color and color-magnitude classification scheme to increase the legacy of the larger *SAGE-LMC* database. In addition, a large number of smaller astrophysical questions can be addressed using the data set provided here, and a rich harvest in scientific results is expected.

This paper gives an overview of the *SAGE-Spec* Legacy program. We outline the observing strategy, describe the data reduction process and discuss the data products that are currently publicly available to the astronomical community (Woods et al. 2010), or will become publicly available in the near future. Existing surveys targeting gas and dust in the LMC are discussed in Sect. 2. This section also includes a description of existing publications of infrared spectroscopy on LMC targets. The observing strategy of the *SAGE-Spec* project is discussed in Sect. 3, along with a description of the data reduction. This paper finishes with some first scientific results of the *SAGE-Spec* project (Sect. 4), and conclusions and an outlook to the future (Sect. 5).

## 2. SURVEYS: THE GAS AND DUST IN THE LMC

In order to study the life-cycle of dust on a galactic scale, the LMC provides a good compromise between distance and size. It is found at a distance of ∼50 kpc (Feast 1999), and as an additional benefit has a favorable viewing angle (35°, van der Marel & Cioni 2001) resulting in low column densities, and typically just a single interstellar cloud, along each line-of-sight. It is possible to observe individual objects in the LMC due to its vicinity, while at the same time the outside viewpoint that we have enables us to obtain a global view of the LMC through surveys like this.

With $Z \approx 0.3 - 0.5\,Z_\odot$, the metallicity of the LMC is sub-solar (Westerlund 1997). As a consequence the dust-to-gas mass ratio is ∼2–4 times lower than that in the Solar neighborhood (Gordon et al. 2003), permitting easier penetration of UV radiation to affect physical processes in the ISM and star formation. Indeed, modeling of photon-dominated regions shows that molecular clouds in the LMC will be larger and less dense than clouds in the Milky Way (Pak et al. 1998). The shape of the UV interstellar extinction curve appears to be independent of metallicity, thus constraining the differences between Galactic and LMC grain properties, although large variations exist between environments within the LMC (Misselt et al. 1999).

### 2.1. *Surveys of the LMC*

Previous infrared surveys of the stellar content of the LMC, performed with, for instance, MSX (Egan et al. 2001) and DENIS (Cioni et al. 2000), are limited to only the brightest sources. Exploration of the stellar content of the LMC was therefore skewed to the tip of the AGB and some bright supergiants. However, with its sensitive arrays, *Spitzer* has allowed for a full census of all objects brighter than ∼ 15th magnitude in the 8.0 μm band (Meixner et al. 2006). *SAGE-LMC* encompasses a field of 7° × 7° covering the majority of the LMC, observed using all bands of the *InfraRed Array Camera* (IRAC; Fazio et al. 2004) and MIPS. The IRAC and MIPS point source catalog contains about 6 million sources, and has been made available to the community[31] (Meixner et al. 2006). The post- and pre-Main Sequence populations uncovered by *SAGE-LMC* are discussed by e.g. Blum et al. (2006) and Whitney et al. (2008).

The extended emission component of the *SAGE-LMC* survey is discussed in more detail by Bernard et al. (2008), who include references to additional LMC surveys in molecular and atomic emission, e.g. Hα (Gaustad et al. 2001), HI (Kim et al. 2003; Staveley-Smith et al. 2003), and CO (Fukui et al. 2008). In addition, a full survey of OH maser emission in the LMC has been performed (Green et al. 2008), as well as photometric surveys in the optical (e.g. Massey 2002; Zaritsky et al. 2004).

### 2.2. *Mid-infrared spectroscopic studies*

Several mid-infrared spectroscopic studies of representative targets in object classes in the LMC have already been performed. Most studies focus on individual objects or small samples, although a few systematic studies of large samples exist. Here we provide an overview of studies not including data from *SAGE-Spec*.

#### 2.2.1. *Silicates*

Prior to the launch of *Spitzer*, Voors et al. (1999) obtained 2–45 μm spectroscopy of R71, a Luminous Blue Variable in the LMC, using the Short Wavelength Spectrometer (SWS; de Graauw et al. 1996) on board the Infrared Space Observatory (*ISO*; Kessler et al. 1996). This spectrum contained the first detection of extragalactic crystalline silicates, and also showed the presence of polycyclic aromatic hydrocarbons (PAHs).

With *Spitzer*-IRS the possibility to obtain mid-infrared spectroscopy of individual objects greatly expanded, allowing the analysis of the dust mineralogy. IRS spectroscopy of two B[e] hypergiants (R126 and R66) revealed the presence of silicate dust, where R66 also shows evidence for crystalline silicates and a dual chemistry with the presence of PAHs (Kastner et al. 2006). Both of

---

[31] The *SAGE-LMC* point source catalog can be accessed on http://irsa.ipac.caltech.edu/applications/Gator/

these sources are known to have disks, which may provide a suitable environment for crystallization. Additional sources found with a silicate mineralogy are IRAS 05003−6712, which shows the characteristic features of crystalline silicates enstatite and forsterite superposed on amorphous silicate features (Zijlstra et al. 2006), and HV 2310, a Mira-type star showing an unusually-shaped 10 $\mu$m resonance, which suggests the presence of both crystalline and amorphous silicates (Sloan et al. 2006a).

### 2.2.2. Carbon-rich and oxygen-rich evolved stars

The late-stage AGB stars that dominate the MSX 8-$\mu$m point source list (Egan et al. 2001) are almost exclusively carbon-rich, as is expected in the low metallicity environment of the LMC (e.g. Zijlstra et al. 2006; Sloan et al. 2008). The $C_2H_2$ molecular absorption bands are deeper than those in their Galactic analogs explained by a higher abundance of this species at low metallicity (Zijlstra et al. 2006). Particularly deep molecular absorption bands are found in IRAS 04496−6958 (Speck et al. 2006), along with a possible detection of SiC at 11.3 $\mu$m in absorption. Another object, SMP LMC 11, is classified as a planetary nebula based on its emission lines although its infrared spectral energy distribution is more reminiscent of a post-AGB star (Bernard-Salas et al. 2006). The spectrum of SMP LMC 11 shows a variety of organic molecular bands in absorption, including several first extragalactic detections. However, Matsuura et al. (2006) have performed a study of molecular bands ($C_2H_2$ and HCN) in a larger sample of carbon stars and find that the abundance of $C_2H_2$ is independent of metallicity, while the HCN bands remain undetected.

An inventory of dust features in the IRS spectra of carbon-rich AGB stars in the LMC is given by Zijlstra et al. (2006), and shows the presence of SiC and MgS solid state components. Leisenring et al. (2008) have added a further 19 sources to this sample, and devised a method to study the dust condensation sequence in environments of differing metallicity. It was also noted that the occurrence of MgS correlates with diminished strength of the SiC feature, suggesting that MgS forms a coating on SiC grains (Lagadec et al. 2007; Leisenring et al. 2008), although this seems contradictory with observations of a sample of 7 of the most extremely reddened carbon stars (Gruendl et al. 2008), where the presence of MgS apparently did not hamper the detection of SiC in absorption.

### 2.2.3. Planetary Nebulae

The prevalence of the carbon-rich phase in stellar evolution is supported by evidence from IRS observations of Planetary Nebulae (PNe). Stanghellini et al. (2007) have observed 41 PNe in both Magellanic Clouds, 25 of which are LMC sources, and which were previously observed using HST. Roughly half of the spectra of the LMC PNe are dominated by atomic emission lines, while the remainder show solid state features, of mostly carbon-rich species. Only two LMC PNe show clear detections of oxygen-rich dust, in particular crystalline silicates. An independent study of atomic lines performed on a sample of 25 LMC/SMC PNe yielded neon and sulfur abundances (Bernard-Salas et al. 2008), both of which are found to be lower than the Galactic values, roughly in the same ratios as the metallicity ratios with respect to the Milky Way.

### 2.2.4. Supernovae and their remnants

A detailed study of supernova remnant N132D by Tappe et al. (2006) included IRS observations and showed the emission lines of [NeIII] and [OIV], as well as PAH emission features – including relatively strong emission from the PAH features at 14-20 $\mu$m. The observations were of part of the shell and a fast-moving knot. In supernova remnant N49 the PAH features are less prominent compared to the atomic emission lines (Williams et al. 2006), which may indicate PAH destruction by UV radiation. The IRS spectrum of recent supernova SN 1987A is dominated by emission from silicate dust, with a few atomic lines (Bouchet et al. 2006). The dust mass derived is $\sim 2.6 \times 10^{-6}\ M_\odot$.

### 2.2.5. Pre-Main Sequence stars

IRAS 05328−6827 is the first YSO to be analyzed with the IRS in the LMC, showing a $CO_2$ ice band that, compared to the $H_2O$ ice band, is deeper than that typically observed in the Milky Way (van Loon et al. 2005b). Seale et al. (2009) have targeted YSO candidates suggested by Gruendl & Chu (2009) and spectrally identified 277 YSOs, thus greatly expanding the sample of known YSOs in the LMC. These YSOs were subdivided in 6 different groups based on the presence of $CO_2$ ice features, silicate features, PAH features and atomic emission lines.

### 2.2.6. Spectral catalogs of point sources

A number of studies have compiled spectral catalogs. Spanning a range of infrared colors, Buchanan et al. (2006) have selected and observed 60 of the brightest 8 $\mu$m sources, and classified 21 red supergiants, 16 carbon-rich and 4 possible oxygen-rich AGB stars, 2 OH/IR stars and the 2 B[e] stars discussed in Sect. 2.2.1. A smaller sample of 28 sources taken from a range of predefined classes is presented by Sloan et al. (2008) and reveals a veritable zoo of spectra. The classification scheme devised by Buchanan et al. (2006) has been used by Kastner et al. (2008) to classify 250 of the most luminous 8 $\mu$m MSX sources in the LMC, arriving at the conclusion that in this flux-limited sample carbon-rich AGB stars indeed dominate (35% of the sources), closely followed by H II regions (32%; some of which might contain massive YSOs), and at some distance Red Supergiants (18%). Less prominent in this sample are the populations of oxygen-rich AGB stars (5%), dusty early-type emission-line stars (3%) and foreground AGB stars (3%) in this sample. The remaining 4% of sources could not be classified. This classification was tested by (Buchanan et al. 2009), who found by studying the IRS spectra of objects which were not previously classified in their earlier work (Buchanan et al. 2006), that 22 out of 31 sources received the correct classification.

### 3. OBSERVATIONS

The *Spitzer SAGE-Spec* program (PID: 40159) consists of 224.6 hours of spectroscopic observations of targets in the LMC (Tab. 1). The targets included point sources

TABLE 1
Summary of observations in the *SAGE-Spec*
program

| observing mode | number of targets | total obs. time |
|---|---|---|
| IRS staring | 196 point sources | 108.7 hrs |
| IRS mapping | 10 atomic clouds | 64.2 hrs |
| | 10 H II regions | |
| | 20 background | |
| MIPS SED | 10 atomic clouds | 20.5 hrs |
| | 10 H II regions | |
| | 20 background | |
| MIPS SED | 48 point sources | 31.2 hrs |



Fig. 1.— [8.0] vs. [8.0]-[24] color-magnitude diagram of infrared point sources in the LMC. The black dots represent the sources for which these colors are available in the *SAGE-LMC* point source catalog (Meixner et al. 2006). Sources selected for observation in the *SAGE-Spec* program are indicated with red circles, whereas archival targets observed in cycles 1–3, and cycles 4–5 are shown as blue triangles and green squares, respectively. The latter group is dominated by targets from PID 40650 (PI: Looney; Seale et al. 2009). The diagonal solid line in the diagram represents the sensitivity limit that we applied to select sources for LL observations. *SAGE-Spec* sources below this line were only observed with SL. The MSX detection limit at 8.0 μm is shown as a horizontal dashed line.

and extended regions, both of which were observed using the IRS low resolution and MIPS SED modes. Observations were done in the IRS staring mode for 196 point sources, and 48 point sources were observed in MIPS SED mode. In addition, 10 extended regions were mapped in both the MIPS SED and IRS observing modes. These *SAGE-Spec* data are discussed in Sect. 3.1 (point sources) and Sect. 3.2 (extended regions).

In addition to the observations made as part of the *SAGE-Spec* program, we also deliver to the scientific community our new, homogeneous reductions of all archival IRS and MIPS SED spectroscopic data within the *SAGE-LMC* footprint, as part of the *SAGE-Spec* legacy. Tab. 1 lists the archival IRS staring mode observations, while the archival IRS maps and MIPS SED observations within the *SAGE-LMC* footprint are discussed in Sect. 3.1.3 and Sect. 3.2.3.

## 3.1. *Point sources*

### 3.1.1. *Target selection*

Spectroscopic studies performed with *Spitzer* prior to the *SAGE-LMC* survey, in observing cycles 1–3, (e.g. Buchanan et al. 2006; Zijlstra et al. 2006) have predominantly targeted (extreme) AGB stars known before the launch of *Spitzer*. These objects are concentrated in the brightest part of the [8.0] vs. [8.0]-[24] color-magnitude diagram (blue triangles in Fig. 1), above the MSX detection limit.

In order to explore the full life-cycle of dust in the LMC and to classify completely the sources in the *SAGE-LMC* photometric catalogs, we have selected additional sources that cover the range in luminosities and colors found in the *SAGE-LMC* photometric survey, focusing predominantly on the unexplored region below the MSX detection limit, and including some additional bright, extremely red sources (red circles in Fig. 1). The *SAGE-Spec* program was executed in observing cycle 4, with the *SAGE-LMC* data becoming available to the *SAGE-LMC*/*SAGE-Spec* team and the community prior to the proposal deadline for that cycle. Several other proposals targeted point sources in the LMC below the MSX detection limit, most notably the program *An Evolutionary Survey of Massive YSOs* (PID: 40650; PI: L. Looney; Seale et al. 2009), in which about ∼300 candidate YSOs were targeted, selected from the *SAGE-LMC* observations using independent photometry from Gruendl & Chu (2009); so this area, too, received substantial coverage with IRS over the lifetime of *Spitzer*. The cycle 4 and 5 targets, dominated by the sample proposed by Seale et al. (2009), are marked with green
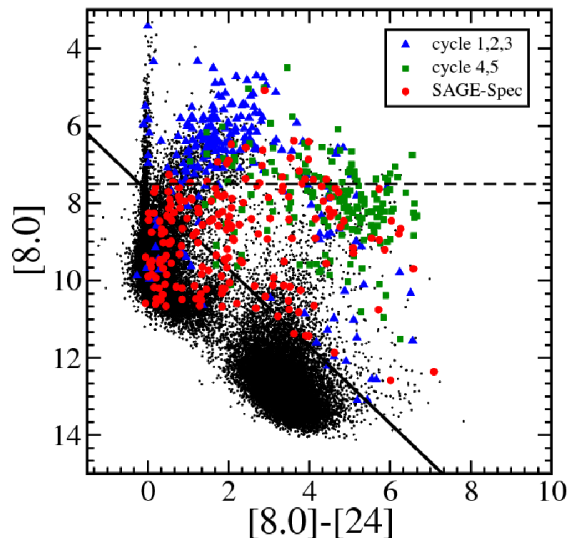
squares in Fig. 1.

For the *SAGE-Spec* program, we arrived at a target list containing 196 pointings, all of which have been observed using the short low (SL) mode on IRS, while 128 of these were also observed in the long low (LL) mode (see Tabs. 1 and 1). We focused on field stars, but also included a small sample of objects from clusters with known metallicities and ages, yielding targets of a much better constrained pedigree than field stars. Cluster stars were mostly overlooked prior to the *SAGE-Spec* survey. The cluster sources are indicated as such in Tab. 1.

We selected candidates in a range of object classes. The sample includes candidate AGB stars, both O-rich and C-rich, selected from the work by Srinivasan et al. (2009); and potential YSO sources taken from the list of candidates selected on their colors and magnitudes (Whitney et al. 2008). Due to the overlapping color-magnitude space with YSOs, we also expected to detect background galaxies (Blum et al. 2006). In addition, we ensured representation of rarer objects, such as post-AGB stars and PNe using additional criteria. For the post-AGB stars the samples of Alcock et al. (1998) and Wood & Cohen (2001) provided a starting point; while the PNe were drawn from lists of LMC PNe assembled by Leisy et al. (1997) and Reid & Parker (2006), representing an adequate sampling of electron density and temperature, morphology, and infrared colors. In order to fully cover the color-magnitude space parametrized by IRAC, MIPS and 2MASS magnitudes, we selected a total of 13 sources from under-represented regions, such as the region defined by $[3.6] − [8.0] > 5$ and the region bordered by $[8.0] > 9$ and $J > 13.3$. The distribution of the selected sources over the LMC is shown in Fig. 2.
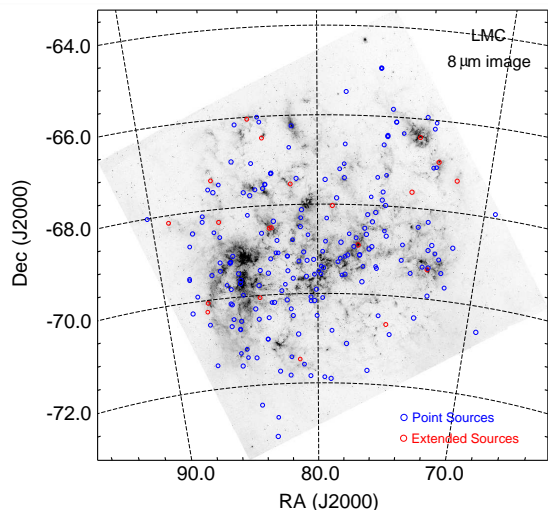
FIG. 2.— Distribution of *SAGE-Spec* IRS targets over the LMC. The blue symbols indicate the positions of point sources targeted with the IRS staring mode, while the red symbols indicate the central positions of the 20 MIPS SED/IRS maps of extended regions. The positions are overplotted on the IRAC 8-$\mu$m footprint of the *SAGE-LMC* survey (Meixner et al. 2006)

*MIPS SED point source target selection*— We observed 48 point sources with MIPS SED (Tables 1 and 1), which is only feasible for the brightest objects in the LMC. A minimum flux level of 100 mJy at 70 $\mu$m is required to obtain a S/N of $\sim$3 for 20 × 10s integrations. We also required all targets selected for MIPS SED observations to have been observed with IRS, either within the context of the *SAGE-Spec* program, or archival programs in cycle 1–3.

### 3.1.2. *IRS staring mode*

*Observations*— The IRS observations of the point sources in the sample are carried out in staring mode. All 196 selected targets were observed using IRS-SL, while the 128 targets with a MIPS-24 $\mu$m flux $\gtrsim$ 5.7 mJy were also observed with IRS-LL. Each target was observed in both nod positions, located one-third and two-thirds along the slit. Integration times were chosen based on the IRAC-8.0 and MIPS-24 $\mu$m flux levels, and targeted to result in a S/N of 60 in SL and 30 in LL, in principle sufficient to analyze and classify dust features on top of a stellar continuum.

Although we observed toward 196 positions, one observation (AOR key 22402560) clearly showed the contribution of two different objects in SL and LL; at short wavelengths the spectrum is due to GV 60, present at the observed location, while the LL spectrum is dominated by nearby Wolf-Rayet star LH$\alpha$ 120–N 82.

*Data reduction SAGE-Spec data*— The processing of data for the *SAGE-Spec* program began with the flat-fielded images produced by the S18.7 version of the data-reduction pipeline at the *Spitzer* Science Center (SSC). To extract spectra from the flat-fielded images and calibrate them spectrophotometrically, we followed the procedure used by several other programs in the Magellanic Clouds and elsewhere in the Local Group (e.g. Sloan et al. 2006b; Zijlstra et al. 2006; Lagadec et al. 2007; Matsuura et al. 2007; Sloan et al. 2008, 2009; Lagadec et al. 2009). The SL and LL

modules each have two apertures, one for the second-order data covering the shorter-wavelength portion, and the other for the first-order data covering the longer-wavelength portion. When the target is in the second-order aperture (SL2 or LL2), a short piece of first-order data is also obtained, which is referred to as the bonus order (SL-bonus or LL-bonus). The bonus order provides overlap with the true first-order data (SL1 or LL1), making it possible to correct the spectra for discontinuities between the orders.

Observations were constructed so that the number and length of integrations in each aperture within a module matched, giving us flexibility on the background subtraction method. Generally, in SL, we chose as the background for a given exposure the corresponding exposure with the target in the other aperture. These aperture differences place the positive and negative beams about 79″ apart, compared to 19″ if we had used nod differences. In SL, nod differences would have placed the positive and negative beams close enough to each other to interfere for extended or complex sources. Consequently, we only reverted to nod differences for those observations where the background emission showed a gradient over the 79″ throw. For LL, the default for background subtraction was a nod difference, which placed the positive and negative beams $\sim$56″ apart. We generally avoided using aperture differences in LL because the beams were 192″ apart, which would often expose us to the more severe background gradients present in the LMC longward of 15 $\mu$m. We examined each image and spectrum carefully to assess when it was necessary to deviate from the default background-subtraction method to avoid either additional sources or complex backgrounds. In some cases, we even reverted to using the image with the target in the other aperture and nod as the background (a cross difference).

In addition to removing the background, differencing the data also corrects most of the *rogue* pixels in an image. These pixels exhibit dark currents different than their usual levels, but generally stable for the duration of a given observation. Some pixels remain problematic for a variety of reasons. Most are flagged as such in the rogue pixel masks provided by the SSC. We built *super-rogue* masks assuming that up to the campaign in which a target was observed, a pixel could be defined as bad if it had been flagged as bad in two previous campaigns. We replaced all flagged pixels using the `imclean` algorithm developed at Cornell and distributed as a part of `irsclean` by the SSC[32]. This algorithm replaces bad pixels by comparing the point-spread functions (PSFs) in adjacent rows.

To extract spectra from the differenced and cleaned images, we used the SSC pipeline modules `profile` (to locate the source in the slit), `ridge` (to map the source position and extraction aperture in the image), and `extract`.[33] The extract module extracts a spectrum from an image by summing the flux within a pseudo-rectangle defined for each wavelength element. When the boundaries of a pseudo-rectangle cross a pixel, the flux

---

[32]     http://ssc.spitzer.caltech.edu/dataanalysistools/ tools/irsclean/

[33] These modules are available in SPICE, the *Spitzer* IRS Custom Extraction package.

| segment  | wavelength ($\mu$m) |
|----------|---------------------|
| SL2      | 5.10–7.59           |
| SL-bonus | 7.23–8.39           |
| SL1      | 7.59–14.20          |
| LL2      | 13.95–20.54         |
| LL-bonus | 19.28–21.23         |
| LL1      | 20.46–37.00         |

is assumed to be evenly distributed within that pixel. The pseudo-rectangles are centered on the center of the PSF at each wavelength element, and their width increases proportionally with wavelength. The tapered-column extraction within SMART (Higdon et al. 2004) was designed to follow this algorithm precisely, and it gives very similar results .

*Spitzer* obtains IRS data in a series of Data Collection Events (DCEs). We extracted spectra separately from each DCE, then co-added them to produce one spectrum per nod position. This step produces a mean flux density and a standard deviation, which we divided by the square root of the number of DCEs to estimate the uncertainty in flux density. To calibrate the co-added spectrum from each nod position, we determined spectral corrections using IRS observations of the standard stars HR 6348 (K0 III), HD 166780 (K4 III) and HD 173511 (K5 III). HR 6348 served as the standard for SL (to avoid any difficulties with the strong SiO absorption in the later K giants), while all three served as standards for LL (to maximize the S/N). We chose to use K giants rather than $\alpha$ Lac (A1 V; e.g. Furlan et al. 2006) because of the difficulty in predicting the strength of the hydrogen recombination lines in the low-resolution modules.

When combining the spectra from the two nod positions for a given order, we replaced the uncertainty when a comparison of the two spectra produced a larger value. When the uncertainty for a given pixel exceeded the average uncertainty in the neighborhood by a factor of five (typically), we used only the data from the nod which were closer to neighboring data. This spike-rejection algorithm removed the occasional spikes and divots which survived the cleaning step above.

Finally, spectra from the six orders were combined into one spectrum (SL2, SL-bonus, SL1, LL2, LL-bonus, LL1; see Table 1). First the bonus-order data were averaged with the first- and second-order data where they overlapped and were within the defined range of valid data. Then the spectra were stitched together to remove discontinuities between segments. These discontinuities arose primarily from mispointings, almost always in SL, with its narrower slit (3.6″ vs. 10.0″). In general, we assumed that the corrections were always upward to the best-centered spectral segment. All corrections were multiplicative and scalar (i.e. not a function of wavelength). To conclude the processing, we trimmed the spectra of those portions at the ends of each segment which proved impossible to calibrate reliably. We also reset uncertainties which indicated a signal/noise ratio > 500, as these values are unlikely and can adversely affect algorithms which use the S/N to weight the data.
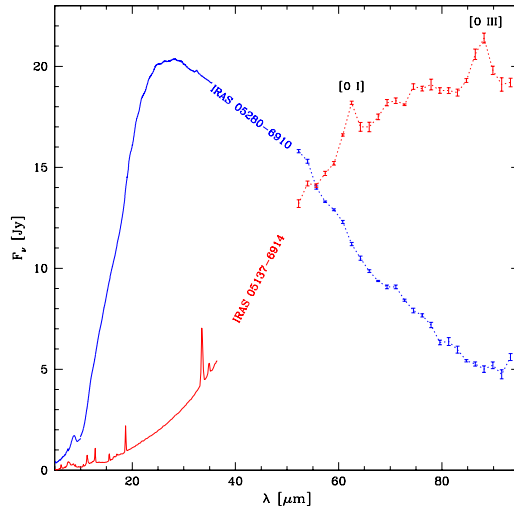


Fig. 3.— Combined MIPS SED (van Loon et al. 2010) and IRS view of two bright, compact IR sources: one, OH/IR star IRAS 05280−6910 is dominated by a warm circumstellar dust envelope with the 10 and 18 $\mu$m silicate features in absorption and a declining, featureless continuum at far-IR wavelengths; the other, ultra-compact H II region IRAS 05137−6914 is dominated by cold dust and an emission-line spectrum both at mid- and far-IR wavelengths.

*Archival data*— We have perused the archive for all staring mode observations within the *SAGE-LMC* footprint, and complemented this list with a few mini-map observations, apparently designed to target point sources. The observations are listed in Tab. 1. Most observations are single pointing staring mode observations, but in some cases more complex settings are used. Examples are the mini-maps, which appear to be designed to cover the entire point-spread-function, and cluster mode observations, where several pointings are strung together in a single AOR. All archival targets were reduced following the scheme described above. One target was only observed with SL2, forcing us to depart from our default background subtraction using aperture differences, since there is no other aperture to extract. For those data, and in other cases where complex backgrounds made aperture differences inadvisable, we used nod differences in SL.

We include both low-resolution (SL and LL) and high-resolution (SH and LH) in the final data delivery. Both Short-High (SH) and Long-High (LH) have short slits, which limit the background-subtraction method. Later in the *Spitzer* mission, the SSC strongly recommended that all SH and LH observations include dedicated background observations, but most observations early in the mission came with no background observations. Where these were available, we subtracted them from the images before extracting. When they were not, then we were forced to skip this important step and continue without background subtraction. In all cases, we performed a full-slit extraction, summing all of the flux in the slit at each wavelength. When stitching high-resolution data, we have not applied different corrections to the orders within SH or LH, because these were all obtained simultaneously and cannot differ due to pointing effects. Sample spectra showing the reduced IRS staring mode data are shown in Fig. 3.

### 3.1.3. *MIPS SED point sources*

*Observations*— For the MIPS SED mode observations, the integration times are determined based on the measured 70 $\mu$m emission, from *SAGE-LMC*, and the slope of the SED. The chop size was chosen to place the background measurement in a region relatively free of emission for the range of dates expected for the observations. Due to the high efficiency of *Spitzer* scheduling, the MIPS SED observations were taken earlier than expected, resulting in some chop regions not being taken in the ideal locations. The chop sizes were normally 1′, except in five cases were a chop of either 2′ or 3′ was employed. Integration times ranged between 24 s and 200 s.

For the LMC, there is one additional point source with MIPS SED observations available in the *Spitzer* archive. This is SN 1987A and has been observed as part of programs 30067, 40149 & 50444 (PI: Dwek). The IRS spectroscopy and MIPS and IRAC photometry associated with these programs is already published (Bouchet et al. 2006).

*Data Reduction*— The MIPS SED point source observations were reduced using the MIPS DAT (see Gordon et al. 2005). The extraction was done for a 5 pixel wide aperture centered on the collapsed profile maximum. For the majority of the sources, the off-source chop observations were used to do the initial background subtraction (except when there was significant emission in the off-source chop position). In addition, background subtraction was done by subtracting the measurements made with the same extraction aperture in a region near the edge of the slit. A wavelength dependent aperture correction was applied to extrapolate to infinite extraction aperture. Finally, a smoothed sensitivity function was applied to convert from instrumental to physical units. The uncertainty due to the absolute calibration is 15% (Lu et al. 2008). Fig. 3 shows the MIPS SED spectrum of point sources IRAS 05280−6910 and IRAS 05137−6914, as examples of the quality of the data. More details on, and first science results from, the MIPS SED observations of point sources in the LMC can be found in van Loon et al. (2010).

## 3.2. *Extended regions*

### 3.2.1. *Target selection*

For the interstellar extended source observations, we distinguish between highly irradiated (ionized) extended regions (i.e. H II regions) and lower-level irradiated clouds, described as atomic and molecular clouds. The H II regions in the *SAGE-Spec* program (see Tab. 1) have been selected on size and the r.m.s. density as derived from the H$\alpha$ emission (Kennicutt & Hodge 1986). The source list covers a range in sizes from 1′ to 16′, while the electron density range spans about two orders of magnitude. H II regions cover only part of IRAC/MIPS color-color space in the LMC (circles in Fig. 4). The atomic regions were selected from the $F_{8.0}/F_{24}$ and $F_{70}/F_{160}$ IRAC/MIPS color-color space, as observed by *SAGE-LMC*, and are chosen to span a wide range of these IRAC and MIPS colors (Fig. 4). Based on the overall pixel statistics, we divided the color-color space into a number of canonical bins (e.g. $5 < F_{8.0}/F_{24} < 10$ and
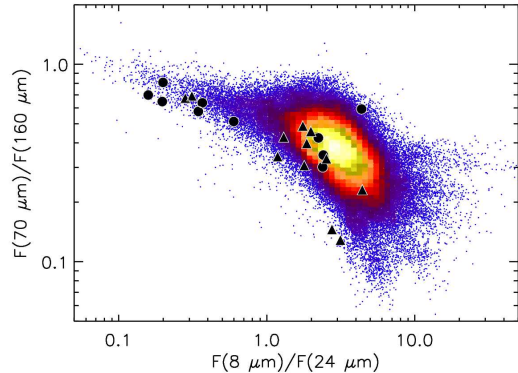


FIG. 4.— IRAC/MIPS color-color diagram for extended regions. The *SAGE-LMC* data for all three MIPS bands and the IRAC 8-$\mu$m band were convolved to the spatial resolution of the MIPS-160 $\mu$m band. The background dots represent the ratios of these bands for each MIPS-160 spatial resolution element. The H II regions that were observed for the *SAGE-Spec* program are plotted as circles and the diffuse regions as triangles.

$F_{70}/F_{160} < 0.1$), and selected regions with high concentrations of pixel values in these bins. As an additional criterion we required these regions to have a distinct identity, for instance a feature in the Spitzer maps or a CO or H I cloud. The selection is somewhat exploratory in nature due to its small size.

While the H II regions in general tend toward $F_8/F_{24}$ ratio $\sim 1$, the atomic regions chosen span higher ratios ranging from 1 to 10, on average. This selection does not guarantee that H II regions are not present in the atomic regions mapped, but samples regions which would be dominated by properties characteristic of atomic ISM. The *SAGE-Spec* sample has been extended by the archival IRS and MIPS SED maps of the 30 Doradus H II region (Indebetouw et al. 2009) and two additional atomic regions in the LMC from PID 40031 (PI: G. Fazio; SSDR 11 and SSDR 12 in Tab. 1), of which the data remain unpublished so far. The central positions and sizes of all 23 extended regions are listed in Tab. 1.

### 3.2.2. *IRS mapping mode*

*Observations*— For the atomic and molecular cloud observations, our sensitivity objective was to obtain spectral maps such that when spatially integrated over a $1' \times 1'$ region, we would achieve a S/N = 10. We used exposure times per pixel of 4×14s (SL) and 4×30s (LL) and spectral mapping to cover each $1' \times 1'$ region. All selected H II regions are mapped in strips that have a width of 1′, and the length being the diameter of the H II region. The mapping is done in such a way that the SL slit is stepped in the cross-slit direction by the diameter of the H II region and contains 2 pointings in the slit direction. The LL slit is stepped in the cross-slit direction by 1′ and again in the slit direction by the diameter of the H II region, thus obtaining a 1′ wide strip in both LL and SL. There are four 6s exposures for both modules, and, since the maximum length of an IRS AOR is 6 hours, the total length of the strip is limited to 5.4′. The largest H II regions in our sample are therefore not mapped to their full diameter. For both the low surface brightness clouds and the H II regions, dedicated off-source observations were obtained to remove the time dependent IRS detector hot pixels and zodiacal light background.
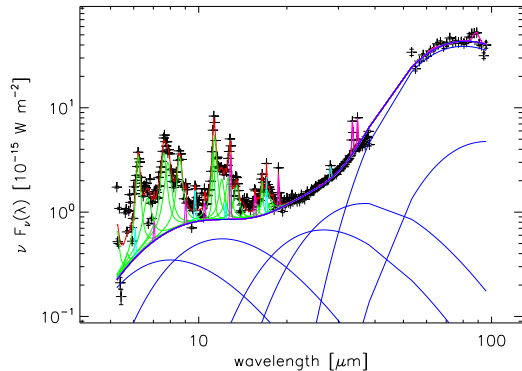
Fig. 5.— Integrated IRS and MIPS SED spectrum of SSDR 1. The spectrum is spatially integrated over a circle with diameter 60", centered on the position listed in Tab. 1. A modified form of the PAHFIT model has been applied (see main text). The pluses indicate the data, and the solid lines are the various components of the PAH fit model, with blue representing the dust continuum, cyan the atomic transitions, and green the PAH bands. The overall fit is indicated with a red line.

*Data Reduction*— We used the standard pipeline data as produced by the SSC. The individual observations were combined into a spectral cube using CUBISM (Smith et al. 2007a), and these spectral cubes were merged together using custom software (Sandstrom et al. 2009). Each independent spectrum in the cube was fit using PAHFIT (Smith et al. 2007b) after convolution to a common resolution using custom convolution kernels (Gordon et al. 2008; Sandstrom et al. 2009). The fit parameters are used to construct the feature maps. For the molecular and atomic regions, we did achieve a S/N of 10, especially at $\lambda > 10$ $\mu$m. For the H II regions, more mixed results emerged, with only 6 of the 10 regions meeting the S/N goal. In those regions with a S/N > 10 it is possible for us to investigate spatial variations in the properties of dust and PAHs, and correlate this with the interstellar radiation field measured through PAH feature strengths and atomic line ratios.

We have also spatially integrated the IRS (and MIPS SED) spectroscopy, as Fig. 5 shows for one of the atomic regions. The integrated SED of this region was extracted from the individual IRS order cubes and MIPS SED cube over the region in common between all the observations. In this example, the extracted region was a $60''$ diameter circle. When studying spatial variations is not possible due to low S/N, the integrated spectra still yield global information on the dust and PAH properties, and the radiation fields in these environments.

### 3.2.3. *MIPS SED*

*Observations*— For the H II regions, the MIPS SED observations roughly coincide with the peak of the SED and pick up any strong [O I] 63 $\mu$m and [O III] 88 $\mu$m lines (Indebetouw et al. 2009). For the atomic and molecular regions the MIPS SED observations constrain dust temperatures, and, in particular, the very small grain emission properties. All *SAGE-Spec* extended regions are mapped with 1/2 slit offsets in both slit dimensions ($9''$ cross-slit and $1.25''$ along-slit), with the minimum exposure time of 3 s. With these exposure times, we aimed to achieve a S/N of 5 per spatial bin for the H II regions, while for the diffuse regions, the objective is for a S/N of 5 for the spatially integrated SED ($1' \times 1'$ region).

Indeed, these S/N goals were met for 7 out of 10 H II regions, and all of the diffuse regions. For all extended regions, dedicated background observations off the LMC were obtained.

For the LMC, there are two additional extended sources with MIPS SED observations available in the *Spitzer* archive. They are 30 Dor (Indebetouw et al. 2009); and the 70 $\mu$m excess (as described by Bernard et al. 2008) region observed in PID 40031, for both of which IRS mapping mode observations are also available (see Sect. 3.2.2).

*Data Reduction*— The MIPS SED extended source observations were reduced using the MIPS DAT v3.10 (Gordon et al. 2005), in a way similar to MIPS imaging data (see, e.g., Dale et al. 2007) and calibrated according to the prescription of Lu et al. (2008). Using the MIPS DAT we constructed three different products: on-source background subtracted, on-source only, and off-source only rectified mosaics combining all the appropriate observations in an AOR. The dedicated off-LMC background observations were subtracted from the on- and off-source mosaics

For each spectral map, and using the on-source and off-source MIPS DAT products, spectral cubes were populated by assuming that the slit is 2 pixels wide and has the coordinates and orientation found in the header of each input image. For any pixel in the output cube where multiple input values are available, the output value is the mean of the input values, weighted by the inverse square of the uncertainty associated with that value. This procedure has been captured in custom IDL software, which parallels that of the similar software for IRS spectra (CUBISM; Smith et al. 2007a). An example of the resulting spectra, integrated over a larger region, is shown in Fig. 5.

### 3.3. *Data products and dissemination*

As part of the *SAGE-Spec* Legacy program we deliver basic and enhanced data products to the astronomical community[34]. Reduced spectra for all point sources and extended sources within the *SAGE-LMC* footprint are included in the delivery in the form of tables and plots. This dataset includes both the *SAGE-Spec* and archival observations within this footprint. The enhanced data products include a spectral catalog of the archival and the SAGE-Spec point sources, along with a source classification. In addition, a photometric classification scheme will be derived, and applied to the entire *SAGE-LMC* point source catalog.

In the cases where spectral maps were performed on extended sources, the data will be spatially averaged into one spectrum. We also deliver spectral data cubes for spectral maps. From those data cubes, maps in selected features or spectral lines will be provided for extended regions with sufficient flux in the intended features. Fig. 6 shows an example of these spectral feature maps.

The first delivery took place on 1 August, 2009, and included the reduced data of all *SAGE-Spec* IRS staring mode observations, along with a first batch of MIPS

---

[34] The *SAGE-Spec* data products are available on http://data.spitzer.caltech.edu/popular/sage-spec/. The unprocessed data are also available through the SSC archive tool Leopard
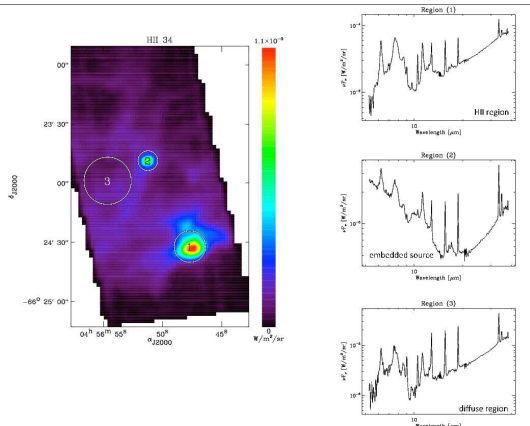
FIG. 6.— Example of a spectral map of an H II region (LHA 120-N 11; DEM L 34) and its surroundings. The map shows the integrated intensity between 6 to 9 $\mu$m for the region where there is full coverage over the entire IRS LL and SL range. The panels on the right show the extracted spectra from different regions in the map. Region 1 is centered on N11B, a compact H II region. Its IRS spectrum shows nebular line and PAH emission on a steeply rising IR continuum. Region 2 is centered on an embedded cluster which shows a strong stellar continuum together with an IR excess due to the surrounding dust. Region 3 represents a more diffuse region and it exhibits very prominent nebular lines in its IRS spectrum. (Hony et al. *in prep.*)

SED point source observations (Woods et al. 2010). The second delivery in March 2010 contains the reduced spectral data cubes for the extended regions observed with MIPS SED and IRS (both *SAGE-Spec* and archival data) and the reduced archival IRS staring mode spectroscopy from Cycles 1–3 (Woods et al. 2010). Two more deliveries are planned at ∼6 month intervals, encompassing archival data from Cycles 4 and 5, and the enhanced data products.

## 4. FIRST RESULTS

Here, we list some first scientific results of the *SAGE-Spec* collaboration, in the context of both program aims: Following the life cycle of gas and dust (Sect. 4.1) and the classification of point sources (Sect. 4.2).

### 4.1. *Life cycle of gas and dust*

#### 4.1.1. *Evolved stars*

*Carbon-rich post-AGB stars*— Four carbon-rich post-AGB objects in the combined *SAGE-Spec* and archival samples can easily be identified by their spectral characteristics: they have strong PAH emission and exhibit the 30 $\mu$m feature generally attributed to MgS grains. In addition, the dust temperature is clearly low compared to that in carbon-stars still on the AGB as judged from the shape of the continuum. These objects most likely have left the AGB within the last few hundred years and are evolving to become planetary nebulae. The IRS spectra of the four objects along with the available photometry in the literature are presented in Figure 7. Three of the objects are *SAGE-Spec* targets and selected as likely post-AGB candidates, while object NGC 1978 WBT 2665 was part of the sample of PID 3591 (Tab. 1), and selected on its infrared colors using the classification by Egan et al. (2001).

IRAS F05192−7009 shows a strong 21 $\mu$m feature, so far only observed in post-AGB objects in our Galaxy (see
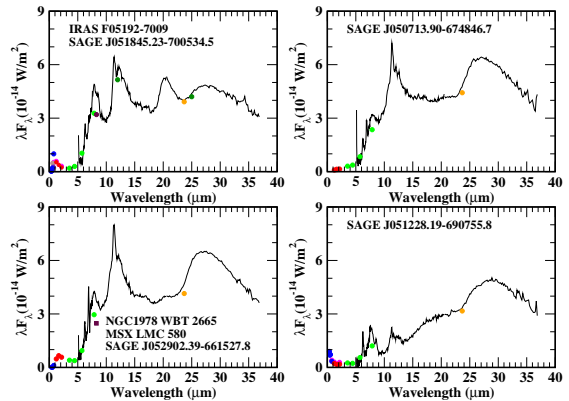


FIG. 7.— IRS spectra of the four post-AGB candidate objects are given all on the same scale for direct comparison. In each panel the available photometry from the literature are also plotted: green for the *SAGE-LMC* IRAC photometry, orange for *SAGE-LMC* MIPS-24 photometry, red for 2MASS photometry (Skrutskie et al. 2006; Cohen et al. 2003), maroon for MSX (from the reject catalog for NGC 1978 WBT 2665; Price et al. 2004), blue for the Magellanic Cloud Photometric Survey photometry (Zaritsky et al. 1997), magenta for DENIS photometry (Fouqué et al. 2000), dark green for IRAS photometry (Beichman et al. 1988), and brown/cyan for Palomar Sky Survey photometry (Monet et al. 2003). No scaling has been applied to any of the data values.

for example Hrivnak et al. 2009, and references therein), thus representing the first extragalactic detection of this feature. In the other three objects it is weak or absent. For object SAGE1C J051228.18−690755.7 the data around the position of the feature possibly contain an artefact, so it is possible that there is a 21 $\mu$m feature present, but if so it is quite weak and it seems more likely that the feature is absent. Preliminary dust radiative transfer modeling for IRAS 05192−7009 shows that that the 21 $\mu$m and 30 $\mu$m feature shapes are the same as those observed in Galactic objects, and suggests that the bulk of the dust in the circumstellar shell is hotter than that found for the Galactic 21 $\mu$m sources. The models indicate that the dust shell for IRAS 05192−7009 is somewhat more massive than those of a number of the well studied Galactic 21 $\mu$m objects such as IRAS 07134+1005 and IRAS 22272+5435. The same may be the case for all four objects which would then suggest that they have left the AGB more recently than most of or all of the Galactic 21 $\mu$m objects.

Compared to Galactic objects of this type, the LMC sources show very strong PAH emission features including the rarely seen 6.9 $\mu$m feature. Comparison of the IRAC colors of these objects to the simulated IRAC/MIPS colors of Galactic 21 $\mu$m objects with good quality ISO SWS data indicates that the [3.6] − [8.0] colors for the LMC objects are larger than those for the Galactic objects, which may be due to some combination of being less evolved off the AGB and having the strong PAH features. All of these objects have a well defined position in a K − [8.0] vs. K − [24] color-color diagram which suggests that further candidate post-AGB objects can be identified from the *SAGE-LMC* data.

*RV Tauri stars*— A specific sub-class of post-AGB stars is formed by the RV Tauri stars. These are pulsating stars which occupy the high-luminosity tail of the population II Cepheids. Their light curves are characterized by a succession of deep and shallow minima. Many ob-
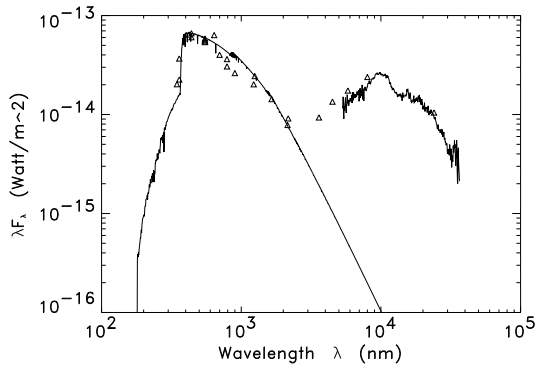
FIG. 8.— The de-reddened SED of RV Tauri star MACHO 82.8405.15 (Gielen et al. 2009). Triangles are broad-band fluxes. The full line is the associated Kurucz stellar atmosphere model. The *SAGE-Spec* infrared spectrum is also shown. Thermal emission from amorphous silicates dominates the spectrum but substructure in the 10 $\mu$m profile as well as the presence of smaller features at longer wavelengths indicate the presence of crystalline silicates (Gielen et al. 2009). This object shows a clear correlation between abundance pattern (Reyniers & van Winckel 2007) and condensation temperature of species, consistent with re-accretion.

jects also show significant cycle-to-cycle variability.

One of the more remarkable properties of RV Tauri stars is that the observed chemical pattern in the photospheres of many Galactic RV Tauri stars is the result of a chemical rather than a nucleosynthetic process: The photospheres are found to be deficient in refractory elements (like Fe and Ca and the s-process elements), while the non-refractory elements are not (or much less) affected (Giridhar et al. 2005; Maas et al. 2005, and references therein). The photospheric patterns can be understood by a process in which gas-dust separation is followed by re-accretion of only the gas, which is poor in refractory elements. This process has likely only taken place in systems which are surrounded by stable dusty disks (Waters et al. 1992), which RV Tauri stars are known to possess (Van Winckel 2003).

These dusty disks around evolved objects are ideal environments to foster strong grain processing and in a *Spitzer* survey of 21 Galactic sources Gielen et al. (2008) showed that very high crystallinity prevails, and is dominated by magnesium-rich end members of olivine and pyroxene silicates. RV Tauri stars in the LMC were found by the microlensing survey MACHO (Alcock et al. 1998) and high resolution optical spectroscopy revealed that depletion of refractory elements is also observed in their photospheres (Reyniers & van Winckel 2007).

Using *SAGE-Spec* data, we showed that also in the LMC, the RV Tauri stars have stable disks, rather than dusty outflows (Gielen et al. 2009) and the close connection between photospheric depletion and the stable dusty environment is illustrated in Fig. 8.

### 4.1.2. *Interstellar medium*

The integrated spectrum of *SAGE-Spec* diffuse region #1, hereafter SSDR 1, which is also known as CO cloud 154 from the NANTEN CO survey (Fukui et al. 2008), or LMC N J0531-6830, with a mass (estimated from the CO) of $1.0 \times 10^6 \ M_\odot$ (Fukui et al. 2008), is shown in Figure 5. The spectrum is dominated by PAH features at 5–15 $\mu$m and a continuum from small grains at
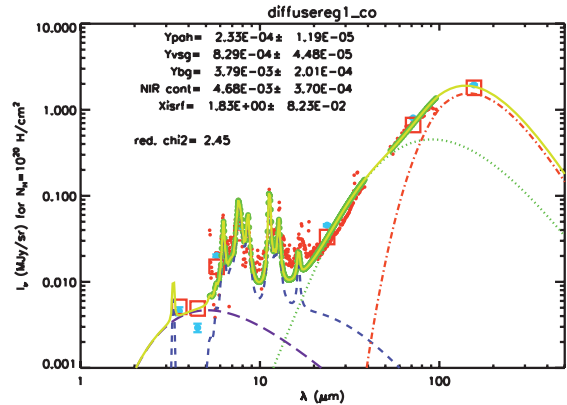


FIG. 9.— Best fit derived using the *DUSTEM* code for the spectrum toward SSDR 1 (CO-154). The red dots show the IRS and MIPS SED *SAGE-Spec* spectrum integrated as discussed in the text. The blue dots show the Spitzer photometry integrated in the SAGE data for the same area. All values are normalized to a total column density of $N_H = 10^{20}$ cm$^{-2}$. The various lines show the contribution of individual dust components: red (dot-dash): Big Grains, green (dashed): Very Small Grains, blue (dashed): PAH, violet (long dash): NIR continuum. The total model spectrum is shown by the continuous yellow line. The squares show the photometry in the Spitzer bands derived from the model spectrum. The best fit values for the free parameters shown are those of Table 1.

longer wavelengths, while big grains dominate the emission longward of $\sim$80 $\mu$m. In order to extract some physical properties of the PAHs and ionic lines in the spectral cube, the spectrum was fitted using an adapted version of *PAHFIT* (Smith et al. 2007b) that handles both the IRS (5–40 $\mu$m) and MIPS SED (70–90 $\mu$m) spectra. To extract abundances of the PAHs and grains populations responsible for the MIR and FIR continuum emission, we used an empirical dust model, *DUSTEM* (see Bernard et al. 2008, for a description) which is based on the emission model of Désert et al. (1990). We fit the integrated spectrum with the *DUSTEM* model allowing the radiation field intensity ($X_{ISRF}$), the abundance of the 3 dust components ($Y_{PAH}$; Very Small Grains: $Y_{VSG}$; and Big Grains: $Y_{BG}$) and the intensity of the NIR continuum to vary simultaneously. The size distribution of the PAHs and BGs remain in the form of a power law as in the Solar Neighborhood (Désert et al. 1990), but we model the VSGs with a flatter size distribution to account for the flatter shape of the far-infrared continuum: $n(a)da \propto a^\alpha$ with $\alpha = -1$, where $a$ is the grain radius and $\alpha$ the index of the size distribution of the VSGs. The best fit is shown in Fig. 9 along with the *SAGE-Spec* spectrum normalized to a total dust column density of $10^{20}$ H cm$^{-2}$ as derived from the HI and CO maps. Fig. 9 also shows the photometry points derived from integrating the *SAGE-LMC* IRAC and MIPS maps over the same region used to extract the spectrum.

The *DUSTEM* fit results are given in Tab. 1, and shows that the dust abundances derived are somewhat in agreement with the results given in Bernard et al. (2008) for cloud CO-154, indicating that the region selected for spectral mapping is representative of the larger region mapped in the *SAGE-LMC* imaging survey. Note that the large value derived for the NIR continuum probably reflects that the stellar contribution was not removed from the data presented here. This does not affect the fit parameters for the PAH, VSG and BG component, as

TABLE 7
Physical parameters derived from the DUSTEM fit compared to those obtained in Bernard et al. (2008) for cloud CO-154. The values labeled with 'H I' are run for a grain size distribution applicable to the Solar Neighborhood, while the values labeled 'CO' are those for *case 2* as described by Bernard et al. (2008), in which the same flattened grain size distribution is used for the VSGs as in the present work.

| | $Y_{\rm PAH}$ $(10^{-4})$ | $Y_{\rm VSG}$ $(10^{-4})$ | $Y_{\rm BG}$ $(10^{-3})$ | NIR cont $(10^{-4}$ MJy/sr) | $X_{\rm ISRF}$ | $\chi^2/{\rm dof}$ |
|---|---|---|---|---|---|---|
| *SAGE-Spec* | 2.33 | 8.29 | 3.79 | 46.8 | 1.83 | 2.44 |
| CO-154(H I) | 1.78 | 8.25 | 2.85 | 4.99 | 2.59 | 6.61 |
| CO-154(CO) | 0.80 | 2.47 | 0.98 | 15.2 | 3.55 | 7.09 |

TABLE 8
Strengths of the major PAH features for SSDR 1, also known as NANTEN CO cloud CO-154.

| Feature name | Strength $({\rm W~m^{-2}~sr^{-1}})$ | Uncertainty $({\rm W~m^{-2}~sr^{-1}})$ |
|---|---|---|
| 6.2 $\mu$m | 1290.8 | 1.2 |
| 7.7 $\mu$m Complex | 3374.8 | 5.2 |
| 8.6 $\mu$m | 1525.4 | 1.4 |
| 11.3 $\mu$m Complex | 2350.9 | 0.7 |
| 12.0 $\mu$m | 674.3 | 0.9 |
| 12.6 $\mu$m Complex | 945.9 | 0.9 |
| 13.6 $\mu$m | 453.6 | 0.8 |
| 14.2 $\mu$m | 49.0 | .8 |
| 16.4 $\mu$m | 171.5 | .4 |
| 17 $\mu$m Complex | 668.7 | 1.2 |
| 17.4 $\mu$m | 53.1 | 0.4 |

the NIR wavelength range is not used to derive the grain properties of those species.

The intensities of the major PAH features derived using *PAHFIT* are shown in Table 1. Figure 10 shows a comparison between the PAH strength ratios in SSDR 1 with those of other nearby galaxies (Smith et al. 2007b). The ISM for all of these extragalactic spectra contain a range of radiation fields. Although SSDR 1 is toward molecular cloud CO-154, there is clearly ionized gas in the line-of-sight, based on the presence of the [Ne III] 15.5 and [Ne II] 12.8 $\mu$m lines. The ratio of these lines, [Ne III]/[Ne II]=0.17, indicating low-ionization gas, is near the median of the ratios for the extragalactic lines-of-sight studied by Smith et al. (2007b). Nonetheless, we separated the high-ionization lines-of-sight in order to keep the comparison as even as possible. It is evident that the 8.6, 11.3 and 12.6 $\mu$m features are significantly stronger for SSDR 1 than the average for the sample of nearby galaxies. The relatively bright 11.3 $\mu$m feature is characteristic of the ISM in the Magellanic Clouds. The features were first detected outside H II regions in the SMC using ISO (Reach et al. 2000), for a region similar in many ways to SSDR 1 considered here; the feature ratios have been interpreted as indicating a different intrinsic set of PAH band strengths in the SMC as compared to those in the Milky Way (Li & Draine 2002).

### 4.1.3. *Young Stellar Objects*

Fig. 11 shows two examples of embedded YSOs in the *SAGE-Spec* sample. Both spectra exhibit strong absorption at 15.2 $\mu$m attributed to the $CO_2$ ice bending mode. These objects also show strong silicate absorption
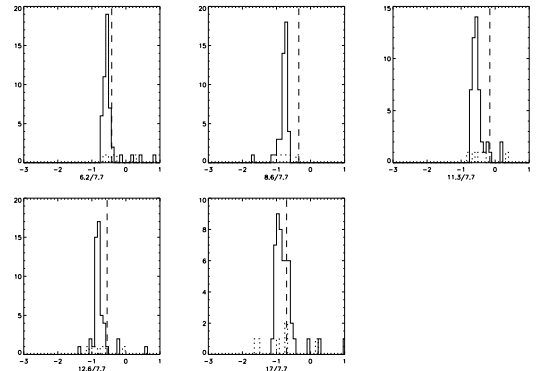


Fig. 10.— Histograms of the ratios of PAH feature strengths from a sample of nearby galaxies (Smith et al. 2007b). Each ratio is normalized to the 7.7 $\mu$m PAH complex. The solid histograms are for the 50 galaxies in the sample with [Ne III]<[Ne II], as observed for SSDR 1, while the dotted histograms are for the 9 others. The feature ratios for SSDR 1 (CO-154) are indicated with vertical dashed lines.

at 10 $\mu$m, as well as emission features due to PAHs, more noticeable at 6, 8 and 11 $\mu$m. The lower spectrum also seems to show an additional broad absorption feature at 6 $\mu$m. This ice band is mainly due to the O−H bending mode of water ice, but it is also thought to include contributions of other minor ice species. We have analyzed in detail the $CO_2$ profiles of a sample of massive embedded YSOs identified in the *SAGE-Spec* survey and from archival data, of which the results are presented in another paper (Oliveira et al. 2009), and summarized here. We compute column densities and compare the observed profiles with laboratory profiles available in the literature. The observed profiles show a varied morphology that, when modeled with the help of lab profiles, provides clues on the ice's admixtures and environmental properties, like temperature. We also investigate the properties of the 5−7 $\mu$m band. By comparing observed properties in LMC and Galactic sample it is possible to get a handle on metallicity effects on ice chemistry (Oliveira et al. 2009).

### 4.2. *The nature of point sources*

#### 4.2.1. *MIPS SED point sources*

Two examples of MIPS SED spectra (van Loon et al. 2010) are shown together with their IRS spectra in Figure 3. These two objects are very different, both in their appearance and in their nature: IRAS 05280−6910 is an OH/IR star of high luminosity (Wood et al. 1992); it is perhaps the most dust-enshrouded supergiant known to
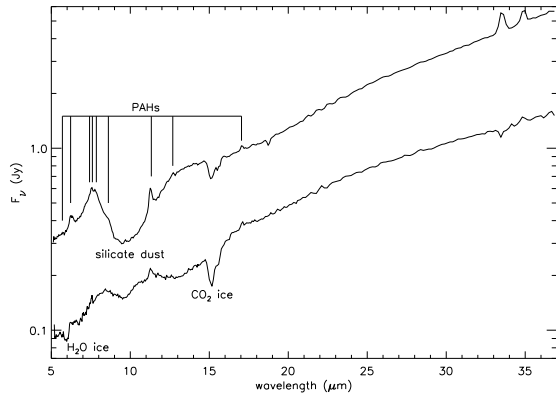
FIG. 11.— Examples of IRS spectra for 2 embedded YSOs in the LMC (Oliveira et al. 2009). Both objects exhibit a red dust continuum characteristic of the early stages of YSO evolution. Both objects show the broad feature at $10\,\mu m$ associated with silicate dust and PAH emission most noticeably at 6, 8 and $13\,\mu m$. Their spectra also show prominent ice signatures: $CO_2$ ice at $15.2\,\mu m$, and the $5-7\,\mu m$ ice complex (for the bottom object) that includes amongst others an important contribution from water ice.

exist in the Magellanic Clouds (van Loon et al. 2005a). We might be dealing with a flattened circumstellar envelope, such as that of WOH G064 (Ohnaka et al. 2008) but in this case viewed edge-on and thus rendering the central star invisible at optical wavelengths. This picture is confirmed by the large optical depth in the silicate features in the IRS range and the absence of cold dust in the MIPS SED range. The other object, IRAS 05137−6914 is an ultra-compact H II region detected at radio wavelengths (Mathewson et al. 1985; Bojičić et al. 2007). It must harbor a massive young, hot star. The cold dust dominating the cocoon around this young star emits an intense far-IR continuum. The excitation and ionization conditions in the gas are traced by the fine-structure line emission of [OI] at $63\,\mu m$ and [OIII] at $88\,\mu m$ in the MIPS SED range; in the IRS range the [SIII] lines at 18 and 33 $\mu m$ are very bright and PAH emission as a consequence of the erosion of small grains is seen. We present a thorough description of the nature of all *SAGE-Spec* MIPS SED point sources in a related study (van Loon et al. 2010).

### 4.2.2. *A background quasar with peculiar properties*

The *SAGE-Spec* program has also yielded IRS spectra of a number of sources that could not easily be classified based on their broad-band colors. Several of these are background sources. One such background source – SAGE 1CJ053634.78−722658.5 – stands out in the IRS spectrum. It has a redshifted spectrum ($z$=0.14) that exhibits extremely prominent silicate emission features at 10 and 18 $\mu m$. We have analyzed the source and discussed its nature (Hony et al. 2010). We argue that the peculiar IRS spectrum and its corresponding broad wavelength energy distribution are indicative of a quasar. We do not detect any emission from the host galaxy; neither the stellar component in the optical or near IR nor the colder ISM in the far-IR (see Fig. 12; Hony et al. 2010), and this may thus be another example of a host-less quasar (Magain et al. 2005).

### 5. OUTLOOK AND CONCLUSIONS

The *SAGE-Spec* program provides useful data for understanding the life cycle of gas and dust in galaxies.
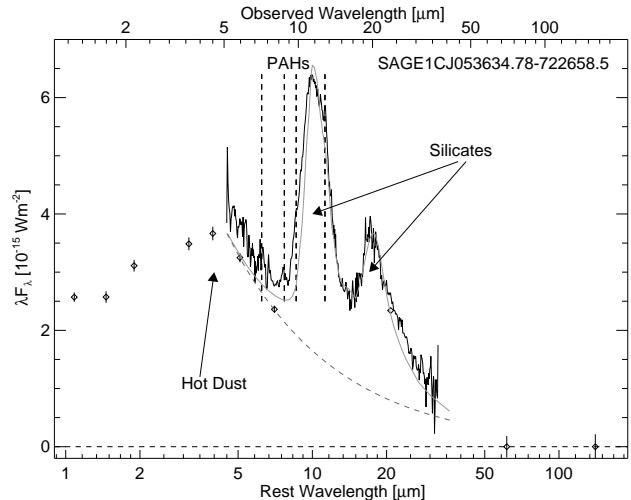


FIG. 12.— Broad wavelength energy distribution of background quasar SAGE 1C J053634.78−722658.5 combined with the remarkable IRS spectrum of the source (Hony et al. 2010). The main contributions that can be identified are the exceptionally strong silicate emission bands at 9.7 and 18 $\mu m$ and the hot continuum peaking near 4 $\mu m$. The weak PAH emission bands have been used to derive the redshift of 0.14.

The extensive dataset of *IRS* and *MIPS SED* spectroscopy, obtained within the *SAGE-Spec* program, complemented with archival data, sample the relevant environments and ultimately provides insights on dust mineralogy and gas properties in these environments. Feeding the results back to the original *SAGE-LMC* data leads to conclusions on stellar populations, and allow us to study the mineralogical dust cycle in the Large Magellanic Cloud, in combination with the global star formation rate (Whitney et al. 2008; Gruendl & Chu 2009) and injection rate of stellar mass loss into the ISM (e.g. Matsuura et al. 2009; Srinivasan et al. 2009). An important outcome of the *SAGE-Spec* program is contributing distinguishing diagnostics to classify sources in the *SAGE-LMC* point source catalog.

The initial results discussed in the paper include the first extragalactic detection of the 21 $\mu m$ feature; the study of crystalline silicates in the disks around RV Tauri stars; the possible detection of a host-less quasar; the analysis of ices towards massive YSOs; and investigations into feature and line ratios in atomic and H II regions to probe physical conditions, such as radiation field and ionization fraction.

True to its legacy status, the *SAGE-Spec* team has delivered a significant fraction of its reduced data to the scientific community already, with further data deliveries planned in the near future. The unprocessed data have been available to the community in the *Spitzer* archive from the date of observing. We will also deliver enhanced data products, particularly spectral feature maps and source and spectral classifications in those future deliveries.

edges support from grant N203 393334 (MNiSW).                SpitzerIRS,MIPS

## REFERENCES

Alcock, C., et al. 1998, AJ, 115, 1921

Beichman, C. A., Neugebauer, G., Habing, H. J., Clegg, P. E., & Chester, T. J. 1988, Infrared astronomical satellite (IRAS) catalogs and atlases. Volume 1: Explanatory supplement

Bernard, J.-P., et al. 2008, AJ, 136, 919

Bernard-Salas, J., Peeters, E., Sloan, G. C., Cami, J., Guiles, S., & Houck, J. R. 2006, ApJ, 652, L29

Bernard-Salas, J., Pottasch, S. R., Gutenkunst, S., Morris, P. W., & Houck, J. R. 2008, ApJ, 672, 274

Blum, R. D., et al. 2006, AJ, 132, 2034

Bojičić, I. S., Filipović, M. D., Parker, Q. A., Payne, J. L., Jones, P. A., Reid, W., Kawamura, A., & Fukui, Y. 2007, MNRAS, 378, 1237

Bouchet, P., et al. 2006, ApJ, 650, 212

Buchanan, C. L., Kastner, J. H., Forrest, W. J., Hrivnak, B. J., Sahai, R., Egan, M., Frank, A., & Barnbaum, C. 2006, AJ, 132, 1890

Buchanan, C. L., Kastner, J. H., Hrivnak, B. J., & Sahai, R. 2009, AJ, 138, 1597

Cioni, M. R., van der Marel, R. P., Loup, C., & Habing, H. J. 2000, A&A, 359, 601

Cohen, M., Wheaton, W. A., & Megeath, S. T. 2003, AJ, 126, 1090

Dale, D. A., et al. 2007, ApJ, 655, 863

Davies, R. D., Elliott, K. H., & Meaburn, J. 1976, MmRAS, 81, 89

de Graauw, T., et al. 1996, A&A, 315, L49

Désert, F.-X., Boulanger, F., & Puget, J. L. 1990, A&A, 237, 215

Egan, M. P., Van Dyk, S. D., & Price, S. D. 2001, AJ, 122, 1844

Fazio, G. G., et al. 2004, ApJS, 154, 10

Feast, M. 1999, PASP, 111, 775

Fouqué, P., et al. 2000, A&AS, 141, 313

Fukui, Y., et al. 2008, ApJS, 178, 56

Furlan, E., et al. 2006, ApJS, 165, 568

Gaustad, J. E., McCullough, P. R., Rosing, W., & Van Buren, D. 2001, PASP, 113, 1326

Gielen, C., van Winckel, H., Min, M., Waters, L. B. F. M., & Lloyd Evans, T. 2008, A&A, 490, 725

Gielen, C., et al. 2009, A&A, 508, 1391

Giridhar, S., Lambert, D. L., Reddy, B. E., Gonzalez, G., & Yong, D. 2005, ApJ, 627, 432

Gordon, K. D., Clayton, G. C., Misselt, K. A., Landolt, A. U., & Wolff, M. J. 2003, ApJ, 594, 279

Gordon, K. D., Engelbracht, C. W., Rieke, G. H., Misselt, K. A., Smith, J.-D. T., & Kennicutt, R. C., Jr. 2008, ApJ, 682, 336

Gordon, K. D., et al. 2005, PASP, 117, 503

Green, J. A., et al. 2008, MNRAS, 385, 948

Gruendl, R. A. & Chu, Y. 2009, ApJS, 184, 172

Gruendl, R. A., Chu, Y.-H., Seale, J. P., Matsuura, M., Speck, A. K., Sloan, G. C., & Looney, L. W. 2008, ApJ, 688, L9

Higdon, S. J. U., et al. 2004, PASP, 116, 975

Hony, S., et al. 2010, ApJ, submitted

Houck, J. R., et al. 2004, ApJS, 154, 18

Hrivnak, B. J., Volk, K., & Kwok, S. 2009, ApJ, 694, 1147

Indebetouw, R., et al. 2009, ApJ, 694, 84

Kastner, J. H., Buchanan, C. L., Sargent, B., & Forrest, W. J. 2006, ApJ, 638, L29

Kastner, J. H., Thorndike, S. L., Romanczyk, P. A., Buchanan, C. L., Hrivnak, B. J., Sahai, R., & Egan, M. 2008, AJ, 136, 1221

Kennicutt, R. C., Jr. & Hodge, P. W. 1986, ApJ, 306, 130

Kessler, M. F., et al. 1996, A&A, 315, L27

Kim, S., Staveley-Smith, L., Dopita, M. A., Sault, R. J., Freeman, K. C., Lee, Y., & Chu, Y.-H. 2003, ApJS, 148, 473

Lagadec, E., et al. 2007, MNRAS, 376, 1270

Lagadec, E., et al. 2009, MNRAS, 396, 598

Leisenring, J. M., Kemper, F., & Sloan, G. C. 2008, ApJ, 681, 1557

Leisy, P., Dennefeld, M., Alard, C., & Guibert, J. 1997, A&AS, 121, 407

Li, A. & Draine, B. T. 2002, ApJ, 576, 762

Lu, N., et al. 2008, PASP, 120, 328

Maas, T., Van Winckel, H., & Lloyd Evans, T. 2005, A&A, 429, 297

Magain, P., Letawe, G., Courbin, F., Jablonka, P., Jahnke, K., Meylan, G., & Wisotzki, L. 2005, Nature, 437, 381

Massey, P. 2002, ApJS, 141, 81

Mathewson, D. S., Ford, V. L., Tuohy, I. R., Mills, B. Y., Turtle, A. J., & Helfand, D. J. 1985, ApJS, 58, 197

Matsuura, M., et al. 2006, MNRAS, 371, 415

— 2007, MNRAS, 382, 1889

— 2009, MNRAS, 396, 918

Meixner, M., et al. 2006, AJ, 132, 2268

Misselt, K. A., Clayton, G. C., & Gordon, K. D. 1999, ApJ, 515, 128

Monet, D. G., et al. 2003, AJ, 125, 984

Ohnaka, K., Driebe, T., Hofmann, K.-H., Weigelt, G., & Wittkowski, M. 2008, A&A, 484, 371

Oliveira, J. M., et al. 2009, ApJ, 707, 1269

Pak, S., Jaffe, D. T., van Dishoeck, E. F., Johansson, L. E. B., & Booth, R. S. 1998, ApJ, 498, 735

Price, S. D., Paxson, C., Engelke, C., & Murdock, T. L. 2004, AJ, 128, 889

Reach, W. T., Boulanger, F., Contursi, A., & Lequeux, J. 2000, A&A, 361, 895

Reid, W. A. & Parker, Q. A. 2006, MNRAS, 373, 521

Reyniers, M. & van Winckel, H. 2007, A&A, 463, L1

Rieke, G. H., et al. 2004, ApJS, 154, 25

Sandstrom, K. M., Bolatto, A. D., Stanimirović, S., van Loon, J. T., & Smith, J. D. T. 2009, ApJ, 696, 2138

Seale, J. P., Looney, L. W., Chu, Y.-H., Gruendl, R. A., Brandl, B., Chen, C.-H. R., Brandner, W., & Blake, G. A. 2009, ApJ, 699, 150

Skrutskie, M. F., et al. 2006, AJ, 131, 1163

Sloan, G. C., Devost, D., Bernard-Salas, J., Wood, P. R., & Houck, J. R. 2006a, ApJ, 638, 472

Sloan, G. C., Kraemer, K. E., Matsuura, M., Wood, P. R., Price, S. D., & Egan, M. P. 2006b, ApJ, 645, 1118

Sloan, G. C., Kraemer, K. E., Wood, P. R., Zijlstra, A. A., Bernard-Salas, J., Devost, D., & Houck, J. R. 2008, ApJ, 686, 1056

Sloan, G. C., et al. 2009, Science, 323, 353

Smith, J. D. T., et al. 2007a, PASP, 119, 1133

— 2007b, ApJ, 656, 770

Speck, A. K., Cami, J., Markwick-Kemper, C., Leisenring, J., Szczerba, R., Dijkstra, C., Van Dyk, S., & Meixner, M. 2006, ApJ, 650, 892

Srinivasan, S., et al. 2009, AJ, 137, 4810

Stanghellini, L., García-Lario, P., García-Hernández, D. A., Perea-Calderón, J. V., Davies, J. E., Manchado, A., Villaver, E., & Shaw, R. A. 2007, ApJ, 671, 1669

Staveley-Smith, L., Kim, S., Calabretta, M. R., Haynes, R. F., & Kesteven, M. J. 2003, MNRAS, 339, 87

Tappe, A., Rho, J., & Reach, W. T. 2006, ApJ, 653, 267

van der Marel, R. P. & Cioni, M. R. L. 2001, AJ, 122, 1807

van Loon, J. T., Marshall, J. R., & Zijlstra, A. A. 2005a, A&A, 442, 597

van Loon, J. T., et al. 2005b, MNRAS, 364, L71

— 2010, AJ, 139, 68

Van Winckel, H. 2003, ARA&A, 41, 391

Voors, R. H. M., Waters, L. B. F. M., Morris, P. W., Trams, N. R., de Koter, A., & Bouwman, J. 1999, A&A, 341, L67

Waters, L. B. F. M., Trams, N. R., & Waelkens, C. 1992, A&A, 262, L37

Werner, M. W., et al. 2004, ApJS, 154, 1

Westerlund, B. E. 1997, The Magellanic Clouds (Cambridge: Cambridge University Press)

Whitney, B. A., et al. 2008, AJ, 136, 18

Williams, R. M., Chu, Y.-H., & Gruendl, R. 2006, AJ, 132, 1877

Wood, P. R. & Cohen, M. 2001, in Post-AGB objects as a phase of stellar evolution, eds. R. Szczerba & S. K. Górny (The Netherlands: Kluwer Academic Publishers), 71–76

Wood, P. R., Whiteoak, J. B., Hughes, S. M. G., Bessell, M. S., Gardner, F. F., & Hyland, A. R. 1992, ApJ, 397, 552

Woods, P. M., Sloan, G. C., Gordon, K. D., Shiao, B., Kemper,
    F., & the SAGE-Spec team 2010, Sage-spectroscopy: The
    life-cycle of dust and gas in the Large Magellanic Cloud. Data
    delivery document v2.0,
    `http://data.spitzer.caltech.edu/popular/sage-spec/`
    `20100301_enhanced/docs/SAGESpecDataDelivery2.pdf`

Zaritsky, D., Harris, J., & Thompson, I. 1997, AJ, 114, 1002
Zaritsky, D., Harris, J., Thompson, I. B., & Grebel, E. K. 2004,
    AJ, 128, 1606
Zijlstra, A. A., et al. 2006, MNRAS, 370, 1961

TABLE 3
Point sources targeted with the IRS staring mode as part of the
SAGE-Spec program.

| Nr. | AORkey IRS | RA (J2000) | Dec (J2000) | SAGE designation SSTISAGE + | mod. | name | AOR key MIPS SED | Remarks |
|---|---|---|---|---|---|---|---|---|
| 1 | 22399232 | 04h37m21.15s | −70d34m44.57s | MC J043721.15−703444.7 | sl | NGC 1651 SAGE IRS 1 | | Cluster |
| 2 | 22399488 | 04h37m27.69s | −67d54m34.94s | MC J043727.61−675435.1 | sl/ll | | 22459648 | |
| 3 | 22399744 | 04h46m27.15s | −68d47m46.83s | MC J044627.10−684747.0 | sl/ll | | | |
| 4 | 22400256 | 04h47m18.63s | −69d42m20.53s | MC J044718.63−694220.6 | sl/ll | | | |
| 5 | 24319488 | 04h48m37.75s | −69d23m36.85s | MC J044837.77−692337.0 | sl/ll | | | |
| 6 | 24318720 | 04h49m34.38s | −69d05m49.17s | MC J044934.31−690549.3 | sl/ll | | | |
| 7 | 22400512 | 04h50m40.57s | −68d58m18.76s | MC J045040.52−685819.0 | sl/ll | MSX LMC 1128 | | |
| 8 | 22400768 | 04h51m28.58s | −69d55m49.92s | MC J045128.58−695550.1 | sl/ll | | | |
| 9 | 22401024 | 04h51m40.63s | −68d47m34.82s | MC J045140.57−684734.6 | sl/ll | IRAS 04518−6852 | | |
| 10 | 22401280 | 04h52m00.38s | −69d18m05.53s | MC J045200.36−691805.6 | sl/ll | | | |
| 11 | 24315136 | 04h52m28.66s | −68d54m51.09s | MC J045228.68−685451.3 | sl/ll | | | |
| 12 | 22401792 | 04h52m32.49s | −67d02m59.30s | MC J045232.54−670259.2 | sl | KDM 764 | | Cluster |
| 13 | 22402048 | 04h53m09.54s | −68d17m10.11s | MC J045309.39−681710.8 | sl | | | |
| 14 | 24317952 | 04h53m11.03s | −67d03m55.96s | 1C J045311.04−670355.6 | sl/ll | IRAS F04532−6709 | | |
| 15 | 22402304 | 04h53m28.71s | −66d03m34.76s | MC J045328.70−660334.4 | sl | | | |
| 16 | 22402560 | 04h53m30.86s | −69d17m49.85s | MC J045330.88−691749.7 | sl | GV 60 | | |
| 17 | 22402560 | 04h53m30.86s | −69d17m49.85s | | ll | LHα 120−N 82 | 22457088 | |
| 18 | 24319232 | 04h53m44.28s | −66d11m45.76s | MC J045344.24−661146.0 | sl/ll | | | |
| 19 | 22403072 | 04h54m22.88s | −70d26m56.64s | MC J045422.82−702657.0 | sl | | | Cluster |
| 20 | 22403328 | 04h55m26.76s | −68d25m07.93s | MC J045526.69−682508.4 | sl/ll | | | |
| 21 | 24318976 | 04h55m34.06s | −65d57m00.92s | MC J045534.07−655701.3 | sl/ll | | | |
| 22 | 22404096 | 04h56m23.27s | −69d27m48.05s | MC J045623.21−692749.0 | sl/ll | | | |
| 23 | 22404864 | 04h58m55.03s | −69d11m18.21s | MC J045855.02−691118.7 | sl | KDM 1238 | | |
| 24 | 22405120 | 04h58m55.29s | −68d50m36.13s | | sl | | | |
| 25 | 22405632 | 05h00m32.59s | −66d21m12.60s | MC J050032.61−662113.0 | sl/ll | | | |
| 26 | 22405888 | 05h00m34.69s | −70d52m00.34s | MC J050034.61−705200.4 | sl/ll | RP 1631 | | |
| 27 | 22406144 | 05h02m21.52s | −66d06m37.98s | MC J050221.46−660638.3 | sl/ll | MSX LMC 1271 | | Cluster |
| 28 | 22406400 | 05h02m24.21s | −66d06m37.46s | MC J050224.17−660637.4 | sl/ll | NGC 1805 SAGE IRS 1 | | Cluster |
| 29 | 22406656 | 05h03m04.98s | −68d40m24.90s | MC J050304.95−684024.7 | sl/ll | HV 2281 | | |
| 30 | 22406912 | 05h03m16.59s | −65d49m44.79s | MC J050316.60−654945.1 | sl | KDM 1656 | | |
| 31 | 22407168 | 05h03m36.89s | −68d33m38.71s | MC J050336.92−683338.5 | sl | KDM 1691 | | |
| 32 | 22407424 | 05h03m42.54s | −67d59m18.83s | MC J050342.57−675919.2 | sl | LMC−BM 11−19 | | |
| 33 | 22407680 | 05h03m53.50s | −70d27m47.53s | MC J050353.40−702747.6 | sl | LMC−BM 12−14 | | |
| 34 | 24317696 | 05h03m54.60s | −67d18m47.69s | MC J050354.55−671848.7 | sl/ll | | | |
| 35 | 22407936 | 05h04m07.38s | −66d26m42.71s | MC J050407.42−662643.0 | sl | NGC 1818 WBT 5 | | Cluster |
| 36 | 22408192 | 05h04m07.73s | −66d25m05.48s | MC J050407.72−662505.9 | sl | NGC 1818 WBT 64 | | Cluster |
| 37 | 22408448 | 05h04m11.09s | −66d26m16.70s | MC J050411.04−662616.8 | sl | NGC 1818 WBT 3 | | Cluster |
| 38 | 22408704 | 05h04m28.91s | −67d41m23.43s | MC J050428.91−674123.9 | sl/ll | MSX LMC 61 | | |
| 39 | 22408960 | 05h04m34.17s | −67d52m21.05s | MC J050434.20−675221.8 | sl/ll | RP 1878 | | |
| 40 | 24317440 | 05h04m51.71s | −66d38m07.41s | MC J050451.70−663807.5 | sl/ll | IRAS 05047−6642 | | |
| 41 | 24314880 | 05h05m03.22s | −69d24m26.51s | MC J050503.21−692426.5 | sl | | | Cluster |
| 42 | 22409216 | 05h05m17.19s | −69d21m57.12s | MC J050517.08−692157.0 | sl/ll | | | |
| 43 | 22409472 | 05h05m55.74s | −67d22m09.24s | MC J050555.66−672210.0 | sl | LMC−BM 13−2 | | |
| 44 | 22409728 | 05h05m58.26s | −68d09m23.79s | MC J050558.23−680923.6 | sl/ll | | | |
| 45 | 22409984 | 05h06m07.51s | −71d41m48.12s | MC J050607.50−714148.4 | sl | | | |
| 46 | 22410240 | 05h06m12.61s | −64d55m37.23s | MC J050612.59−645537.5 | sl | KDM 1961 | | Cluster |
| 47 | 22410496 | 05h06m18.95s | −64d56m10.88s | MC J050618.98−645610.2 | sl | KDM 1966 | | Cluster |
| 48 | 22410752 | 05h06m20.13s | −64d54m58.01s | MC J050620.12−645458.6 | sl | | | Cluster |
| 49 | 22411008 | 05h06m29.62s | −68d55m34.54s | MC J050629.61−685534.9 | sl | | | |
| 50 | 22411264 | 05h06m39.24s | −68d22m09.32s | MC J050639.14−682209.3 | sl/ll | | | |
| 51 | 22411520 | 05h07m09.47s | −68d58m50.18s | 2C J050709.45−685849.3 | sl/ll | SHV 0507252−690238 | | Cluster |
| 52 | 24317184 | 05h07m14.00s | −67d48m46.46s | MC J050713.90−674846.7 | sl/ll | | | |
| 53 | 22411776 | 05h07m53.01s | −68d12m46.38s | MC J050752.93−681246.5 | sl/ll | | | |
| 54 | 22412032 | 05h07m59.36s | −68d39m25.71s | MC J050759.35−683925.8 | sl/ll | | | |
| 55 | 22412288 | 05h08m26.27s | −68d31m15.01s | MC J050826.35−683115.1 | sl/ll | | | |
| 56 | 22412544 | 05h08m30.62s | −69d22m37.39s | MC J050830.51−692237.4 | sl/ll | | | |
| 57 | 22412800 | 05h08m36.42s | −69d43m15.11s | MC J050836.39−694315.7 | sl | KDM 2187 | | |
| 58 | 22413056 | 05h09m26.44s | −69d06m56.99s | MC J050926.57−690656.3 | sl | BMB−BW 180 | | Cluster |
| 59 | 22413312 | 05h09m29.54s | −69d07m50.90s | MC J050929.53−690750.3 | sl | NGC 1856 SAGE IRS 1 | | Cluster |
| 60 | 22414080 | 05h10m28.38s | −68d44m31.44s | 1C J051028.32−684431.4 | sl | | | Cluster |
| 61 | 22414336 | 05h10m59.06s | −68d56m13.82s | MC J051059.07−685613.7 | sl/ll | | | |
| 62 | 22414592 | 05h12m09.19s | −71d06m49.52s | MC J051209.02−710649.7 | sl/ll | MSX LMC 209 | | |
| 63 | 22414848 | 05h12m13.57s | −68d39m22.47s | MC J051213.54−683922.8 | sl | | | |
| 64 | 24316928 | 05h12m28.17s | −69d07m56.15s | MC J051228.19−690755.8 | sl/ll | | | |
| 65 | 22415104 | 05h13m01.80s | −69d33m51.21s | MC J051301.75−693351.0 | sl/ll | IRAS 05133−6937 | | |
| 66 | 22415360 | 05h13m06.43s | −69d09m46.53s | 1C J051306.40−690946.3 | sl/ll | OGLE J051306.52−690946.4 | | |
| 67 | 22415616 | 05h13m39.87s | −66d38m52.70s | MC J051339.94−663852.5 | sl | | | |
| 68 | 22416128 | 05h13m41.42s | −65d28m27.91s | MC J051341.40−652828.2 | sl | NGC 1866 Robb B136 | | Cluster |
| 69 | 22416384 | 05h13m42.83s | −67d24m10.44s | MC J051342.63−672409.9 | sl/ll | BSDL 923 | | |
| 70 | 24316672 | 05h13m47.79s | −69d35m05.06s | MC J051347.72−693505.2 | sl/ll | | | |
| 71 | 22416640 | 05h13m48.33s | −67d05m26.87s | MC J051348.38−670527.0 | sl/ll | | | |
| 72 | 22416896 | 05h14m12.32s | −68d50m58.29s | MC J051412.33−685058.0 | sl | | | |
| 73 | 22417152 | 05h14m18.15s | −69d12m35.06s | MC J051418.09−691234.9 | sl/ll | HV 915 | | |

TABLE 3 — *Continued*

| Nr. | AORkey IRS | RA (J2000) | Dec (J2000) | SAGE designation SSTISAGE + | mod. | name | AOR key MIPS SED | Remarks |
|-----|-----------|-----------|-------------|------------------------------|------|------|------------------|---------|
| 74 | 24316416 | 05h14m49.41s | −67d12m22.24s | MC J051449.43−671221.4 | sl/ll | | | |
| 75 | 22417408 | 05h14m53.12s | −69d17m23.70s | MC J051453.10−691723.5 | sl/ll | | | |
| 76 | 22417664 | 05h15m26.47s | −67d51m26.91s | MC J051526.44−675126.9 | sl | | | |
| 77 | 22417920 | 05h16m12.52s | −70d49m30.18s | MC J051612.42−704930.3 | sl | | | |
| 78 | 22418176 | 05h16m18.69s | −71d53m59.21s | MC J051618.69−715359.0 | sl/ll | IRAS 05170−7156 | | |
| 79 | 22418688 | 05h17m47.16s | −68d18m42.64s | MC J051747.18−681842.6 | sl | | | |
| 80 | 22418944 | 05h18m03.28s | −68d49m50.29s | 1C J051803.23−684950.7 | sl/ll | | | |
| 81 | 22419200 | 05h18m07.94s | −71d51m53.66s | MC J051807.93−715153.7 | sl | KDM 3196 | | |
| 82 | 22419456 | 05h18m11.05s | −67d26m48.92s | MC J051811.08−672648.5 | sl/ll | HV 5715 | | |
| 83 | 22419712 | 05h18m32.63s | −69d25m25.59s | MC J051832.64−692525.5 | sl | | | Cluster |
| 84 | 24314624 | 05h18m45.27s | −70d05m34.70s | MC J051845.23−700534.5 | sl/ll | IRAS F05192−7008 | | |
| 85 | 27037952 | 05h18m45.46s | −69d03m21.65s | MC J051845.47−690321.8 | sl/ll | HV 2444 | | |
| 86 | 22419968 | 05h19m08.52s | −69d23m14.44s | MC J051908.46−692314.3 | sl | | | |
| 87 | 22420224 | 05h19m10.63s | −69d33m46.51s | MC J051910.49−693345.3 | sl | 2MASS J05191049−6933453 | | |
| 88 | 22420480 | 05h19m44.87s | −69d29m59.84s | MC J051944.81−692959.4 | sl | 2MASS J05194483−6929594 | | |
| 89 | 22420736 | 05h20m14.31s | −70d29m31.33s | MC J052014.24−702931.0 | sl | | | |
| 90 | 22420992 | 05h20m23.97s | −69d54m23.08s | MC J052023.97−695423.2 | sl/ll | | | |
| 91 | 22421248 | 05h20m51.86s | −69d34m08.04s | MC J052051.83−693407.6 | sl | | | |
| 92 | 22421504 | 05h20m52.44s | −70d09m35.60s | MC J052052.42−700935.5 | sl/ll | LHα 120−N 125 | | |
| 93 | 22421760 | 05h21m01.71s | −69d14m17.07s | MC J052101.66−691417.5 | sl/ll | | | |
| 94 | 22422016 | 05h21m47.99s | −70d09m57.22s | MC J052147.95−700957.0 | sl/ll | HV 942 | | |
| 95 | 22422272 | 05h21m49.40s | −70d04m35.26s | MC J052149.11−700434.2 | sl/ll | MACHO 78.6698.38 | | |
| 96 | 22422528 | 05h22m06.91s | −71d50m17.89s | MC J052206.92−715017.7 | sl/ll | | | |
| 97 | 22422784 | 05h22m22.98s | −68d41m00.72s | MC J052222.95−684101.2 | sl/ll | | 22457856 | |
| 98 | 22423040 | 05h22m42.01s | −69d15m26.04s | MC J052241.93−691526.2 | sl/ll | OGLE 052242.09−691526.2 | | |
| 99 | 22423552 | 05h22m54.96s | −69d36m52.34s | MC J052254.97−693651.7 | sl | SHV 0523185−693932 | | |
| 100 | 22423808 | 05h23m31.25s | −69d04m04.56s | MC J052331.11−690404.6 | sl/ll | LHα 120−N 136 | | |
| 101 | 22424320 | 05h23m51.14s | −68d07m12.37s | MC J052351.13−680712.2 | sl/ll | IRAS 05240−6809 | | |
| 102 | 22424576 | 05h23m53.95s | −71d34m43.97s | MC J052353.92−713443.9 | sl/ll | IRAS 05246−7137 | 22458112 | |
| 103 | 22424832 | 05h24m05.25s | −68d18m01.99s | MC J052405.31−681802.5 | sl/ll | | | |
| 104 | 22425088 | 05h24m14.30s | −68d29m58.98s | MC J052413.36−682958.8 | sl/ll | MSX LMC 464 | | |
| 105 | 22425344 | 05h24m45.36s | −69d16m05.53s | MC J052445.38−691605.3 | sl/ll | OGLE J052445.53−691605.6 | | |
| 106 | 22425600 | 05h24m57.86s | −67d24m58.43s | MC J052457.85−672458.3 | sl/ll | LHα 120−S 33 | | |
| 107 | 24314368 | 05h25m19.52s | −70d54m09.84s | MC J052519.48−705410.0 | sl/ll | HV 5829 | | |
| 108 | 24319744 | 05h25m46.52s | −66d14m11.30s | MC J052546.51−661411.5 | sl/ll | | | |
| 109 | 24315904 | 05h26m13.35s | −68d47m15.24s | MC J052613.39−684715.0 | sl/ll | | | |
| 110 | 22426112 | 05h26m20.15s | −69d39m02.59s | MC J052620.10−693902.1 | sl | OGLE J052620.25−693902.4 | | |
| 111 | 27038208 | 05h26m27.19s | −66d42m58.66s | MC J052627.23−664258.7 | sl/ll | HV 2522 | | |
| 112 | 22426368 | 05h26m37.58s | −70d29m07.18s | MC J052637.81−702906.7 | sl | RP 589 | | |
| 113 | 22426624 | 05h27m07.14s | −70d20m02.12s | MC J052707.10−702001.9 | sl/ll | | | |
| 114 | 22426880 | 05h27m23.24s | −71d24m25.41s | MC J052723.14−712426.3 | sl/ll | | 22458624 | |
| 115 | 22427136 | 05h27m35.64s | −69d08m56.22s | MC J052735.63−690856.3 | sl | LHα 120−N 145 | | Cluster |
| 116 | 22427392 | 05h27m38.76s | −69d28m45.57s | MC J052738.58−692843.9 | sl/ll | HV 2551 | | |
| 117 | 22427648 | 05h27m39.62s | −69d09m01.57s | MC J052739.63−690901.4 | sl/ll | W61 11−16 | | Cluster |
| 118 | 22427904 | 05h27m47.60s | −71d48m52.75s | MC J052747.62−714852.8 | sl/ll | | | |
| 119 | 22428160 | 05h28m05.91s | −70d07m54.03s | MC J052805.91−700753.4 | sl/ll | SHV 0528350−701014 | | |
| 120 | 22428416 | 05h28m25.86s | −69d46m47.45s | MC J052825.81−694647.3 | sl | OGLE J052825.96−694647.4 | | |
| 121 | 27084288 | 05h29m24.61s | −69d55m14.19s | 1C J052924.59−695513.4 | sl/ll | IRAS 05298−6957 | 22448896 | |
| 122 | 22428672 | 05h29m54.80s | −69d04m15.73s | MC J052954.73−690415.7 | sl/ll | HV 5879 | | |
| 123 | 22428928 | 05h30m04.67s | −68d47m29.08s | MC J053004.56−684728.8 | sl/ll | SP77 46−50 | | |
| 124 | 22429184 | 05h30m27.56s | −69d03m59.04s | MC J053027.49−690358.3 | sl | SHV 0530472−690607 | | |
| 125 | 22429440 | 05h30m44.72s | −71d42m59.62s | MC J053044.71−714259.4 | sl/ll | IRAS 05315−7145 | | |
| 126 | 22429696 | 05h30m45.03s | −68d21m29.11s | 1C J053044.97−682129.1 | sl/ll | KDM 4554 | | |
| 127 | 22429952 | 05h30m46.74s | −67d16m56.92s | MC J053046.81−671657.2 | sl | NGC 2004 Robb B45 | | Cluster |
| 128 | 22430208 | 05h30m48.40s | −67d16m45.88s | MC J053048.42−671645.8 | sl/ll | NGC 2004 Wes 18−13 | | Cluster |
| 129 | 22430464 | 05h30m52.25s | −67d17m34.22s | MC J053052.28−671734.4 | sl/ll | NGC 2004 Wes 6−14 | | Cluster |
| 130 | 22430720 | 05h31m28.43s | −70d10m27.65s | MC J053128.44−701027.1 | sl/ll | | | |
| 131 | 22430976 | 05h31m51.01s | −69d11m46.56s | MC J053150.98−691146.4 | sl/ll | MACHO 82.8405.15 | | |
| 132 | 22431232 | 05h31m58.96s | −72d44m36.35s | MC J053158.92−724436.0 | sl | KDM 4665 | | |
| 133 | 22431488 | 05h32m06.64s | −70d10m25.34s | MC J053206.70−701024.8 | sl | | | Cluster |
| 134 | 22431744 | 05h32m18.66s | −67d31m46.16s | MC J053218.64−673145.9 | sl | | | Cluster |
| 135 | 22432000 | 05h32m19.31s | −67d31m20.34s | MC J053219.33−673120.5 | sl/ll | NGC 2011 SAGE IRS 1 | | Cluster |
| 136 | 22432256 | 05h32m26.52s | −73d10m06.99s | MC J053226.51−731006.8 | sl | KDM 4718 | | |
| 137 | 24318208 | 05h32m39.71s | −69d30m49.25s | MC J053239.68−693049.4 | sl/ll | RP 774 | | |
| 138 | 22432768 | 05h32m53.35s | −66d07m27.17s | MC J053253.36−660727.8 | sl/ll | | | |
| 139 | 22433024 | 05h32m54.98s | −67d36m47.10s | MC J053254.99−673647.2 | sl | KDM 4774 | | |
| 140 | 24314112 | 05h33m06.86s | −70d30m34.22s | MC J053306.86−703033.9 | sl/ll | MSX LMC 736 | | |
| 141 | 22433280 | 05h33m18.61s | −66d00m39.91s | MC J053318.58−660040.2 | sl/ll | | | |
| 142 | 22433536 | 05h33m43.18s | −70d59m21.16s | MC J053343.27−705921.1 | sl | | | Cluster |
| 143 | 22433792 | 05h33m44.00s | −70d59m01.14s | MC J053343.98−705901.9 | sl | | | Cluster |
| 144 | 22434048 | 05h33m46.97s | −68d36m44.08s | MC J053346.97−683644.2 | sl/ll | LHα 120−N 151 | | |
| 145 | 22434304 | 05h34m41.46s | −69d26m30.74s | MC J053441.40−692630.6 | sl/ll | | | |
| 146 | 22434560 | 05h34m44.20s | −67d37m50.82s | MC J053444.17−673750.1 | sl/ll | SHP LMC 256 | | |
| 147 | 22434816 | 05h35m19.01s | −67d02m19.50s | MC J053518.91−670219.5 | sl/ll | HV 2700 | | |
| 148 | 22435072 | 05h35m48.02s | −70d31m46.92s | MC J053548.07−703146.6 | sl | | | |

TABLE 3 — *Continued*

| Nr. | AORkey IRS | RA (J2000) | Dec (J2000) | SAGE designation SSTISAGE + | mod. | name | AOR key MIPS SED | Remarks |
|---|---|---|---|---|---|---|---|---|
| 149 | 22435328 | 05h36m02.42s | −67d45m17.41s | MC J053602.36−674517.3 | sl/ll | | | |
| 150 | 24315648 | 05h36m32.48s | −70d17m38.81s | MC J053632.56−701738.4 | sl/ll | IRAS 05370−7019 | | |
| 151 | 22435584 | 05h36m34.82s | −72d26m58.67s | MC J053634.77−722658.6 | sl/ll | | | |
| 152 | 22436096 | 05h36m55.68s | −68d11m24.31s | MC J053655.60−681124.6 | sl | | | |
| 153 | 22436352 | 05h37m10.12s | −71d23m14.06s | MC J053710.26−712314.3 | sl | RP 493 | | |
| 154 | 22436608 | 05h37m30.63s | −67d40m41.19s | MC J053730.59−674041.6 | sl | | | |
| 155 | 22437120 | 05h38m23.66s | −66d09m00.91s | MC J053823.58−660900.3 | sl | KDM 5345 | | |
| 156 | 22437376 | 05h39m29.94s | −69d57m56.27s | 1C J053929.96−695755.6 | sl/ll | OGLE J053930.16−695755.8 | | |
| 157 | 22437632 | 05h39m33.17s | −71d21m55.45s | 1C J053932.66−712154.7 | sl/ll | HV 12631 | | |
| 158 | 22437888 | 05h39m42.37s | −71d10m45.03s | MC J053942.45−711044.5 | sl/ll | | | |
| 159 | 22438144 | 05h39m45.46s | −66d58m09.75s | MC J053945.40−665809.4 | sl | WOH G 449 | | |
| 160 | 22438400 | 05h39m49.22s | −69d37m47.03s | MC J053949.23−693747.0 | sl/ll | | | |
| 161 | 22438912 | 05h40m00.47s | −69d42m14.85s | MC J054000.52−694214.6 | sl | MACHO 81.9728.14 | | |
| 162 | 22439424 | 05h40m14.78s | −69d28m49.33s | MC J054014.83−692849.1 | sl/ll | MSX LMC 949 | | |
| 163 | 22439680 | 05h40m33.51s | −70d32m41.06s | MC J054033.54−703240.8 | sl/ll | RP 85 | 22460160 | |
| 164 | 22439936 | 05h40m59.28s | −70d44m02.82s | MC J054059.31−704402.5 | sl/ll | | | |
| 165 | 22440192 | 05h41m02.04s | −70d43m10.55s | 1C J054101.91−704311.0 | sl/ll | MSX LMC 947 | | |
| 166 | 22440448 | 05h41m14.58s | −71d32m36.01s | MC J054114.56−713236.0 | sl/ll | | | |
| 167 | 22440704 | 05h41m20.69s | −69d04m44.46s | 1C J054120.72−690443.5 | sl/ll | IRAS 05416−6906 | | |
| 168 | 24315392 | 05h41m25.08s | −71d15m32.74s | MC J054125.09−711532.6 | sl/ll | IRAS 05421−7116 | | |
| 169 | 22440960 | 05h41m57.43s | −69d12m18.61s | MC J054157.40−691218.1 | sl/ll | W61 6−24 | | |
| 170 | 22441472 | 05h42m03.91s | −69d13m07.64s | 1C J054203.85−691307.1 | sl/ll | NGC 2100 Robb 4 | | Cluster |
| 171 | 22441728 | 05h42m06.76s | −69d12m31.35s | MC J054206.76−691231.1 | sl/ll | 2MASS J05420676−6912312 | | Cluster |
| 172 | 22441984 | 05h42m09.98s | −69d13m28.76s | MC J054209.95−691328.7 | sl/ll | W61 6−57 | | Cluster |
| 173 | 22442240 | 05h42m30.51s | −69d48m57.47s | MC J054230.55−694857.3 | sl | WOH G 494 | | |
| 174 | 22442496 | 05h42m33.35s | −70d29m24.18s | MC J054233.17−702924.1 | sl/ll | LM 2−42 | | |
| 175 | 22443008 | 05h42m36.63s | −70d09m32.50s | MC J054236.65−700932.0 | sl/ll | LHα 120−N 178 | | |
| 176 | 22443264 | 05h42m54.62s | −70d08m07.74s | MC J054254.38−700807.4 | sl | | | |
| 177 | 22443520 | 05h43m10.87s | −67d27m28.42s | MC J054310.86−672728.0 | sl/ll | IRAS F05432−6728 | | |
| 178 | 22443776 | 05h43m14.23s | −70d38m35.12s | MC J054314.12−703835.1 | sl | | | |
| 179 | 22444032 | 05h43m28.77s | −69d42m43.88s | MC J054328.84−694243.7 | sl | KDM 5841 | | |
| 180 | 22444288 | 05h44m06.10s | −68d37m53.68s | MC J054406.01−683753.6 | sl/ll | | | |
| 181 | 22444544 | 05h44m37.92s | −67d36m58.17s | MC J054437.87−673657.7 | sl/ll | | | |
| 182 | 22444800 | 05h44m40.08s | −69d11m49.11s | MC J054440.11−691149.0 | sl/ll | | | |
| 183 | 22445056 | 05h44m50.23s | −69d23m04.72s | MC J054450.23−692304.2 | sl/ll | IRAS 05452−6924 | | |
| 184 | 22445312 | 05h45m24.23s | −68d30m41.61s | MC J054524.23−683041.4 | sl/ll | | | |
| 185 | 22445824 | 05h45m46.35s | −67d32m39.16s | MC J054546.32−673239.4 | sl/ll | | | |
| 186 | 22446080 | 05h47m04.62s | −69d27m34.24s | MC J054704.54−692733.9 | sl/ll | LHα 120−N 170 | | |
| 187 | 22446336 | 05h47m45.80s | −68d07m34.26s | MC J054745.79−680734.1 | sl/ll | | | |
| 188 | 22446592 | 05h47m57.25s | −68d14m56.90s | MC J054757.37−681457.0 | sl | KDM 6247 | | |
| 189 | 22446848 | 05h48m16.84s | −71d28m39.64s | MC J054816.79−712839.3 | sl | NGC 2121 LE 6 | | Cluster |
| 190 | 22447104 | 05h49m00.12s | −70d33m22.51s | MC J054900.01−703322.5 | sl/ll | IRAS 05495−7034 | | |
| 191 | 22447360 | 05h50m36.62s | −68d28m52.27s | MC J055036.69−682852.4 | sl | KDM 6486 | | |
| 192 | 27038464 | 05h51m22.58s | −69d53m51.05s | MC J055122.52−695351.4 | sl/ll | HV 2862 | | |
| 193 | 22447616 | 05h51m43.25s | −68d45m42.79s | MC J055143.27−684543.0 | sl/ll | | | |
| 194 | 22447872 | 05h52m51.07s | −69d28m39.09s | MC J055251.05−692839.6 | sl | PMP 337 | | Cluster |
| 195 | 22448128 | 05h52m52.51s | −69d30m35.54s | MC J055252.50−693035.6 | sl | PMP 133 | | Cluster |
| 196 | 27084032 | 05h53m12.04s | −70d15m22.71s | MC J055311.98−701522.5 | sl/ll | IRAS 05537−7015 | | |
| 197 | 22448384 | 06h00m53.60s | −68d00m39.08s | MC J060053.62−680038.8 | sl | | | |

TABLE 4
POINT SOURCES TARGETED WITH THE IRS STARING MODE AS PART OF THE
*SAGE-Spec* PROGRAM, PART II.

| Nr. | J | H | K | [3.6] | [4.5] | [5.8] | [8.0] | [24] |
|---|---|---|---|---|---|---|---|---|
| 1 | 12.41 | 11.49 | 11.19 | 10.91 | 10.81 | 10.69 | 10.49 | 9.64 |
| 2 | 16.02 | 15.16 | 14.45 | 14.02 | 13.52 | 13.09 | 10.12 | 7.03 |
| 3 | 15.02 | 13.28 | 11.72 | 9.86 | 8.97 | 8.55 | 8.12 | 7.33 |
| 4 | 10.10 | 9.27 | 9.00 | 8.87 | 9.05 | 8.87 | 8.75 | 7.55 |
| 5 | ⋯ | ⋯ | 12.92 | 10.36 | 9.48 | 8.68 | 7.85 | 4.86 |
| 6 | 12.18 | 11.78 | 11.24 | 10.07 | 9.60 | 9.21 | 8.56 | 7.21 |
| 7 | 13.22 | 11.56 | 10.37 | 9.37 | 8.94 | 8.57 | 8.14 | 7.62 |
| 8 | 15.05 | 13.78 | 12.94 | 11.12 | 10.61 | 10.04 | 9.19 | 7.23 |
| 9 | ⋯ | ⋯ | ⋯ | 12.61 | 10.38 | 8.63 | 7.02 | 4.20 |
| 10 | ⋯ | 16.89 | 15.83 | 13.65 | 12.35 | 11.11 | 9.70 | 3.12 |
| 11 | ⋯ | ⋯ | 12.36 | 11.18 | 10.07 | 8.61 | 3.84 |
| 12 | 12.02 | 10.79 | 10.03 | 9.22 | 9.36 | 9.35 | 8.80 | 8.46 |
| 13 | 12.26 | 11.31 | 10.99 | 10.74 | 10.77 | 10.59 | 10.49 | 10.16 |
| 14 | 16.94 | 16.14 | 14.89 | 12.85 | 11.63 | 10.25 | 8.95 | 3.22 |
| 15 | 12.54 | 11.30 | 10.43 | 9.40 | 9.26 | 8.96 | 8.46 | 8.17 |

TABLE 4  — *Continued*

| Nr. | $J$ | $H$ | $K$ | [3.6] | [4.5] | [5.8] | [8.0] | [24] |
|-----|-----|-----|-----|-------|-------|-------|-------|------|
| 16 | 9.32 | 8.46 | 8.06 | 7.50 | 7.46 | 7.13 | 6.51 | $\cdots$ |
| 17 | $\cdots$ | $\cdots$ | $\cdots$ | $\cdots$ | $\cdots$ | $\cdots$ | $\cdots$ | 1.86[a] |
| 18 | $\cdots$ | $\cdots$ | $\cdots$ | 11.55 | 9.71 | 8.18 | 7.56 | 4.22 |
| 19 | 9.19 | 8.67 | 8.60 | 8.92 | 8.54 | 8.47 | 8.44 | 8.41 |
| 20 | 16.79 | 15.27 | 13.77 | 11.76 | 11.03 | 10.07 | 8.66 | 2.40 |
| 21 | 17.32 | 16.32 | 14.38 | 11.11 | 9.92 | 8.89 | 7.68 | 4.35 |
| 22 | 12.42 | 11.74 | 11.43 | 10.53 | 10.42 | 10.07 | 9.49 | 7.19 |
| 23 | 12.40 | 11.23 | 10.68 | 10.02 | 10.07 | 9.97 | 9.56 | 9.51 |
| 24 | $\cdots$ | $\cdots$ | $\cdots$ | $\cdots$ | $\cdots$ | $\cdots$ | $\cdots$ | $\cdots$ |
| 25 | 17.65 | 16.72 | 15.71 | 13.97 | 13.14 | 11.99 | 10.52 | 7.04 |
| 26 | $\cdots$ | 15.22 | $\cdots$ | 10.51 | 9.67 | 9.00 | 8.34 | 6.32 |
| 27 | 8.94 | 8.10 | 7.73 | 7.56 | 7.67 | 7.34 | 6.88 | 4.89 |
| 28 | $\cdots$ | $\cdots$ | $\cdots$ | 11.08 | 10.22 | 9.52 | 8.56 | 6.29 |
| 29 | 13.75 | 13.41 | 13.09 | 11.53 | 10.59 | 9.73 | 8.59 | 6.52 |
| 30 | 11.59 | 10.43 | 9.78 | 9.06 | 9.09 | 8.90 | 8.26 | 8.23 |
| 31 | 11.49 | 10.31 | 9.69 | 8.97 | 9.08 | 8.93 | 8.44 | 7.85 |
| 32 | 12.05 | 11.13 | 10.83 | 10.54 | 10.73 | 10.56 | 10.37 | 10.00 |
| 33 | 11.67 | 10.55 | 9.95 | 9.21 | 9.30 | 9.21 | 8.74 | 8.33 |
| 34 | 16.15 | 14.13 | 12.35 | 10.15 | 9.26 | 8.51 | 7.49 | 3.67 |
| 35 | 10.65 | 9.87 | 9.63 | 9.45 | 9.65 | 9.54 | 9.50 | 9.39 |
| 36 | 12.41 | 11.34 | 10.85 | 10.33 | 10.15 | 9.88 | 9.55 | 8.97 |
| 37 | 10.31 | 9.51 | 9.26 | 9.07 | 9.25 | 9.11 | 8.99 | 8.41 |
| 38 | 10.93 | 9.97 | 9.39 | 9.21 | 8.98 | 8.73 | 7.99 | 5.62 |
| 39 | 16.39 | 15.27 | 14.33 | 12.53 | 11.77 | 11.05 | 10.14 | 7.50 |
| 40 | 13.98 | 13.17 | 12.22 | 10.49 | 9.87 | 9.06 | 7.94 | 3.60 |
| 41 | 12.44 | 11.35 | $\cdots$ | 10.13 | 10.20 | 10.10 | 9.65 | 9.56 |
| 42 | $\cdots$ | $\cdots$ | $\cdots$ | 14.28 | 13.18 | 11.96 | 10.65 | 6.54 |
| 43 | 14.13 | 12.58 | 11.71 | 10.18 | 9.83 | 9.43 | 9.01 | 8.49 |
| 44 | 14.68 | 13.89 | 13.47 | 13.18 | 12.55 | 12.04 | 10.82 | 7.08 |
| 45 | 12.64 | 11.39 | 10.49 | 9.71 | 9.27 | 8.92 | 8.67 | 8.33 |
| 46 | 12.96 | 11.97 | 11.59 | 10.93 | 10.91 | 10.75 | 10.61 | 10.42 |
| 47 | 12.67 | 11.68 | 11.29 | 10.88 | 10.97 | 10.80 | 10.51 | 10.21 |
| 48 | 11.86 | 10.71 | 10.09 | 9.33 | 9.40 | 9.33 | 8.75 | 8.65 |
| 49 | 12.88 | 11.60 | 11.01 | 10.24 | 10.40 | 10.53 | 9.85 | 9.74 |
| 50 | 13.10 | 13.09 | 13.10 | 13.06 | 13.04 | 12.91 | 12.58 | 6.57 |
| 51 | 12.63 | 11.15 | 10.06 | 8.55 | 8.35 | 8.05 | 7.72 | 7.56 |
| 52 | 16.62 | 15.38 | 14.50 | 12.22 | 11.32 | 9.68 | 7.57 | 3.26 |
| 53 | 15.51 | 13.72 | 12.13 | 9.74 | 9.06 | 8.51 | 8.05 | 7.48 |
| 54 | 13.30 | 12.32 | 11.96 | 11.18 | 10.56 | 9.91 | 8.95 | 6.82 |
| 55 | 15.34 | 13.32 | 11.74 | 9.36 | 8.88 | 8.37 | 7.90 | 7.36 |
| 56 | 12.46 | 11.54 | 11.09 | 10.49 | 10.25 | 9.88 | 8.40 | 5.36 |
| 57 | 12.98 | 11.91 | 11.42 | 10.79 | 10.83 | 10.52 | 10.16 | 9.46 |
| 58 | 11.61 | 10.71 | 10.38 | 10.23 | 10.38 | 10.23 | 10.18 | 10.02 |
| 59 | 13.15 | 12.75 | 12.62 | $\cdots$ | 11.89 | 11.41 | 10.59 | 8.39 |
| 60 | 15.36 | 13.13 | 11.35 | 9.86 | 8.89 | 8.16 | 7.47 | 6.42 |
| 61 | 10.81 | 9.85 | 9.53 | 9.12 | 9.18 | 8.92 | 8.58 | 6.83 |
| 62 | 13.71 | 13.19 | 12.11 | 10.11 | 9.32 | 8.60 | 7.48 | 4.71 |
| 63 | 12.28 | 11.33 | 10.97 | 10.68 | 10.65 | 10.49 | 10.05 | 8.03 |
| 64 | 15.63 | 15.11 | 14.27 | 12.42 | 11.80 | 10.11 | 8.25 | 3.64 |
| 65 | $\cdots$ | 16.44 | $\cdots$ | 15.82 | 13.70 | 10.68 | 7.85 | 3.32 |
| 66 | 14.16 | 12.30 | 10.89 | 9.13 | 8.47 | 7.93 | 7.45 | 6.83 |
| 67 | 12.26 | 11.32 | 10.99 | 10.76 | 10.75 | 10.59 | 10.34 | 9.03 |
| 68 | 11.41 | 10.50 | 10.23 | 10.00 | 10.17 | 9.99 | 9.93 | 9.73 |
| 69 | 12.93 | 12.84 | 12.69 | 13.01 | 12.93 | 12.82 | 12.36 | 5.27 |
| 70 | $\cdots$ | $\cdots$ | 15.58 | $\cdots$ | 11.90 | 10.36 | 8.90 | 3.36 |
| 71 | 18.06 | 17.08 | 16.01 | 14.16 | 13.38 | 12.53 | 11.43 | 7.51 |
| 72 | 12.33 | 11.37 | 11.07 | 10.87 | 10.87 | 10.69 | 10.51 | 9.18 |
| 73 | 13.09 | 12.63 | 12.09 | 10.14 | 9.39 | 8.67 | 7.84 | 6.01 |
| 74 | 17.43 | 15.21 | 13.20 | 10.41 | 9.30 | 8.38 | 7.38 | 3.49 |
| 75 | 13.48 | 12.71 | 12.51 | 12.15 | 11.77 | 10.94 | 9.51 | 6.13 |
| 76 | 12.13 | 11.25 | 10.89 | 10.60 | 10.76 | 10.59 | 10.47 | 10.26 |
| 77 | 12.26 | 11.35 | 11.08 | 10.78 | 10.83 | 10.68 | 10.47 | 9.28 |
| 78 | $\cdots$ | 16.21 | $\cdots$ | 11.61 | 10.38 | 9.20 | 7.61 | 2.97 |
| 79 | 13.14 | 12.18 | 11.90 | 11.68 | 11.59 | 11.40 | 10.68 | 8.84 |
| 80 | $\cdots$ | $\cdots$ | $\cdots$ | 9.38 | 9.20 | 8.69 | 8.32 | 7.85 |
| 81 | 11.97 | 10.95 | 10.58 | 10.18 | 10.20 | 10.04 | 9.85 | 9.38 |
| 82 | 10.36 | 9.43 | 9.06 | 8.80 | 8.92 | 8.63 | 8.46 | 6.93 |
| 83 | 12.26 | 11.09 | 10.43 | 9.76 | 9.93 | 9.99 | 9.46 | 9.16 |
| 84 | 14.66 | 14.22 | 13.99 | 12.70 | 11.53 | 9.43 | 7.16 | 3.41 |
| 85 | 13.54 | 13.17 | 12.66 | 10.79 | 10.14 | 9.57 | 8.68 | 6.73 |
| 86 | 11.78 | 10.65 | 10.05 | 9.54 | 9.66 | 9.60 | 9.06 | 8.53 |
| 87 | 11.78 | 10.56 | 9.86 | 9.16 | 9.37 | 9.47 | 8.83 | 7.71 |
| 88 | 12.54 | 11.62 | 11.28 | 11.05 | 11.09 | 10.92 | 10.72 | $\cdots$ |
| 89 | 12.53 | 11.57 | 11.28 | 11.11 | 11.04 | 10.90 | 10.65 | 9.37 |
| 90 | 15.63 | 14.94 | 13.80 | 11.34 | 10.34 | 9.50 | 8.46 | 3.61 |
| 91 | 12.36 | 11.41 | 11.08 | 10.83 | 10.80 | 10.62 | 10.20 | 8.36 |
| 92 | 15.97 | 15.61 | 14.27 | 11.73 | 10.69 | 9.17 | 7.40 | 3.30 |

TABLE 4 — *Continued*

| Nr. | $J$ | $H$ | $K$ | [3.6] | [4.5] | [5.8] | [8.0] | [24] |
|---|---|---|---|---|---|---|---|---|
| 93 | 11.72 | 10.81 | 10.52 | 10.22 | 10.34 | 10.11 | 9.40 | 7.41 |
| 94 | 13.36 | 12.82 | 11.89 | 9.85 | 8.99 | 8.22 | 7.43 | 5.97 |
| 95 | 14.35 | 13.77 | 13.60 | 12.27 | 11.42 | 10.56 | 9.53 | 7.19 |
| 96 | 12.40 | 11.47 | 11.20 | 11.00 | 10.95 | 10.74 | 9.66 | 7.70 |
| 97 | 15.57 | 14.66 | 13.67 | 11.90 | 11.28 | 9.96 | 8.42 | 4.92 |
| 98 | 15.79 | 13.60 | 11.81 | 9.46 | 8.72 | 8.16 | 7.60 | 6.83 |
| 99 | 12.74 | 11.77 | 11.44 | 11.19 | 11.05 | 10.84 | 10.34 | 8.51 |
| 100 | $\cdots$ | $\cdots$ | 15.07 | 13.36 | 12.45 | 11.72 | 10.13 | 6.76 |
| 101 | 12.99 | 12.28 | 11.79 | 10.24 | 9.33 | 8.59 | 7.63 | 1.90 |
| 102 | $\cdots$ | 15.59 | 12.98 | 9.78 | 8.65 | 7.73 | 6.83 | 3.29 |
| 103 | 15.12 | 13.34 | 11.78 | 9.63 | 9.10 | 8.63 | 8.24 | 7.60 |
| 104 | 14.24 | 12.51 | 11.06 | 9.11 | 8.26 | 7.44 | 6.41 | 2.43 |
| 105 | 12.26 | 10.90 | 9.93 | 9.06 | 8.56 | 8.12 | 7.82 | 7.05 |
| 106 | 13.92 | 13.28 | 12.51 | 11.00 | 10.44 | 9.98 | 9.35 | 7.65 |
| 107 | 14.22 | 13.83 | 13.46 | 10.90 | 10.12 | 9.50 | 8.65 | 6.59 |
| 108 | $\cdots$ | 15.46 | 12.92 | 9.93 | 8.75 | 7.90 | 6.87 | 2.89 |
| 109 | 15.66 | 14.97 | 14.14 | 12.38 | 11.59 | 10.20 | 8.17 | 3.68 |
| 110 | 12.26 | 11.38 | 11.10 | 10.65 | 10.82 | 10.54 | 10.21 | 8.30 |
| 111 | 13.58 | 13.14 | 12.74 | 11.15 | 10.28 | 9.50 | 8.51 | 6.52 |
| 112 | $\cdots$ | $\cdots$ | $\cdots$ | 13.53 | 12.59 | 11.73 | 10.71 | 8.03 |
| 113 | $\cdots$ | $\cdots$ | $\cdots$ | 11.44 | 10.67 | 10.17 | 9.48 | 7.56 |
| 114 | 17.33 | $\cdots$ | 15.91 | 13.85 | 13.45 | 11.02 | 9.15 | 4.07 |
| 115 | 15.06 | 14.47 | 12.88 | 9.95 | 8.76 | 7.79 | 6.56 | 4.14 |
| 116 | 9.33 | 8.52 | 8.22 | 8.03 | 8.18 | 7.98 | 7.79 | 5.88 |
| 117 | 9.06 | 8.25 | 7.97 | 7.70 | 7.91 | 7.70 | 7.59 | 7.40 |
| 118 | 13.48 | 12.75 | 11.77 | 10.07 | 9.39 | 8.89 | 8.12 | 6.04 |
| 119 | 12.34 | 10.97 | 9.99 | 8.95 | 8.84 | 8.75 | 8.29 | 6.53 |
| 120 | 11.84 | 10.83 | 10.40 | 9.89 | 9.93 | 9.77 | 9.36 | 8.90 |
| 121 | $\cdots$ | $\cdots$ | 11.38 | 7.47 | 6.67 | 5.99 | 5.08 | 2.19 |
| 122 | 9.42 | 8.69 | 8.41 | 8.25 | 8.38 | 8.15 | 7.90 | 6.80 |
| 123 | 9.80 | 9.03 | 8.77 | 8.58 | 8.80 | 8.58 | 8.40 | 7.42 |
| 124 | 12.46 | 11.76 | 11.46 | 10.65 | 10.61 | 10.32 | 10.10 | 9.68 |
| 125 | $\cdots$ | $\cdots$ | $\cdots$ | 13.88 | 12.19 | 10.23 | 7.83 | 2.75 |
| 126 | $\cdots$ | 12.63 | 11.14 | 9.10 | 8.62 | 7.75 | 7.70 | 7.19 |
| 127 | 10.76 | 10.01 | 9.77 | 9.65 | 9.82 | 9.69 | 9.69 | 9.31 |
| 128 | 9.98 | 9.15 | 8.91 | 8.78 | 8.99 | 8.76 | 8.66 | 7.80 |
| 129 | 9.87 | 9.04 | 8.83 | 8.63 | 8.77 | 8.60 | 8.42 | 6.81 |
| 130 | 12.42 | 11.27 | 10.45 | 9.59 | 9.29 | 8.82 | 7.88 | 5.80 |
| 131 | 13.11 | 12.88 | 12.57 | 11.05 | 9.91 | 8.88 | 7.55 | 4.84 |
| 132 | 12.59 | 11.53 | 11.13 | 10.60 | 10.66 | 10.46 | 10.19 | 9.34 |
| 133 | 11.74 | 10.81 | 10.54 | 10.36 | 10.44 | 10.27 | 10.20 | 9.92 |
| 134 | 9.70 | 8.94 | 8.64 | 8.47 | 8.65 | 8.45 | 8.37 | 7.84 |
| 135 | 9.26 | 8.38 | 8.05 | 7.82 | 7.83 | 7.47 | 6.93 | 5.20 |
| 136 | 12.17 | 11.02 | 10.45 | 9.87 | 10.02 | 9.98 | 9.55 | 9.26 |
| 137 | 16.97 | 16.04 | 14.93 | 12.18 | 11.33 | 10.31 | 8.91 | 5.34 |
| 138 | $\cdots$ | $\cdots$ | $\cdots$ | 14.79 | 13.97 | 12.98 | 11.87 | 7.24 |
| 139 | 11.94 | 10.89 | 10.41 | 9.81 | 9.78 | 9.53 | 9.11 | 8.27 |
| 140 | 13.76 | 13.05 | 12.46 | 10.12 | 8.58 | 7.52 | 6.47 | 4.41 |
| 141 | 15.13 | 13.31 | 11.76 | 9.60 | 9.00 | 8.48 | 7.87 | 6.81 |
| 142 | 10.89 | 9.95 | 9.65 | 9.42 | 9.57 | 9.38 | 9.32 | 8.53 |
| 143 | 11.50 | 10.56 | 10.23 | 10.08 | 10.15 | 9.94 | 9.84 | 8.51 |
| 144 | 15.64 | 15.17 | 13.98 | 11.91 | 11.30 | 9.34 | 7.32 | 3.99 |
| 145 | 12.47 | 10.99 | 9.91 | 9.01 | 8.28 | 7.79 | 7.26 | 6.74 |
| 146 | 14.51 | 14.20 | 13.55 | 11.49 | 10.55 | 9.70 | 8.80 | 6.06 |
| 147 | 9.54 | 8.71 | 8.34 | 7.97 | 8.03 | 7.77 | 7.37 | 4.95 |
| 148 | 12.06 | 11.14 | 10.77 | 10.52 | 10.60 | 10.46 | 10.23 | 8.77 |
| 149 | 16.87 | 15.81 | 14.60 | 12.80 | 12.14 | 11.32 | 10.25 | 6.47 |
| 150 | 17.25 | 16.30 | 15.21 | 11.93 | 10.84 | 9.20 | 7.39 | 2.96 |
| 151 | 15.59 | 14.78 | 13.83 | 12.21 | 11.43 | 10.80 | 10.16 | 6.64 |
| 152 | 12.24 | 11.28 | 10.95 | 10.80 | 10.95 | 10.72 | 10.28 | 8.42 |
| 153 | 17.58 | 16.58 | 15.43 | 13.78 | 13.01 | 12.39 | 11.37 | 7.75 |
| 154 | 16.70 | 15.77 | 14.51 | 12.18 | 11.26 | 10.51 | 9.56 | 5.14 |
| 155 | 13.15 | 11.99 | 11.31 | 10.18 | 10.02 | 9.68 | 9.02 | 7.78 |
| 156 | 14.21 | 12.42 | 10.98 | 9.55 | 8.98 | 8.47 | 7.94 | 7.03 |
| 157 | 13.24 | 12.38 | 12.18 | 11.97 | 12.89 | 11.47 | 10.75 | 7.25 |
| 158 | $\cdots$ | $\cdots$ | 14.95 | 12.11 | 11.21 | 10.19 | 8.93 | 5.97 |
| 159 | 12.11 | 11.15 | 10.87 | 10.62 | 10.60 | 10.42 | 9.89 | 8.07 |
| 160 | 15.06 | 14.72 | 14.56 | 14.29 | 13.81 | 12.67 | 10.76 | 5.04 |
| 161 | 13.20 | 12.63 | 12.10 | 10.38 | 9.59 | 8.97 | 8.21 | 6.37 |
| 162 | 15.37 | 14.54 | 12.95 | 10.11 | 8.76 | 7.71 | 6.39 | 2.77 |
| 163 | $\cdots$ | $\cdots$ | $\cdots$ | 12.98 | 12.14 | 10.74 | 8.91 | 4.76 |
| 164 | $\cdots$ | 16.38 | 14.83 | 11.99 | 10.60 | 9.56 | 8.34 | 3.82 |
| 165 | 10.14 | 9.25 | 8.78 | 8.43 | 8.11 | 7.74 | 6.97 | 5.02 |
| 166 | 13.23 | 12.28 | 11.94 | 11.21 | 10.78 | 10.26 | 9.45 | 7.55 |
| 167 | $\cdots$ | $\cdots$ | $\cdots$ | 12.70 | 10.20 | 8.24 | 6.63 | 3.78 |
| 168 | 16.44 | 15.43 | 14.29 | 12.20 | 11.63 | 10.46 | 9.21 | 3.34 |
| 169 | 9.81 | 9.04 | 8.74 | 8.55 | 8.64 | 8.42 | 8.14 | 6.89 |

TABLE 4  — *Continued*

| Nr. | $J$ | $H$ | $K$ | [3.6] | [4.5] | [5.8] | [8.0] | [24] |
|---|---|---|---|---|---|---|---|---|
| 170 | 9.84 | 9.00 | 8.74 | 8.50 | 8.67 | 8.36 | 7.94 | 6.37 |
| 171 | 9.98 | 9.15 | 8.81 | 8.54 | 8.56 | 8.19 | 7.62 | 5.94 |
| 172 | 10.02 | 9.15 | 8.82 | 8.48 | 8.58 | 8.24 | 7.78 | 6.05 |
| 173 | 10.80 | 9.87 | 9.52 | 9.30 | 9.46 | 9.24 | 9.02 | 8.64 |
| 174 | 15.30 | 14.69 | 14.32 | 13.42 | 12.78 | 12.37 | 11.44 | 7.45 |
| 175 | 15.78 | 15.50 | $\cdots$ | 12.71 | 11.98 | 10.39 | 8.40 | 4.25 |
| 176 | 11.66 | 10.65 | 10.24 | 10.02 | 10.09 | 9.89 | 9.74 | 8.23 |
| 177 | 11.90 | 11.02 | 10.82 | 10.49 | 10.14 | 9.52 | 7.84 | 4.34 |
| 178 | 11.16 | 10.21 | 9.88 | 9.61 | 9.74 | 9.54 | 9.45 | 9.07 |
| 179 | 12.93 | 11.70 | 11.09 | 10.31 | 10.40 | 10.27 | 9.65 | 8.30 |
| 180 | 10.45 | 9.48 | 9.13 | 8.73 | 8.76 | 8.48 | 8.24 | 6.99 |
| 181 | 14.09 | 12.40 | 10.98 | 9.42 | 8.78 | 8.44 | 7.93 | 7.13 |
| 182 | 13.06 | 12.15 | 11.91 | 11.75 | 11.79 | 11.59 | 10.41 | 7.50 |
| 183 | 17.08 | 16.18 | 14.55 | 12.69 | 11.74 | 10.32 | 8.80 | 2.58 |
| 184 | 16.46 | 15.69 | 14.84 | 13.72 | 13.13 | 12.44 | 10.93 | 7.71 |
| 185 | 15.96 | 14.51 | 13.34 | 11.47 | 10.63 | 9.83 | 8.91 | 6.80 |
| 186 | $\cdots$ | $\cdots$ | $\cdots$ | 13.17 | 12.41 | 11.05 | 9.29 | 4.20 |
| 187 | 13.76 | 13.45 | 12.65 | 10.79 | 10.09 | 9.53 | 8.62 | 6.61 |
| 188 | 12.65 | 11.73 | 11.34 | 10.80 | 10.94 | 10.78 | 10.59 | 10.65 |
| 189 | 12.97 | 11.44 | 10.36 | 9.17 | 8.95 | 8.67 | 8.26 | 8.11 |
| 190 | $\cdots$ | $\cdots$ | $\cdots$ | 15.37 | 13.71 | 11.31 | 8.46 | 2.42 |
| 191 | 12.98 | 11.99 | 11.55 | 11.08 | 11.09 | 10.86 | 10.66 | 10.21 |
| 192 | 13.72 | 13.32 | 13.10 | 11.67 | 10.68 | 9.68 | 8.41 | 5.84 |
| 193 | 15.66 | 15.00 | 14.10 | 12.11 | 11.42 | 10.69 | 9.92 | 6.80 |
| 194 | 12.20 | 11.11 | 10.60 | 10.18 | 10.27 | 10.18 | 9.90 | 9.89 |
| 195 | 10.14 | 9.61 | 9.48 | 9.40 | 9.45 | 9.44 | 9.39 | 9.45 |
| 196 | 16.28 | 15.74 | 14.95 | 12.79 | 11.89 | 9.90 | 7.72 | 3.00 |
| 197 | 11.90 | 11.03 | 10.68 | 10.50 | 10.45 | 10.31 | 10.14 | 8.98 |

[a] MIPS-[24] from nearby LH$\alpha$ 120$-$N 82, which appears to be the main contributor to the LL spectrum.

TABLE 5
Archival IRS staring mode observations within the *SAGE-LMC*
footprint

| AOR key IRS | RA (J2000) requested | Dec (J2000) requested | Proposal ID | PI | AOR key MIPS SED |
|---|---|---|---|---|---|
| 10972672 | 04h28m30.17s | $-$69d30m50.0s | 3426 | Kastner | |
| 19012352 | 04h32m57.38s | $-$69d26m33.0s | 30788 | Sahai | |
| 19012864 | 04h33m43.69s | $-$70d09m50.0s | 30788 | Sahai | |
| 19012608 | 04h35m24.10s | $-$66d56m49.0s | 30788 | Sahai | |
| 10972928 | 04h37m22.73s | $-$68d25m03.3s | 3426 | Kastner | |
| 24325120 | 04h38m49.80s | $-$69d27m14.0s | 464 | Cohen | |
| 23882240 | 04h40m05.79s | $-$67d16m38.4s | 40650 | Looney | |
| 6077440 | 04h40m28.51s | $-$69d55m13.8s | 1094 | Kemper | |
| 10957824 | 04h40m28.51s | $-$69d55m13.8s | 3426 | Kastner | |
| 23888896 | 04h40m50.35s | $-$67d52m17.5s | 40650 | Looney | |
| 4946944 | 04h40m56.67s | $-$67d48m01.6s | 103 | Houck | |
| 23881472 | 04h41m12.26s | $-$67d40m30.7s | 40650 | Looney | |
| 23883776 | 04h41m14.98s | $-$67d39m02.4s | 40650 | Looney | |
| 19009024 | 04h42m57.33s | $-$70d12m25.0s | 30788 | Sahai | |
| 23890688 | 04h44m18.99s | $-$66d56m32.4s | 40650 | Looney | |
| 33292288 | 04h44m58.40s | $-$70d35m22.5s | 50092 | Gielen | |
| 11182080 | 04h47m04.45s | $-$67d06m53.1s | 3578 | Misselt | |
| 10958080 | 04h47m16.08s | $-$68d24m25.5s | 3426 | Kastner | |
| 23882240 | 04h47m17.50s | $-$69d09m30.3s | 40650 | Looney | |
| 23889664 | 04h48m49.85s | $-$69d09m30.6s | 40650 | Looney | |
| 23888896 | 04h48m54.41s | $-$69d09m48.3s | 40650 | Looney | |
| 11239168 | 04h48m54.66s | $-$69d09m46.1s | 3591 | Kemper | |
| 9069312 | 04h49m18.50s | $-$69d53m14.3s | 1094 | Kemper | |
| 10958336 | 04h49m22.46s | $-$69d24m34.6s | 3426 | Kastner | |
| 23881472 | 04h49m27.29s | $-$69d12m06.3s | 40650 | Looney | |
| 6076672 | 04h49m41.46s | $-$68d37m51.2s | 1094 | Kemper | |
| 25648128 | 04h49m41.48s | $-$68d37m51.5s | 50147 | Sloan | |
| 25648384 | 04h49m41.48s | $-$68d37m21.5s | 50147 | Sloan | |
| 23889664 | 04h50m09.52s | $-$69d29m06.4s | 40650 | Looney | |
| 4947456 | 04h50m13.20s | $-$69d33m56.6s | 103 | Houck | |
| 15902464 | 04h50m13.20s | $-$69d33m56.0s | 103 | Houck | |
| 19009792 | 04h50m23.38s | $-$69d37m56.0s | 30788 | Sahai | |
| 14705920 | 04h50m24.71s | $-$68d13m17.0s | 20443 | Stanghellini | |
| 6022400 | 04h50m40.46s | $-$69d17m31.9s | 200 | Houck | |
| 23888896 | 04h51m00.16s | $-$69d19m34.4s | 40650 | Looney | |
| 14700032 | 04h51m08.90s | $-$68d49m05.8s | 20443 | Stanghellini | |

TABLE 5 — *Continued*

| AOR key IRS | RA (J2000) requested | Dec (J2000) requested | Proposal ID | PI | AOR key MIPS SED |
|---|---|---|---|---|---|
| 11239168 | 04h51m10.96s | −69d20m14.7s | 3591 | Kemper | |
| 23881472 | 04h51m11.39s | −69d26m46.7s | 40650 | Looney | |
| 11239168 | 04h51m11.47s | −69d26m46.9s | 3591 | Kemper | |
| 11239168 | 04h51m15.48s | −68d41m40.3s | 3591 | Kemper | |
| 6020096 | 04h51m29.00s | −68d57m50.1s | 200 | Houck | |
| 4947712 | 04h51m37.89s | −67d05m16.3s | 103 | Houck | 22450432 |
| 27984640 | 04h51m40.56s | −68d47m04.9s | 50338 | Matsuura | |
| 27985664 | 04h51m40.56s | −68d47m34.9s | 50338 | Matsuura | |
| 27986432 | 04h51m40.56s | −68d48m04.9s | 50338 | Matsuura | |
| 23883776 | 04h51m53.29s | −69d23m28.6s | 40650 | Looney | |
| 11239168 | 04h51m53.69s | −69d23m28.7s | 3591 | Kemper | |
| 23888896 | 04h52m00.43s | −69d23m42.6s | 40650 | Looney | |
| 23888896 | 04h52m01.15s | −69d20m07.7s | 40650 | Looney | |
| 23888896 | 04h52m04.56s | −69d20m46.4s | 40650 | Looney | |
| 23885568 | 04h52m05.39s | −66d55m13.8s | 40650 | Looney | |
| 23881984 | 04h52m06.97s | −66d55m16.4s | 40650 | Looney | |
| 23884544 | 04h52m08.94s | −66d55m37.4s | 40650 | Looney | |
| 23893504 | 04h52m09.22s | −66d55m21.9s | 40650 | Looney | |
| 11239168 | 04h52m20.18s | −68d43m30.1s | 3591 | Kemper | |
| 11239168 | 04h52m32.54s | −69d21m44.2s | 3591 | Kemper | |
| 33283584 | 04h52m43.19s | −70d47m37.2s | 50092 | Gielen | |
| 6023936 | 04h52m45.00s | −69d11m48.0s | 200 | Houck | 22453504 |
| 23883776 | 04h52m45.62s | −69d11m49.5s | 40650 | Looney | 22453504 |
| 23881472 | 04h52m58.09s | −68d03m36.1s | 40650 | Looney | |
| 23890688 | 04h52m58.67s | −68d02m56.0s | 40650 | Looney | |
| 10958592 | 04h52m58.80s | −68d02m56.8s | 3426 | Kastner | |
| 27576832 | 04h53m29.91s | −69d17m48.52s | 485 | Ardila | |
| 11239168 | 04h53m32.32s | −69d01m17.5s | 3591 | Kemper | |
| 19010048 | 04h53m46.37s | −68d16m13.0s | 30788 | Sahai | |
| 23885568 | 04h53m58.55s | −66d47m22.8s | 40650 | Looney | |
| 23881472 | 04h53m58.57s | −69d11m06.7s | 40650 | Looney | |
| 23881472 | 04h54m00.10s | −69d11m55.5s | 40650 | Looney | |
| 23881472 | 04h54m01.14s | −69d11m52.9s | 40650 | Looney | |
| 19009280 | 04h54m01.61s | −65d04m52.0s | 30788 | Sahai | |
| 23888896 | 04h54m03.04s | −69d11m39.7s | 40650 | Looney | |
| 23890688 | 04h54m03.62s | −67d16m18.5s | 40650 | Looney | |
| 25996800 | 04h54m03.62s | −67d16m18.2s | 50338 | Matsuura | |
| 23889408 | 04h54m05.74s | −66d45m07.2s | 40650 | Looney | |
| 23881728 | 04h54m06.43s | −66d46m01.4s | 40650 | Looney | |
| 23884544 | 04h54m08.28s | −66d46m31.4s | 40650 | Looney | |
| 6020352 | 04h54m09.90s | −69d55m58.0s | 200 | Houck | |
| 17399808 | 04h54m09.90s | −69d55m58.0s | 30345 | Houck | |
| 17400064 | 04h54m09.90s | −69d55m28.0s | 30345 | Houck | |
| 11219200 | 04h54m14.29s | −68d44m14.1s | 3583 | Onaka | |
| 11219456 | 04h54m14.29s | −68d44m14.1s | 3583 | Onaka | |
| 11219712 | 04h54m14.29s | −68d44m14.1s | 3583 | Onaka | |
| 11219968 | 04h54m14.29s | −68d44m14.1s | 3583 | Onaka | |
| 11220224 | 04h54m14.29s | −68d44m14.1s | 3583 | Onaka | |
| 11220480 | 04h54m14.29s | −68d44m14.1s | 3583 | Onaka | |
| 3824384 | 04h54m22.30s | −69d11m04.00s | 18 | Houck | |
| 23883776 | 04h54m26.06s | −69d11m02.3s | 40650 | Looney | |
| 11239168 | 04h54m33.87s | −69d20m36.2s | 3591 | Kemper | |
| 10958848 | 04h55m03.07s | −69d29m12.8s | 3426 | Kastner | |
| 23888896 | 04h55m06.50s | −69d17m08.8s | 40650 | Looney | 22460416 |
| 11239168 | 04h55m06.56s | −69d17m08.7s | 3591 | Kemper | 22460416 |
| 23893504 | 04h55m07.49s | −65d12m32.7s | 40650 | Looney | |
| 5056256 | 04h55m10.20s | −68d20m35.0s | 129 | Gehrz | |
| 10973952 | 04h55m10.49s | −68d20m29.8s | 3426 | Kastner | 22448640 |
| 10959104 | 04h55m16.03s | −69d19m12s | 3426 | Kastner | |
| 11239168 | 04h55m18.88s | −68d46m30.7s | 3591 | Kemper | |
| 23889408 | 04h55m20.40s | −66d44m17.6s | 40650 | Looney | |
| 10959360 | 04h55m21.65s | −69d47m16.8s | 3426 | Kastner | |
| 23881728 | 04h55m24.38s | −66d31m17.9s | 40650 | Looney | |
| 23890688 | 04h55m26.71s | −68d25m28.6s | 40650 | Looney | |
| 11239168 | 04h55m33.54s | −69d24m59.3s | 3591 | Kemper | |
| 23890176 | 04h55m37.28s | −66d34m23.0s | 40650 | Looney | |
| 12929792 | 04h55m38.98s | −67d49m10.7s | 3505 | Wood | |
| 23890176 | 04h55m40.01s | −66d34m24.2s | 40650 | Looney | |
| 23888640 | 04h55m41.59s | −66d34m34.1s | 40650 | Looney | |
| 23888640 | 04h55m42.46s | −66d34m25.8s | 40650 | Looney | |
| 23888640 | 04h55m46.40s | −66d25m09.1s | 40650 | Looney | |
| 23893504 | 04h55m50.62s | −66d34m34.6s | 40650 | Looney | 22457344 |
| 23881728 | 04h56m22.61s | −66d36m56.9s | 40650 | Looney | 22457600 |
| 23890176 | 04h56m25.99s | −66d31m55.5s | 40650 | Looney | |
| 23890176 | 04h56m29.02s | −66d31m59.3s | 40650 | Looney | |
| 11239168 | 04h56m32.15s | −68d52m51.0s | 3591 | Kemper | |

TABLE 5 — *Continued*

| AOR key IRS | RA (J2000) requested | Dec (J2000) requested | Proposal ID | PI | AOR key MIPS SED |
|---|---|---|---|---|---|
| 23890176 | 04h56m38.76s | −66d24m46.2s | 40650 | Looney | |
| 23893504 | 04h56m40.79s | −66d32m30.5s | 40650 | Looney | |
| 10959616 | 04h56m47.04s | −69d50m24.7s | 3426 | Kastner | 22453760 |
| 6724352 | 04h56m47.08s | −69d50m24.8s | 653 | Houck | 22453760 |
| 7459328 | 04h56m47.08s | −69d50m24.8s | 665 | Houck | 22453760 |
| 23881984 | 04h56m47.23s | −66d24m31.8s | 40650 | Looney | |
| 23890176 | 04h56m51.82s | −66d31m33.0s | 40650 | Looney | |
| 23893504 | 04h56m57.25s | −66d25m13.0s | 40650 | Looney | |
| 23890176 | 04h56m59.85s | −66d24m25.9s | 40650 | Looney | |
| 11182336 | 04h57m04.47s | −66d34m38.5s | 3578 | Misselt | |
| 23881728 | 04h57m05.03s | −66d42m35.8s | 40650 | Looney | |
| 23881472 | 04h57m09.73s | −68d44m48.2s | 40650 | Looney | |
| 23888640 | 04h57m13.47s | −66d19m00.1s | 40650 | Looney | |
| 19150592 | 04h57m14.33s | −68d26m30.0s | 30869 | Kastner | |
| 23889408 | 04h57m14.98s | −68d26m29.5s | 40650 | Looney | |
| 23885568 | 04h57m16.25s | −66d23m19.9s | 40650 | Looney | |
| 23889408 | 04h57m16.82s | −68d26m48.0s | 40650 | Looney | |
| 23882240 | 04h57m19.77s | −68d25m26.4s | 40650 | Looney | |
| 23888640 | 04h57m20.72s | −66d28m14.4s | 40650 | Looney | |
| 9531392 | 04h57m24.10s | −68d23m57.5s | 1406 | Armus | |
| 19151616 | 04h57m36.80s | −67d47m37.0s | 30869 | Kastner | |
| 23881728 | 04h57m42.00s | −66d26m34.4s | 40650 | Looney | |
| 10959872 | 04h57m43.30s | −70d08m50.3s | 3426 | Kastner | |
| 23885568 | 04h57m47.68s | −66d28m16.9s | 40650 | Looney | |
| 23881984 | 04h57m47.96s | −66d28m44.7s | 40650 | Looney | |
| 23890176 | 04h57m47.97s | −66d18m42.4s | 40650 | Looney | |
| 23881728 | 04h57m49.22s | −66d29m00.3s | 40650 | Looney | |
| 23881728 | 04h58m11.70s | −66d22m11.3s | 40650 | Looney | |
| 23894272 | 04h58m31.57s | −70d15m35.3s | 40650 | Looney | |
| 23881728 | 04h58m42.47s | −66d08m35.7s | 40650 | Looney | |
| 19010304 | 04h58m46.26s | −68d20m43.0s | 30788 | Sahai | |
| 23888640 | 04h58m51.63s | −66d09m44.6s | 40650 | Looney | |
| 23885568 | 04h58m54.30s | −66d07m18.9s | 40650 | Looney | |
| 27575552 | 04h58m56.37s | −68d48m04.28s | 485 | Ardila | |
| 25997056 | 04h59m07.39s | −65d43m13.3s | 50338 | Matsuura | |
| 23888640 | 04h59m44.28s | −65d38m01.2s | 40650 | Looney | |
| 4947968 | 05h00m00.15s | −70d27m40.5s | 103 | Houck | |
| 23888640 | 05h00m02.03s | −66d30m11.5s | 40650 | Looney | |
| 23888640 | 05h00m06.21s | −66d15m56.8s | 40650 | Looney | |
| 23881728 | 05h00m16.18s | −66d15m31.3s | 40650 | Looney | |
| 12930048 | 05h00m19.00s | −67d07m58.0s | 3505 | Wood | |
| 10960128 | 05h00m19.03s | −67d07m58.1s | 3426 | Kastner | |
| 19006464 | 05h00m32.27s | −72d09m02.0s | 30788 | Sahai | |
| 24325376 | 05h00m32.73s | −64d23m39.0s | 464 | Cohen | |
| 11196416 | 05h00m49.53s | −68d07m10.3s | 3578 | Misselt | |
| 23885568 | 05h00m51.45s | −66d23m59.9s | 40650 | Looney | |
| 10960384 | 05h01m00.86s | −67d35m23.6s | 3426 | Kastner | |
| 12929536 | 05h01m04.43s | −66d12m40.4s | 3505 | Wood | |
| 23893248 | 05h01m16.82s | −67d10m23.6s | 40650 | Looney | |
| 11196672 | 05h01m20.00s | −67d20m12.0s | 3578 | Misselt | |
| 11182592 | 05h01m30.00s | −68d10m42.0s | 3578 | Misselt | |
| 8569088 | 05h01m39.83s | −67d55m24.3s | 1402 | Armus | |
| 33287680 | 05h01m43.45s | −69d40m48.4s | 50092 | Gielen | |
| 7870976 | 05h01m44.84s | −66d45m55.04s | 667 | Houck | |
| 14700288 | 05h02m01.91s | −69d48m54.4s | 20443 | Stanghellini | |
| 9108224 | 05h02m06.84s | −66d45m46.3s | 1404 | Armus | |
| 9108736 | 05h02m07.39s | −71d20m13.1s | 1404 | Armus | 22454016 |
| 9857536 | 05h02m07.39s | −71d20m13.1s | 1408 | Armus | 22454016 |
| 11812096 | 05h02m07.39s | −71d20m13.1s | 1411 | Armus | 22454016 |
| 12003328 | 05h02m07.39s | −71d20m13.1s | 1412 | Armus | 22454016 |
| 12129792 | 05h02m07.39s | −71d20m13.1s | 1413 | Armus | 22454016 |
| 13050368 | 05h02m07.39s | −71d20m13.1s | 1417 | Armus | 22454016 |
| 13359872 | 05h02m07.39s | −71d20m13.1s | 1419 | Armus | 22454016 |
| 23886592 | 05h02m12.66s | −72d08m40.0s | 40650 | Looney | |
| 25991680 | 05h02m31.47s | −68d05m35.0s | 50338 | Matsuura | |
| 23889408 | 05h02m31.49s | −68d05m35.8s | 40650 | Looney | |
| 6939904 | 05h02m41.83s | −67d50m35.3s | 659 | Houck | |
| 7266304 | 05h02m41.83s | −67d50m35.20s | 663 | Houck | |
| 7266560 | 05h02m41.83s | −67d50m35.20s | 663 | Houck | |
| 7269632 | 05h02m41.83s | −67d50m35.3s | 663 | Houck | |
| 7449600 | 05h02m41.83s | −67d50m35.20s | 665 | Houck | |
| 8569088 | 05h02m41.83s | −67d50m35.3s | 1402 | Armus | |
| 11677696 | 05h02m41.83s | −67d50m35.20s | 1409 | Armus | |
| 7269632 | 05h02m50.83s | −67d45m45.3s | 663 | Houck | |
| 7870720 | 05h03m08.84s | −66d40m57.3s | 667 | Houck | |
| 7870976 | 05h03m08.84s | −66d40m57.3s | 667 | Houck | |

TABLE 5 — *Continued*

| AOR key IRS | RA (J2000) requested | Dec (J2000) requested | Proposal ID | PI | AOR key MIPS SED |
|---|---|---|---|---|---|
| 9107968 | 05h03m08.84s | −66d40m57.3s | 1404 | Armus | |
| 9108224 | 05h03m08.84s | −66d40m57.3s | 1404 | Armus | |
| 9108480 | 05h03m08.84s | −66d40m57.3s | 1404 | Armus | |
| 9760512 | 05h03m08.84s | −66d40m57.3s | 1407 | Armus | |
| 23895040 | 05h03m35.19s | −68d43m12.0s | 40650 | Looney | |
| 14700800 | 05h03m41.30s | −70d13m53.6s | 20443 | Stanghellini | |
| 14700544 | 05h03m42.64s | −70d06m47.8s | 20443 | Stanghellini | |
| 23890688 | 05h03m48.17s | −67d18m28.0s | 40650 | Looney | |
| 23889408 | 05h03m55.87s | −67d20m45.1s | 40650 | Looney | |
| 23889408 | 05h03m56.03s | −67d18m45.2s | 40650 | Looney | |
| 23890432 | 05h03m56.13s | −67d20m38.8s | 40650 | Looney | |
| 9108224 | 05h03m58.84s | −66d45m41.3s | 1404 | Armus | |
| 23889408 | 05h04m05.60s | −68d23m40.3s | 40650 | Looney | |
| 7870976 | 05h04m06.44s | −66d45m50.4s | 667 | Houck | |
| 23891712 | 05h04m08.12s | −68d43m26.4s | 40650 | Looney | |
| 6015488 | 05h04m14.10s | −67d16m16.0s | 200 | Houck | |
| 23887616 | 05h04m16.15s | −65d06m02.6s | 40650 | Looney | |
| 23886592 | 05h04m24.82s | −70d43m43.7s | 40650 | Looney | |
| 23895296 | 05h04m30.29s | −65d06m09.4s | 40650 | Looney | |
| 23881216 | 05h04m35.85s | −70d54m30.1s | 40650 | Looney | |
| 23881216 | 05h04m38.09s | −70d54m43.1s | 40650 | Looney | |
| 23881216 | 05h04m39.86s | −70d54m19.0s | 40650 | Looney | |
| 14701056 | 05h04m40.14s | −69d21m39.3s | 20443 | Stanghellini | |
| 10960640 | 05h04m47.14s | −66d40m30.4s | 3426 | Kastner | 22451456 |
| 7269632 | 05h04m50.83s | −67d45m45.3s | 663 | Houck | |
| 14701312 | 05h04m51.90s | −68d39m10.0s | 20443 | Stanghellini | 22450688 |
| 25991168 | 05h05m04.81s | −68d57m48.0s | 50338 | Matsuura | |
| 23893504 | 05h05m20.27s | −66d55m06.5s | 40650 | Looney | |
| 10960896 | 05h05m33.48s | −70d33m46.8s | 3426 | Kastner | |
| 23887872 | 05h05m46.23s | −69d26m12.3s | 40650 | Looney | |
| 23886336 | 05h06m01.35s | −71d13m01.3s | 40650 | Looney | |
| 19006720 | 05h06m03.67s | −69d03m58.0s | 30788 | Sahai | |
| 23883008 | 05h06m11.60s | −67d30m41.1s | 40650 | Looney | |
| 14701568 | 05h06m24.00s | −69d03m19.2s | 20443 | Stanghellini | |
| 6014976 | 05h06m27.40s | −68d12m04.0s | 200 | Houck | |
| 19005440 | 05h06m35.11s | −70d16m50.0s | 30788 | Sahai | |
| 25991936 | 05h07m18.33s | −69d07m42.0s | 50338 | Matsuura | |
| 14701824 | 05h07m54.90s | −66d57m46.1s | 20443 | Stanghellini | |
| 4948224 | 05h07m57.71s | −68d51m46.2s | 103 | Houck | 22450944 |
| 23882752 | 05h08m24.37s | −66d55m32.0s | 40650 | Looney | |
| 25990656 | 05h08m25.59s | −68d53m59.0s | 50338 | Matsuura | |
| 23894272 | 05h08m34.72s | −69d25m25.1s | 40650 | Looney | |
| 25992448 | 05h08m35.92s | −71d17m30.0s | 50338 | Matsuura | |
| 23106304 | 05h08m58.10s | −68d43m26.0s | 40604 | Reynolds | |
| 23106048 | 05h08m58.70s | −68d43m32.0s | 40604 | Reynolds | |
| 23891456 | 05h09m14.52s | −68d30m17.1s | 40650 | Looney | |
| 14702080 | 05h09m19.00s | −66d53m42.0s | 20443 | Stanghellini | |
| 23886592 | 05h09m41.94s | −71d27m42.1s | 40650 | Looney | |
| 23887872 | 05h09m49.11s | −68d52m30.6s | 40650 | Looney | |
| 23884288 | 05h09m50.53s | −68d53m05.5s | 40650 | Looney | |
| 23895040 | 05h09m52.26s | −68d53m27.3s | 40650 | Looney | |
| 23883008 | 05h09m52.73s | −68d53m00.7s | 40650 | Looney | |
| 23882752 | 05h09m53.89s | −68d53m36.7s | 40650 | Looney | |
| 23893248 | 05h09m54.63s | −68d49m47.2s | 40650 | Looney | |
| 10961152 | 05h10m00.00s | −69d56m9.6s | 3426 | Kastner | |
| 24324352 | 05h10m04.54s | −66d25m23.0s | 464 | Cohen | |
| 14702336 | 05h10m17.18s | −68d48m23.0s | 20443 | Stanghellini | |
| 10961408 | 05h10m19.63s | −69d49m51.2s | 3426 | Kastner | |
| 23884288 | 05h10m21.89s | −67d32m09.8s | 40650 | Looney | |
| 23887872 | 05h10m23.69s | −69d26m20.2s | 40650 | Looney | |
| 23895040 | 05h10m24.09s | −70d14m06.5s | 40650 | Looney | |
| 23888640 | 05h10m30.10s | −67d08m33.3s | 40650 | Looney | |
| 16604928 | 05h10m32.68s | −69d12m35.70s | 263 | Woodward | |
| 4949248 | 05h10m39.68s | −68d36m04.0s | 103 | Houck | 22449664 |
| 4948736 | 05h10m49.97s | −65d29m30.4s | 103 | Houck | |
| 23890432 | 05h11m07.74s | −65d37m07.9s | 40650 | Looney | |
| 23894528 | 05h11m07.74s | −65d37m07.9s | 40650 | Looney | |
| 12939008 | 05h11m10.47s | −67d52m10.5s | 3505 | Wood | |
| 25992704 | 05h11m10.65s | −66d12m53.0s | 50338 | Matsuura | |
| 12937984 | 05h11m13.89s | −67d36m16.1s | 3505 | Wood | |
| 12939264 | 05h11m19.52s | −68d42m27.9s | 3505 | Wood | |
| 12633600 | 05h11m23.78s | −70d01m56.5s | 103 | Houck | |
| 24324096 | 05h11m28.18s | −69d32m45.0s | 464 | Cohen | |
| 12937216 | 05h11m38.65s | −66d51m09.8s | 3505 | Wood | |
| 33292800 | 05h11m59.42s | −69d25m32.9s | 50092 | Gielen | |
| 6078464 | 05h12m00.82s | −70d32m24.0s | 1094 | Kemper | |

TABLE 5  — *Continued*

| AOR key IRS | RA (J2000) requested | Dec (J2000) requested | Proposal ID | PI | AOR key MIPS SED |
|---|---|---|---|---|---|
| 4949504 | 05h12m15.76s | −66d22m56.1s | 103 | Houck | |
| 23886336 | 05h12m17.33s | −70d27m18.4s | 40650 | Looney | |
| 23888640 | 05h12m29.69s | −67d09m18.6s | 40650 | Looney | |
| 19151360 | 05h12m30.17s | −70d24m22.0s | 30869 | Kastner | |
| 10961664 | 05h12m32.06s | −69d15m40.7s | 3426 | Kastner | |
| 12938752 | 05h12m51.07s | −69d37m50.3s | 3505 | Wood | |
| 23891712 | 05h12m59.82s | −69d34m36.9s | 40650 | Looney | |
| 6024192 | 05h13m04.60s | −64d51m40.0s | 200 | Houck | |
| 23895040 | 05h13m15.73s | −69d21m35.9s | 40650 | Looney | |
| 10961920 | 05h13m16.39s | −68d44m10s | 3426 | Kastner | |
| 23884288 | 05h13m17.69s | −69d22m25.0s | 40650 | Looney | |
| 23891712 | 05h13m18.26s | −69d21m35.5s | 40650 | Looney | |
| 23895040 | 05h13m19.14s | −69d21m51.0s | 40650 | Looney | |
| 3823616 | 05h13m19.80s | −69d22m15.0s | 18 | Houck | |
| 23883008 | 05h13m21.43s | −69d22m41.5s | 40650 | Looney | |
| 23883008 | 05h13m24.50s | −69d10m48.3s | 40650 | Looney | 22452992 |
| 10962176 | 05h13m24.67s | −69d10m48.4s | 3426 | Kastner | 22452992 |
| 23884288 | 05h13m25.09s | −69d22m45.1s | 40650 | Looney | |
| 33283328 | 05h13m33.74s | −66d34m19.2s | 50092 | Gielen | |
| 23891456 | 05h13m38.34s | −69d23m00.7s | 40650 | Looney | |
| 23887872 | 05h13m40.92s | −69d23m01.6s | 40650 | Looney | |
| 23895040 | 05h13m41.85s | −69d35m28.4s | 40650 | Looney | 22451712 |
| 10962432 | 05h13m42.48s | −69d35m21.8s | 3426 | Kastner | |
| 23887872 | 05h13m44.99s | −69d35m10.6s | 40650 | Looney | |
| 23894528 | 05h13m51.51s | −67d27m21.9s | 40650 | Looney | |
| 23891456 | 05h13m51.97s | −67d55m34.7s | 40650 | Looney | |
| 19149056 | 05h13m52.99s | −67d26m54.0s | 30869 | Kastner | |
| 23892736 | 05h13m54.06s | −67d20m18.9s | 40650 | Looney | |
| 27575808 | 05h13m54.40s | −69d31m46.09s | 485 | Ardila | |
| 23888384 | 05h13m59.84s | −67d22m51.4s | 40650 | Looney | |
| 11183616 | 05h14m04.42s | −67d15m50.5s | 3578 | Misselt | |
| 23893248 | 05h14m08.66s | −67d23m10.3s | 40650 | Looney | |
| 6016768 | 05h14m29.40s | −68d54m35.0s | 200 | Houck | |
| 23890432 | 05h14m45.43s | −67d12m04.2s | 40650 | Looney | |
| 10962688 | 05h14m49.75s | −67d27m19.8s | 3426 | Kastner | |
| 23894272 | 05h15m03.26s | −70d33m51.0s | 40650 | Looney | |
| 23893760 | 05h15m18.17s | −66d09m34.1s | 40650 | Looney | |
| 23892736 | 05h15m19.98s | −66d48m27.9s | 40650 | Looney | |
| 10962944 | 05h15m41.28s | −73d47m13.9s | 3426 | Kastner | |
| 24241920 | 05h15m44.15s | −67d58m52.5s | 40031 | Fazio | |
| 19149312 | 05h16m31.80s | −68d22m09.0s | 30869 | Kastner | |
| 23890432 | 05h16m54.05s | −67d20m05.1s | 40650 | Looney | |
| 23895296 | 05h17m07.26s | −65d59m33.5s | 40650 | Looney | |
| 17329920 | 05h17m11.94s | −70d46m58.0s | 30180 | Fazio | |
| 12938240 | 05h17m26.94s | −68d54m58.2s | 3505 | Wood | 22449920 |
| 23894528 | 05h17m28.44s | −66d43m07.0s | 40650 | Looney | |
| 23894528 | 05h17m30.66s | −66d43m37.4s | 40650 | Looney | |
| 19012096 | 05h17m32.82s | −68d20m41.0s | 30788 | Sahai | |
| 23891968 | 05h17m34.73s | −71d14m56.5s | 40650 | Looney | |
| 23889920 | 05h17m41.05s | −66d42m18.8s | 40650 | Looney | |
| 23887872 | 05h18m11.70s | −70d30m27.0s | 40650 | Looney | |
| 5030144 | 05h18m14.30s | −69d14m59.0s | 124 | Gehrz | |
| 7870464 | 05h18m14.30s | −69d14m59.0s | 667 | Houck | |
| 9107712 | 05h18m14.30s | −69d14m59.0s | 1404 | Armus | |
| 11812864 | 05h18m14.30s | −69d14m59.0s | 1411 | Armus | |
| 12004096 | 05h18m14.30s | −69d14m59.0s | 1412 | Armus | |
| 12130304 | 05h18m14.30s | −69d14m59.0s | 1413 | Armus | |
| 25996288 | 05h18m25.67s | −70d05m32.6s | 50338 | Matsuura | |
| 19011840 | 05h18m28.17s | −68d04m04.0s | 30788 | Sahai | |
| 23886336 | 05h18m48.36s | −69d33m34.7s | 40650 | Looney | |
| 12938496 | 05h18m56.26s | −67d45m04.4s | 3505 | Wood | |
| 23895040 | 05h19m03.42s | −69d38m12.9s | 40650 | Looney | |
| 23886336 | 05h19m05.93s | −69d38m41.2s | 40650 | Looney | |
| 23890944 | 05h19m06.69s | −68d21m37.4s | 40650 | Looney | |
| 19011584 | 05h19m06.80s | −68d21m36.0s | 30788 | Sahai | |
| 23891456 | 05h19m07.31s | −69d38m42.0s | 40650 | Looney | |
| 23887872 | 05h19m09.02s | −69d11m56.1s | 40650 | Looney | |
| 23884288 | 05h19m12.27s | −69d09m07.3s | 40650 | Looney | |
| 23891456 | 05h19m16.87s | −69d37m57.5s | 40650 | Looney | |
| 23891712 | 05h19m16.98s | −69d38m16.4s | 40650 | Looney | |
| 14702592 | 05h19m21.00s | −66d58m13.0s | 20443 | Stanghellini | |
| 14702848 | 05h19m29.72s | −68d51m09.1s | 20443 | Stanghellini | |
| 9753856 | 05h19m30.43s | −67d52m44.1s | 1407 | Armus | |
| 9753856 | 05h19m30.63s | −67d52m44.1s | 1407 | Armus | |
| 9753856 | 05h19m30.83s | −67d52m44.1s | 1407 | Armus | |
| 9753856 | 05h19m31.03s | −67d52m44.1s | 1407 | Armus | |

TABLE 5 — *Continued*

| AOR key IRS | RA (J2000) requested | Dec (J2000) requested | Proposal ID | PI | AOR key MIPS SED |
|---|---|---|---|---|---|
| 9753856 | 05h19m31.23s | −67d52m44.1s | 1407 | Armus | |
| 9753856 | 05h19m31.43s | −67d52m44.1s | 1407 | Armus | |
| 9753856 | 05h19m31.63s | −67d52m44.1s | 1407 | Armus | |
| 9753856 | 05h19m31.83s | −67d52m44.1s | 1407 | Armus | |
| 9753856 | 05h19m32.03s | −67d52m44.1s | 1407 | Armus | |
| 9753856 | 05h19m32.23s | −67d52m44.1s | 1407 | Armus | |
| 9753856 | 05h19m32.33s | −67d52m44.1s | 1407 | Armus | |
| 9753856 | 05h19m32.43s | −67d52m44.1s | 1407 | Armus | |
| 9753856 | 05h19m32.83s | −67d52m44.1s | 1407 | Armus | |
| 9753856 | 05h19m33.03s | −67d52m44.1s | 1407 | Armus | |
| 9753856 | 05h19m33.23s | −67d52m44.1s | 1407 | Armus | |
| 9753856 | 05h19m33.43s | −67d52m44.1s | 1407 | Armus | |
| 23894272 | 05h19m33.46s | −69d41m06.7s | 40650 | Looney | |
| 9753856 | 05h19m33.63s | −67d52m44.1s | 1407 | Armus | |
| 9753856 | 05h19m33.83s | −67d52m44.1s | 1407 | Armus | |
| 9753856 | 05h19m34.03s | −67d52m44.1s | 1407 | Armus | |
| 9753856 | 05h19m34.23s | −67d52m44.1s | 1407 | Armus | |
| 9753856 | 05h19m34.43s | −67d52m44.1s | 1407 | Armus | |
| 9753856 | 05h19m34.63s | −67d52m44.1s | 1407 | Armus | |
| 9753856 | 05h19m34.83s | −67d52m44.1s | 1407 | Armus | |
| 9753856 | 05h19m35.03s | −67d52m44.1s | 1407 | Armus | |
| 9753856 | 05h19m35.23s | −67d52m44.1s | 1407 | Armus | |
| 11183360 | 05h19m51.99s | −69d53m08.7s | 3578 | Misselt | |
| 25688064 | 05h19m53.34s | −69d27m33.4s | 50167 | Clayton | |
| 11217664 | 05h20m01.57s | −67d34m42.1s | 3583 | Onaka | |
| 11217920 | 05h20m01.57s | −67d34m42.1s | 3583 | Onaka | |
| 11218176 | 05h20m01.57s | −67d34m42.1s | 3583 | Onaka | |
| 11218432 | 05h20m01.57s | −67d34m42.1s | 3583 | Onaka | |
| 11218688 | 05h20m01.57s | −67d34m42.1s | 3583 | Onaka | |
| 11218944 | 05h20m01.57s | −67d34m42.1s | 3583 | Onaka | |
| 14703104 | 05h20m09.66s | −69d53m39.2s | 20443 | Stanghellini | |
| 23892736 | 05h20m11.56s | −68d37m53.7s | 40650 | Looney | |
| 23893760 | 05h20m11.96s | −66d52m38.9s | 40650 | Looney | |
| 23894528 | 05h20m16.71s | −66d52m54.1s | 40650 | Looney | |
| 12939520 | 05h20m19.38s | −66d35m47.8s | 3505 | Wood | |
| 25688320 | 05h20m23.69s | −69d33m26.6s | 50167 | Clayton | |
| 27985920 | 05h20m43.58s | −69d23m41.4s | 50338 | Matsuura | |
| 23893248 | 05h20m46.55s | −67d52m55.0s | 40650 | Looney | |
| 25990400 | 05h20m48.21s | −70d12m12.0s | 50338 | Matsuura | |
| 12937728 | 05h21m00.37s | −69d20m55.3s | 3505 | Wood | |
| 23885056 | 05h21m17.24s | −69d59m50.2s | 40650 | Looney | |
| 23888128 | 05h21m17.49s | −68d02m04.4s | 40650 | Looney | |
| 23891712 | 05h21m21.50s | −69d59m01.9s | 40650 | Looney | |
| 23890944 | 05h21m21.99s | −67d47m28.9s | 40650 | Looney | |
| 25996544 | 05h21m23.83s | −68d35m33.5s | 50338 | Matsuura | |
| 23895296 | 05h21m24.90s | −66d04m12.9s | 40650 | Looney | |
| 6076160 | 05h21m29.63s | −67d51m07.0s | 1094 | Kemper | 22451968 |
| 15902720 | 05h21m32.89s | −67d00m04.0s | 103 | Houck | |
| 23895296 | 05h21m33.20s | −65d29m20.8s | 40650 | Looney | |
| 23891712 | 05h21m33.23s | −69d40m19.9s | 40650 | Looney | |
| 23888128 | 05h21m41.84s | −67d53m24.0s | 40650 | Looney | |
| 23882752 | 05h21m47.09s | −67d56m56.8s | 40650 | Looney | |
| 23888128 | 05h21m55.18s | −67d47m30.4s | 40650 | Looney | |
| 23893760 | 05h21m56.97s | −67d57m00.1s | 40650 | Looney | |
| 8406528 | 05h21m57.73s | −68d06m35.3s | 1401 | Armus | |
| 3824128 | 05h22m01.30s | −67d57m47.00s | 18 | Houck | |
| 23890944 | 05h22m02.11s | −67d57m53.6s | 40650 | Looney | |
| 23882752 | 05h22m02.72s | −67d47m02.1s | 40650 | Looney | |
| 23882752 | 05h22m03.30s | −67d57m47.0s | 40650 | Looney | |
| 23882752 | 05h22m04.85s | −67d58m00.3s | 40650 | Looney | |
| 23893760 | 05h22m07.27s | −67d58m19.7s | 40650 | Looney | |
| 23888128 | 05h22m08.77s | −67d53m24.9s | 40650 | Looney | |
| 23888384 | 05h22m10.08s | −67d34m59.6s | 40650 | Looney | |
| 23882496 | 05h22m12.57s | −67d58m32.4s | 40650 | Looney | |
| 23892224 | 05h22m16.87s | −68d04m03.9s | 40650 | Looney | |
| 23892992 | 05h22m19.69s | −68d04m37.4s | 40650 | Looney | |
| 23887616 | 05h22m19.71s | −65d43m19.0s | 40650 | Looney | |
| 33284352 | 05h22m21.13s | −65d55m51.6s | 50092 | Gielen | |
| 23886592 | 05h22m22.46s | −71d35m32.2s | 40650 | Looney | |
| 23895040 | 05h22m24.89s | −69d42m32.8s | 40650 | Looney | |
| 23892224 | 05h22m27.70s | −67d54m12.8s | 40650 | Looney | |
| 23888128 | 05h22m28.98s | −67d53m39.3s | 40650 | Looney | |
| 23892224 | 05h22m31.72s | −68d03m19.2s | 40650 | Looney | |
| 23888128 | 05h22m32.65s | −68d03m01.7s | 40650 | Looney | |
| 23888128 | 05h22m41.97s | −67d55m00.5s | 40650 | Looney | |
| 12937472 | 05h22m44.00s | −69d38m28.1s | 3505 | Wood | |

F. Kemper et al.

TABLE 5 — *Continued*

| AOR key IRS | RA (J2000) requested | Dec (J2000) requested | Proposal ID | PI | AOR key MIPS SED |
|---|---|---|---|---|---|
| 23885312 | 05h22m45.13s | −71d36m10.2s | 40650 | Looney | |
| 23892224 | 05h22m49.13s | −68d01m29.1s | 40650 | Looney | |
| 23894528 | 05h22m49.88s | −66d40m56.1s | 40650 | Looney | |
| 23887872 | 05h22m53.27s | −69d51m11.1s | 40650 | Looney | |
| 23890944 | 05h22m55.12s | −68d04m09.4s | 40650 | Looney | |
| 23892736 | 05h22m56.79s | −68d04m06.8s | 40650 | Looney | |
| 8406528 | 05h22m59.73s | −68d01m46.3s | 1401 | Armus | |
| 8406784 | 05h22m59.73s | −68d01m46.3s | 1401 | Armus | |
| 23893760 | 05h23m08.60s | −68d00m06.5s | 40650 | Looney | |
| 12936960 | 05h23m09.11s | −69d17m49.1s | 3505 | Wood | |
| 23882752 | 05h23m15.18s | −68d00m17.1s | 40650 | Looney | |
| 23888128 | 05h23m31.37s | −68d01m08.0s | 40650 | Looney | |
| 23891456 | 05h23m33.40s | −69d37m12.2s | 40650 | Looney | |
| 23890944 | 05h23m35.54s | −67d52m35.6s | 40650 | Looney | |
| 23885056 | 05h23m37.88s | −69d38m54.4s | 40650 | Looney | |
| 19007488 | 05h23m38.33s | −66d53m24.0s | 30788 | Sahai | |
| 23892992 | 05h23m43.48s | −68d00m33.9s | 40650 | Looney | |
| 10963200 | 05h23m43.63s | −65d41m59.6s | 3426 | Kastner | |
| 23890944 | 05h23m50.04s | −67d57m19.6s | 40650 | Looney | |
| 6014464 | 05h24m07.02s | −69d23m36.9s | 200 | Houck | |
| 6076928 | 05h24m19.35s | −69d38m50.0s | 1094 | Kemper | |
| 4950784 | 05h24m20.86s | −70d05m00.5s | 103 | Houck | |
| 23891456 | 05h24m23.39s | −69d39m04.7s | 40650 | Looney | |
| 12633856 | 05h24m36.02s | −73d40m39.4s | 103 | Houck | |
| 9532160 | 05h24m36.60s | −73d40m46.0s | 1406 | Armus | |
| 12936448 | 05h24m38.62s | −70d23m57.1s | 3505 | Wood | |
| 19007232 | 05h24m43.69s | −71d47m26.0s | 30788 | Sahai | |
| 18143488 | 05h24m54.93s | −69d38m24.1s | 30372 | Tappe | |
| 4951040 | 05h24m55.04s | −71d32m55.4s | 103 | Houck | 22451200 |
| 18143488 | 05h25m03.02s | −69d38m12.4s | 30372 | Tappe | |
| 23882496 | 05h25m04.10s | −68d28m24.5s | 40650 | Looney | |
| 18143488 | 05h25m05.56s | −69d38m13.5s | 30372 | Tappe | |
| 12935936 | 05h25m05.69s | −70d10m10.6s | 3505 | Wood | |
| 11019776 | 05h25m07.26s | −69d38m54.1s | 3483 | Rho | |
| 18143488 | 05h25m07.31s | −69d39m04.8s | 30372 | Tappe | |
| 10963456 | 05h25m19.51s | −71d04m02.6s | 3426 | Kastner | |
| 25996032 | 05h25m20.75s | −70d50m07.3s | 50338 | Matsuura | |
| 23893760 | 05h25m21.16s | −67d29m37.6s | 40650 | Looney | |
| 23885056 | 05h25m31.03s | −70d26m34.5s | 40650 | Looney | |
| 23886336 | 05h25m40.63s | −70d08m27.2s | 40650 | Looney | |
| 23892224 | 05h25m41.54s | −66d15m28.6s | 40650 | Looney | |
| 11184128 | 05h25m42.00s | −66d15m00.0s | 3578 | Misselt | |
| 25687552 | 05h25m44.95s | −69d04m48.9s | 50167 | Clayton | |
| 10963712 | 05h25m49.25s | −66d15m8.3s | 3426 | Kastner | |
| 23894528 | 05h25m49.27s | −66d15m08.7s | 40650 | Looney | |
| 25992192 | 05h25m51.85s | −68d46m34.0s | 50338 | Matsuura | |
| 11239680 | 05h26m01.08s | −66d16m19.1s | 3591 | Kemper | |
| 23895552 | 05h26m01.20s | −67d30m12.1s | 40650 | Looney | 22458368 |
| 6586112 | 05h26m01.56s | −66d05m03.8s | 124 | Gehrz | 22454272 |
| 27576064 | 05h26m03.94s | −67d29m56.98s | 485 | Ardila | |
| 23891712 | 05h26m05.26s | −68d36m09.3s | 40650 | Looney | |
| 10963968 | 05h26m11.38s | −66d12m10.8s | 3426 | Kastner | |
| 18144000 | 05h26m16.70s | −69d35m08.8s | 30372 | Tappe | |
| 18143488 | 05h26m18.56s | −69d34m44.3s | 30372 | Tappe | |
| 18144000 | 05h26m18.56s | −69d34m44.3s | 30372 | Tappe | |
| 6023424 | 05h26m19.40s | −69d41m39.0s | 200 | Houck | |
| 6023425 | 05h26m19.40s | −69d41m24.00s | 200 | Houck | |
| 6586112 | 05h26m21.56s | −66d04m53.8s | 124 | Gehrz | |
| 23887872 | 05h26m21.74s | −68d39m59.1s | 40650 | Looney | |
| 11239680 | 05h26m22.18s | −66d21m28.5s | 3591 | Kemper | |
| 11238912 | 05h26m23.10s | −69d11m20.3s | 3591 | Kemper | |
| 17741312 | 05h26m24.52s | −71d11m11.8s | 30077 | Evans | |
| 23885056 | 05h26m29.01s | −69d17m56.1s | 40650 | Looney | |
| 23892224 | 05h26m29.60s | −67d41m44.7s | 40650 | Looney | |
| 23888384 | 05h26m30.65s | −67d40m36.7s | 40650 | Looney | 22455296 |
| 19007744 | 05h26m30.69s | −67d40m36.0s | 30788 | Sahai | 22455296 |
| 10964224 | 05h26m34.80s | −68d51m40s | 3426 | Kastner | |
| 11238912 | 05h26m35.70s | −69d08m22.7s | 3591 | Kemper | |
| 23895552 | 05h26m38.55s | −67d39m23.2s | 40650 | Looney | |
| 6021632 | 05h26m40.40s | −69d23m11.0s | 200 | Houck | |
| 24324864 | 05h26m41.14s | −72d56m57.0s | 464 | Cohen | |
| 23884288 | 05h26m46.61s | −68d48m47.2s | 40650 | Looney | |
| 12935424 | 05h26m50.83s | −69d31m36.9s | 3505 | Wood | |
| 6023680 | 05h27m04.30s | −69d38m17.0s | 200 | Houck | |
| 11239680 | 05h27m17.84s | −66d22m05.6s | 3591 | Kemper | |
| 6022144 | 05h27m18.00s | −69d36m25.0s | 200 | Houck | |

TABLE 5 — *Continued*

| AOR key IRS | RA (J2000) requested | Dec (J2000) requested | Proposal ID | PI | AOR key MIPS SED |
|---|---|---|---|---|---|
| 12932864 | 05h27m24.12s | −69d39m45.0s | 3505 | Wood | |
| 11239680 | 05h27m34.35s | −66d53m30.0s | 3591 | Kemper | |
| 23888384 | 05h27m36.93s | −67d27m28.6s | 40650 | Looney | |
| 6077952 | 05h27m40.22s | −69d08m04.6s | 1094 | Kemper | 22454528 |
| 23889920 | 05h27m43.47s | −67d26m24.2s | 40650 | Looney | |
| 23891968 | 05h27m49.05s | −72d53m15.7s | 40650 | Looney | |
| 23888384 | 05h27m57.09s | −67d25m22.3s | 40650 | Looney | |
| 23890944 | 05h27m58.18s | −66d34m05.0s | 40650 | Looney | |
| 23895552 | 05h28m03.20s | −67d25m25.6s | 40650 | Looney | |
| 23883264 | 05h28m04.78s | −68d59m47.2s | 40650 | Looney | |
| 11238912 | 05h28m04.83s | −68d59m47.2s | 3591 | Kemper | |
| 6021120 | 05h28m06.20s | −69d32m29.0s | 200 | Houck | |
| 12932352 | 05h28m11.48s | −70d33m58.7s | 3505 | Wood | |
| 19151104 | 05h28m22.20s | −69d08m33.0s | 30869 | Kastner | |
| 6021376 | 05h28m26.20s | −69d14m43.0s | 200 | Houck | |
| 10964480 | 05h28m28.87s | −68d07m08s | 3426 | Kastner | |
| 6020864 | 05h28m33.30s | −69d29m54.0s | 200 | Houck | |
| 6014208 | 05h28m36.70s | −69d20m05.0s | 200 | Houck | |
| 12933888 | 05h28m40.17s | −66d13m54.2s | 3505 | Wood | |
| 14703616 | 05h28m41.20s | −67d33m39.0s | 20443 | Stanghellini | |
| 23888128 | 05h28m42.10s | −66d28m01.0s | 40650 | Looney | |
| 23888384 | 05h28m42.10s | −66d28m01.0s | 40650 | Looney | |
| 23889920 | 05h28m42.10s | −66d28m01.0s | 40650 | Looney | |
| 23892224 | 05h28m42.10s | −66d28m01.0s | 40650 | Looney | |
| 23895552 | 05h28m42.10s | −66d28m01.0s | 40650 | Looney | |
| 12933376 | 05h28m44.50s | −66d14m04.0s | 3505 | Wood | |
| 12935168 | 05h28m44.50s | −66d14m04.0s | 3505 | Wood | |
| 12929024 | 05h28m46.62s | −71d19m12.5s | 3505 | Wood | |
| 12934400 | 05h28m47.20s | −66d14m14.2s | 3505 | Wood | |
| 10964992 | 05h28m48.14s | −71d02m28.7s | 3426 | Kastner | |
| 12931840 | 05h28m48.62s | −69d48m01.3s | 3505 | Wood | |
| 23882496 | 05h28m58.76s | −66d35m27.6s | 40650 | Looney | |
| 6016256 | 05h29m00.00s | −67d45m01.0s | 200 | Houck | |
| 11184384 | 05h29m00.00s | −66d39m00.0s | 3578 | Misselt | |
| 17399552 | 05h29m00.00s | −67d45m01.0s | 30332 | Houck | |
| 11239680 | 05h29m02.41s | −66d15m27.8s | 3591 | Kemper | |
| 6014720 | 05h29m03.00s | −69d48m09.0s | 200 | Houck | |
| 11238912 | 05h29m03.48s | −69d06m46.2s | 3591 | Kemper | |
| 12929280 | 05h29m07.60s | −66d58m15.0s | 3505 | Wood | 22450176 |
| 23885312 | 05h29m37.89s | −72d49m52.9s | 40650 | Looney | |
| 10965248 | 05h29m42.24s | −68d57m17.3s | 3426 | Kastner | |
| 6024704 | 05h30m04.20s | −66d49m23.0s | 200 | Houck | |
| 19005696 | 05h30m05.55s | −70d30m34.0s | 30788 | Sahai | |
| 11238912 | 05h30m10.32s | −69d09m33.8s | 3591 | Kemper | |
| 23884032 | 05h30m10.33s | −69d09m33.9s | 40650 | Looney | |
| 23894784 | 05h30m20.32s | −71d07m48.9s | 40650 | Looney | |
| 10965504 | 05h30m20.66s | −66d53m01.7s | 3426 | Kastner | |
| 23894784 | 05h30m20.79s | −71d07m38.6s | 40650 | Looney | |
| 23884032 | 05h30m23.18s | −71d05m56.3s | 40650 | Looney | |
| 14703872 | 05h30m33.22s | −70d44m38.4s | 20443 | Stanghellini | |
| 6021888 | 05h30m40.90s | −69d59m03.0s | 200 | Houck | |
| 14704128 | 05h30m45.98s | −70d50m16.4s | 20443 | Stanghellini | |
| 19150336 | 05h30m47.88s | −71d07m55.0s | 30869 | Kastner | |
| 9532416 | 05h30m51.48s | −69d02m58.6s | 1406 | Armus | |
| 10065920 | 05h30m51.48s | −69d02m58.6s | 1410 | Armus | |
| 11183104 | 05h30m54.00s | −66d53m12.0s | 3578 | Misselt | |
| 23882496 | 05h30m54.24s | −68d34m28.3s | 40650 | Looney | |
| 23888384 | 05h30m55.56s | −67d20m06.2s | 40650 | Looney | |
| 10965760 | 05h31m04.15s | −69d19m3.3s | 3426 | Kastner | |
| 11239680 | 05h31m10.65s | −66d35m31.6s | 3591 | Kemper | |
| 11239680 | 05h31m13.12s | −66d09m41.2s | 3591 | Kemper | |
| 23891968 | 05h31m22.85s | −71d04m09.9s | 40650 | Looney | |
| 10966016 | 05h31m36.82s | −66d30m7.9s | 3426 | Kastner | |
| 11238912 | 05h31m40.90s | −69d39m19.8s | 3591 | Kemper | |
| 10966272 | 05h31m42.41s | −68d34m53.7s | 3426 | Kastner | |
| 23884800 | 05h31m42.44s | −68d34m54.3s | 40650 | Looney | |
| 24241920 | 05h31m48.61s | −68d30m23.5s | 40031 | Fazio | |
| 23892992 | 05h31m54.43s | −68d26m40.6s | 40650 | Looney | |
| 11239680 | 05h31m59.34s | −66d38m38.6s | 3591 | Kemper | |
| 11238912 | 05h32m03.31s | −69d17m30.4s | 3591 | Kemper | |
| 23882496 | 05h32m03.43s | −67d42m25.7s | 40650 | Looney | |
| 23889920 | 05h32m03.82s | −67d42m56.8s | 40650 | Looney | |
| 23885312 | 05h32m07.82s | −71d13m36.4s | 40650 | Looney | |
| 23886848 | 05h32m14.97s | −71d13m23.9s | 40650 | Looney | |
| 23895552 | 05h32m17.49s | −67d41m55.6s | 40650 | Looney | |
| 23885056 | 05h32m24.97s | −68d39m04.1s | 40650 | Looney | |

F. Kemper et al.

TABLE 5 — *Continued*

| AOR key IRS | RA (J2000) requested | Dec (J2000) requested | Proposal ID | PI | AOR key MIPS SED |
|---|---|---|---|---|---|
| 23890944 | 05h32m27.42s | −67d41m32.9s | 40650 | Looney | |
| 10966528 | 05h32m31.99s | −66d27m15.1s | 3426 | Kastner | 22452224 |
| 23889920 | 05h32m32.06s | −66d27m15.2s | 40650 | Looney | 22452224 |
| 6015744 | 05h32m35.62s | −67d55m09.0s | 200 | Houck | |
| 10966784 | 05h32m37.15s | −67d06m56.5s | 3426 | Kastner | |
| 12931328 | 05h32m38.59s | −68d25m22.2s | 3505 | Wood | 22452480 |
| 23885056 | 05h32m44.25s | −69d30m05.7s | 40650 | Looney | 22459904 |
| 17400576 | 05h32m46.48s | −67d06m51.0s | 30345 | Houck | |
| 23890944 | 05h32m51.50s | −67d40m59.4s | 40650 | Looney | |
| 6023168 | 05h32m51.60s | −67d06m51.0s | 200 | Houck | 22449152 |
| 17400320 | 05h32m51.60s | −67d06m51.0s | 30345 | Houck | 22449152 |
| 23892992 | 05h32m52.29s | −67d41m09.0s | 40650 | Looney | |
| 23883520 | 05h32m52.46s | −69d46m18.6s | 40650 | Looney | |
| 10967040 | 05h32m52.68s | −69d46m22.8s | 3426 | Kastner | |
| 11238912 | 05h32m55.47s | −69d20m26.6s | 3591 | Kemper | 22455552 |
| 10967296 | 05h32m56.18s | −68d12m49s | 3426 | Kastner | |
| 6016000 | 05h32m59.40s | −70d41m25.0s | 200 | Houck | |
| 25993216 | 05h33m06.80s | −70d30m34.0s | 50338 | Matsuura | |
| 25993472 | 05h33m06.80s | −70d31m04.0s | 50338 | Matsuura | |
| 25993728 | 05h33m06.80s | −70d30m04.0s | 50338 | Matsuura | |
| 11238912 | 05h33m11.02s | −68d58m20.5s | 3591 | Kemper | |
| 27985408 | 05h33m36.07s | −69d23m12.7s | 50338 | Matsuura | |
| 23892992 | 05h33m42.15s | −68d46m02.8s | 40650 | Looney | |
| 25993984 | 05h33m46.99s | −68d36m44.0s | 50338 | Matsuura | |
| 25994240 | 05h33m46.99s | −68d37m31.0s | 50338 | Matsuura | |
| 25994496 | 05h33m46.99s | −68d36m11.0s | 50338 | Matsuura | |
| 18144512 | 05h33m48.94s | −70d13m23.0s | 30380 | Clayton | 22454784 |
| 4951296 | 05h33m56.17s | −67d53m08.3s | 103 | Houck | |
| 14704384 | 05h34m08.76s | −74d20m06.6s | 20443 | Stanghellini | |
| 23888384 | 05h34m10.23s | −67d25m29.4s | 40650 | Looney | |
| 5056512 | 05h34m14.20s | −69d47m21.0s | 129 | Gehrz | |
| 6024448 | 05h34m16.10s | −70d22m53.0s | 200 | Houck | |
| 15902208 | 05h34m21.27s | −68d58m24.0s | 103 | Houck | |
| 23886080 | 05h34m31.46s | −68d35m13.9s | 40650 | Looney | |
| 23892992 | 05h34m36.26s | −66d47m49.7s | 40650 | Looney | |
| 14704640 | 05h34m38.87s | −70d19m56.9s | 20443 | Stanghellini | |
| 11238912 | 05h34m53.67s | −68d46m39.6s | 3591 | Kemper | |
| 12930816 | 05h34m53.74s | −70d29m24.8s | 3505 | Wood | |
| 33293568 | 05h34m53.77s | −69d08m02.1s | 50092 | Gielen | |
| 11238912 | 05h34m56.21s | −69d09m16.5s | 3591 | Kemper | |
| 11239424 | 05h35m03.55s | −69d52m45.5s | 3591 | Kemper | |
| 10967552 | 05h35m14.09s | −67d43m55.6s | 3426 | Kastner | |
| 8082688 | 05h35m18.50s | −67d23m03.0s | 667 | Houck | |
| 11239424 | 05h35m20.00s | −69d48m45.9s | 3591 | Kemper | |
| 14704896 | 05h35m20.92s | −73d55m30.1s | 20443 | Stanghellini | |
| 23890944 | 05h35m24.05s | −67d34m55.6s | 40650 | Looney | |
| 11238912 | 05h35m24.52s | −69d04m03.4s | 3591 | Kemper | |
| 17719552 | 05h35m25.43s | −69d16m28.7s | 30067 | Dwek | |
| 17720832 | 05h35m25.43s | −69d16m28.7s | 30067 | Dwek | |
| 22392576 | 05h35m25.43s | −69d16m28.7s | 40149 | Dwek | |
| 22393856 | 05h35m25.43s | −69d16m28.7s | 40149 | Dwek | |
| 19008256 | 05h35m25.84s | −71d19m56.0s | 30788 | Sahai | 22455808 |
| 12930560 | 05h35m26.86s | −69d52m27.9s | 3505 | Wood | |
| 5031168 | 05h35m28.01s | −69d16m11.6s | 124 | Gehrz | |
| 13983232 | 05h35m28.01s | −69d16m10.9s | 20080 | Polomski | |
| 17719552 | 05h35m28.01s | −69d16m10.9s | 30067 | Dwek | |
| 17720832 | 05h35m28.01s | −69d16m10.9s | 30067 | Dwek | |
| 22392576 | 05h35m28.01s | −69d16m10.9s | 40149 | Dwek | |
| 22393856 | 05h35m28.01s | −69d16m10.9s | 40149 | Dwek | |
| 26172160 | 05h35m28.01s | −69d16m10.9s | 50444 | Dwek | |
| 10967808 | 05h35m28.32s | −66d56m2.4s | 3426 | Kastner | |
| 23887360 | 05h35m36.88s | −69d12m14.1s | 40650 | Looney | |
| 19008512 | 05h35m39.72s | −65d19m56.0s | 30788 | Sahai | |
| 10968064 | 05h35m41.14s | −69d11m59.6s | 3426 | Kastner | |
| 23887360 | 05h35m54.36s | −69d38m48.1s | 40650 | Looney | |
| 23891200 | 05h35m54.94s | −69d39m03.0s | 40650 | Looney | |
| 11238912 | 05h35m55.23s | −69d09m59.5s | 3591 | Kemper | |
| 12936704 | 05h36m01.24s | −66d46m39.7s | 3505 | Wood | |
| 11182848 | 05h36m03.81s | −69d01m29.8s | 3578 | Misselt | |
| 33291520 | 05h36m05.88s | −69d58m02.6s | 50092 | Gielen | |
| 23886080 | 05h36m15.84s | −69d31m51.5s | 40650 | Looney | |
| 7571200 | 05h36m20.50s | −67d18m14.0s | 662 | Houck | |
| 7857664 | 05h36m20.50s | −67d18m14.0s | 665 | Houck | |
| 8082688 | 05h36m20.50s | −67d18m14.0s | 667 | Houck | |
| 9189376 | 05h36m20.50s | −67d18m14.0s | 1404 | Armus | |
| 19008000 | 05h36m24.13s | −72d41m32.0s | 30788 | Sahai | |

TABLE 5  — *Continued*

| AOR key IRS | RA (J2000) requested | Dec (J2000) requested | Proposal ID | PI | AOR key MIPS SED |
|---|---|---|---|---|---|
| 10968320 | 05h36m25.87s | −69d22m55.9s | 3426 | Kastner | 22455040 |
| 23883520 | 05h36m30.81s | −69d18m17.2s | 40650 | Looney | |
| 11238912 | 05h36m30.82s | −69d18m17.2s | 3591 | Kemper | |
| 12930304 | 05h36m36.71s | −69d47m22.6s | 3505 | Wood | |
| 23889152 | 05h36m42.42s | −70d07m46.7s | 40650 | Looney | |
| 27576320 | 05h36m43.50s | −69d29m44.99s | 485 | Ardila | |
| 11238912 | 05h36m51.20s | −69d13m35.9s | 3591 | Kemper | |
| 23887104 | 05h37m04.78s | −66d22m07.2s | 40650 | Looney | |
| 8082688 | 05h37m10.50s | −67d22m58.0s | 667 | Houck | |
| 23885824 | 05h37m16.29s | −66d26m54.7s | 40650 | Looney | |
| 11238912 | 05h37m28.07s | −69d08m48.0s | 3591 | Kemper | 22452736 |
| 11239424 | 05h37m28.07s | −69d08m48.0s | 3591 | Kemper | 22452736 |
| 23885056 | 05h37m46.08s | −69d10m50.3s | 40650 | Looney | |
| 12081152 | 05h37m50.36s | −69d11m07.1s | 63 | Houck | |
| 23886080 | 05h37m54.82s | −69d34m35.8s | 40650 | Looney | |
| 12081152 | 05h38m00.00s | −69d10m30.0s | 63 | Houck | |
| 23892480 | 05h38m05.65s | −69d09m09.7s | 40650 | Looney | |
| 11239424 | 05h38m16.01s | −69d10m11.2s | 3591 | Kemper | |
| 11239424 | 05h38m20.23s | −69d37m32.4s | 3591 | Kemper | |
| 12081408 | 05h38m30.13s | −69d06m25.1s | 63 | Houck | |
| 12081152 | 05h38m31.58s | −69d02m14.4s | 63 | Houck | |
| 10968576 | 05h38m31.63s | −69d02m14.6s | 3426 | Kastner | |
| 6076416 | 05h38m33.96s | −69d20m31.6s | 1094 | Kemper | |
| 12081152 | 05h38m34.01s | −69d04m52.1s | 63 | Houck | |
| 12081152 | 05h38m34.58s | −69d05m57.5s | 63 | Houck | |
| 12081408 | 05h38m38.44s | −69d06m31.0s | 63 | Houck | |
| 23894016 | 05h38m39.23s | −69d05m52.2s | 40650 | Looney | |
| 23883520 | 05h38m39.69s | −69d05m38.2s | 40650 | Looney | |
| 12081408 | 05h38m42.43s | −69d06m02.2s | 63 | Houck | |
| 10968832 | 05h38m44.71s | −69d24m39.6s | 3426 | Kastner | 22460672 |
| 23883520 | 05h38m45.15s | −69d05m07.9s | 40650 | Looney | |
| 12081152 | 05h38m46.93s | −69d05m02.5s | 63 | Houck | |
| 12081152 | 05h38m47.99s | −69d04m42.9s | 63 | Houck | |
| 12081408 | 05h38m48.11s | −69d04m12.2s | 63 | Houck | |
| 12081152 | 05h38m48.41s | −69d05m32.9s | 63 | Houck | |
| 23883520 | 05h38m49.27s | −69d04m44.4s | 40650 | Looney | |
| 11239424 | 05h38m49.33s | −69d27m06.5s | 3591 | Kemper | |
| 12081408 | 05h38m49.76s | −69d06m43.1s | 63 | Houck | |
| 4382720 | 05h38m50.70s | −69d04m15.0s | 63 | Houck | |
| 23894016 | 05h38m52.67s | −69d04m37.5s | 40650 | Looney | |
| 23887360 | 05h38m53.88s | −69d09m31.3s | 40650 | Looney | |
| 12081152 | 05h38m56.47s | −69d04m16.7s | 63 | Houck | |
| 23886080 | 05h38m58.42s | −69d04m34.7s | 40650 | Looney | |
| 12081408 | 05h39m01.30s | −69d04m00.5s | 63 | Houck | |
| 12081408 | 05h39m03.80s | −69d08m06.5s | 63 | Houck | |
| 23892480 | 05h39m04.42s | −69d04m13.9s | 40650 | Looney | |
| 23887360 | 05h39m04.88s | −69d29m49.9s | 40650 | Looney | |
| 23883264 | 05h39m06.31s | −69d30m43.8s | 40650 | Looney | |
| 25995776 | 05h39m11.60s | −69d31m25.6s | 50338 | Matsuura | |
| 27985152 | 05h39m11.60s | −69d31m00.0s | 50338 | Matsuura | |
| 23883520 | 05h39m15.77s | −69d30m39.9s | 40650 | Looney | |
| 10969088 | 05h39m15.86s | −69d30m38.5s | 3426 | Kastner | |
| 23892480 | 05h39m29.21s | −69d47m19.0s | 40650 | Looney | |
| 23883520 | 05h39m31.19s | −70d12m16.9s | 40650 | Looney | |
| 11239424 | 05h39m32.34s | −69d34m50.1s | 3591 | Kemper | |
| 23887360 | 05h39m35.99s | −69d46m04.1s | 40650 | Looney | |
| 23894016 | 05h39m37.04s | −69d45m36.7s | 40650 | Looney | |
| 23883520 | 05h39m37.53s | −69d46m09.8s | 40650 | Looney | |
| 23883520 | 05h39m37.60s | −69d45m25.0s | 40650 | Looney | |
| 23883520 | 05h39m38.73s | −69d39m04.3s | 40650 | Looney | |
| 23883520 | 05h39m39.02s | −69d39m11.4s | 40650 | Looney | |
| 23886080 | 05h39m39.15s | −69d17m54.6s | 40650 | Looney | |
| 27984896 | 05h39m41.00s | −69d29m0.0s | 50338 | Matsuura | |
| 27986176 | 05h39m41.08s | −69d29m16.7s | 50338 | Matsuura | |
| 23884800 | 05h39m41.89s | −69d46m12.0s | 40650 | Looney | 22453248 |
| 12548352 | 05h39m41.96s | −69d46m11.9s | 124 | Gehrz | 22453248 |
| 23884800 | 05h39m43.26s | −69d38m54.6s | 40650 | Looney | |
| 23884800 | 05h39m43.82s | −69d38m34.0s | 40650 | Looney | |
| 3823872 | 05h39m44.00s | −69d38m48.0s | 18 | Houck | |
| 23884800 | 05h39m44.33s | −69d38m47.5s | 40650 | Looney | |
| 6020608 | 05h39m44.89s | −69d55m18.1s | 200 | Houck | |
| 25648640 | 05h39m44.89s | −69d55m18.1s | 50147 | Sloan | |
| 25648896 | 05h39m44.89s | −69d55m38.1s | 50147 | Sloan | |
| 23892480 | 05h39m45.18s | −69d44m50.4s | 40650 | Looney | |
| 23884800 | 05h39m45.94s | −69d38m39.2s | 40650 | Looney | |
| 8242944 | 05h39m46.10s | −69d38m36.0s | 1401 | Armus | |

F. Kemper et al.

TABLE 5  — *Continued*

| AOR key IRS | RA (J2000) requested | Dec (J2000) requested | Proposal ID | PI | AOR key MIPS SED |
|---|---|---|---|---|---|
| 8568832 | 05h39m46.10s | −69d38m36.0s | 1402 | Armus | |
| 8579328 | 05h39m46.10s | −69d38m36.0s | 1402 | Armus | |
| 11812352 | 05h39m46.10s | −69d38m36.0s | 1411 | Armus | |
| 12003584 | 05h39m46.10s | −69d38m36.0s | 1412 | Armus | |
| 12130048 | 05h39m46.10s | −69d38m36.0s | 1413 | Armus | |
| 12606208 | 05h39m46.10s | −69d38m36.0s | 1415 | Armus | |
| 12902656 | 05h39m46.10s | −69d38m36.0s | 1416 | Armus | |
| 13048576 | 05h39m46.10s | −69d38m36.0s | 1417 | Armus | |
| 13162752 | 05h39m46.10s | −69d38m36.0s | 1418 | Armus | |
| 13358336 | 05h39m46.10s | −69d38m36.0s | 1419 | Armus | |
| 13529088 | 05h39m46.10s | −69d38m36.0s | 1420 | Armus | |
| 15672064 | 05h39m46.10s | −69d38m36.0s | 1423 | Armus | |
| 16295936 | 05h39m46.10s | −69d38m36.0s | 1426 | Armus | |
| 16702976 | 05h39m46.10s | −69d38m36.0s | 1429 | Armus | |
| 23892480 | 05h39m51.60s | −69d45m10.5s | 40650 | Looney | |
| 11239424 | 05h39m51.85s | −70d01m17.0s | 3591 | Kemper | |
| 23885312 | 05h39m52.11s | −71d09m30.7s | 40650 | Looney | |
| 23892480 | 05h39m52.29s | −69d45m16.5s | 40650 | Looney | |
| 23891968 | 05h39m53.43s | −71d09m53.1s | 40650 | Looney | |
| 23891968 | 05h39m55.66s | −71d10m00.9s | 40650 | Looney | |
| 23891968 | 05h39m58.39s | −71d10m05.5s | 40650 | Looney | |
| 23891968 | 05h39m58.52s | −71d10m14.6s | 40650 | Looney | |
| 23884800 | 05h39m59.34s | −69d45m26.3s | 40650 | Looney | |
| 12548608 | 05h39m59.44s | −69d45m26.3s | 124 | Gehrz | |
| 23894016 | 05h39m59.51s | −69d37m30.4s | 40650 | Looney | 22458880 |
| 12081408 | 05h40m00.00s | −69d05m45.0s | 63 | Houck | |
| 33289472 | 05h40m00.51s | −69d42m14.6s | 50092 | Gielen | |
| 23894016 | 05h40m00.69s | −69d47m13.4s | 40650 | Looney | 22459136 |
| 8889856 | 05h40m04.00s | −69d45m49.0s | 1403 | Armus | |
| 23883264 | 05h40m04.19s | −69d38m12.4s | 40650 | Looney | |
| 23883520 | 05h40m04.40s | −69d44m37.6s | 40650 | Looney | |
| 3823360 | 05h40m04.80s | −69d44m37.50s | 18 | Houck | |
| 23892480 | 05h40m09.49s | −69d44m53.5s | 40650 | Looney | |
| 23892480 | 05h40m09.50s | −69d40m23.0s | 40650 | Looney | |
| 15097088 | 05h40m11.17s | −69d19m48s | 20752 | Reynolds | |
| 23891200 | 05h40m12.00s | −70d09m16.0s | 40650 | Looney | |
| 16943616 | 05h40m12.05s | −70d10m05.6s | 249 | Indebetouw | 22456064 |
| 16943616 | 05h40m12.15s | −70d09m15.4s | 249 | Indebetouw | |
| 5032192 | 05h40m12.17s | −69d40m04.8s | 124 | Gehrz | |
| 11239424 | 05h40m13.33s | −69d22m46.5s | 3591 | Kemper | |
| 19149824 | 05h40m13.61s | −69d22m48.0s | 30869 | Kastner | |
| 12813056 | 05h40m20.62s | −66d14m44.2s | 3426 | Kastner | |
| 11239424 | 05h40m24.45s | −69d21m17.0s | 3591 | Kemper | |
| 23883520 | 05h40m25.15s | −69d40m12.1s | 40650 | Looney | |
| 4952320 | 05h40m30.91s | −66d17m37.0s | 103 | Houck | |
| 23886080 | 05h40m33.97s | −69d25m09.9s | 40650 | Looney | |
| 11239424 | 05h40m36.06s | −69d52m49.8s | 3591 | Kemper | |
| 16943616 | 05h40m43.17s | −70d11m10.1s | 249 | Indebetouw | 22456320 |
| 10969600 | 05h40m43.73s | −69d21m57.9s | 3426 | Kastner | |
| 10969856 | 05h40m43.99s | −69d25m54.5s | 3426 | Kastner | 22456576 |
| 23886080 | 05h40m44.03s | −69d25m54.6s | 40650 | Looney | 22456576 |
| 23886848 | 05h40m44.98s | −70d28m07.0s | 40650 | Looney | |
| 16943616 | 05h40m46.12s | −70d11m18.7s | 249 | Indebetouw | |
| 16943616 | 05h40m46.86s | −70d11m22.5s | 249 | Indebetouw | |
| 10970112 | 05h40m48.48s | −69d33m36s | 3426 | Kastner | |
| 16943616 | 05h40m49.49s | −70d10m15.8s | 249 | Indebetouw | 22456832 |
| 23884032 | 05h40m54.25s | −69d33m18.7s | 40650 | Looney | |
| 25688576 | 05h40m55.30s | −69d23m25.1s | 50167 | Clayton | |
| 23889152 | 05h40m55.77s | −69d40m47.3s | 40650 | Looney | |
| 25995520 | 05h40m55.81s | −69d16m14.6s | 50338 | Matsuura | |
| 11239424 | 05h40m58.18s | −69d53m12.7s | 3591 | Kemper | |
| 23885312 | 05h40m58.36s | −72d47m38.3s | 40650 | Looney | |
| 23894784 | 05h40m58.36s | −72d47m38.3s | 40650 | Looney | |
| 11239424 | 05h40m59.20s | −69d18m36.2s | 3591 | Kemper | |
| 8889856 | 05h41m06.00s | −69d41m00.0s | 1403 | Armus | |
| 25688832 | 05h41m06.94s | −69d17m14.8s | 50167 | Clayton | |
| 4952576 | 05h41m08.04s | −72d42m07.8s | 103 | Houck | |
| 10970368 | 05h41m10.63s | −69d38m3.8s | 3426 | Kastner | |
| 23894784 | 05h41m25.95s | −71d17m53.9s | 40650 | Looney | |
| 23886848 | 05h41m37.57s | −71d19m02.0s | 40650 | Looney | |
| 23891968 | 05h41m38.76s | −71d19m13.9s | 40650 | Looney | |
| 8889600 | 05h41m42.00s | −69d35m00.0s | 1403 | Armus | |
| 8889856 | 05h41m56.00s | −69d45m44.0s | 1403 | Armus | |
| 25689088 | 05h42m00.84s | −69d11m37.0s | 50167 | Clayton | |
| 23891200 | 05h42m21.16s | −69d06m21.0s | 40650 | Looney | |
| 25990912 | 05h42m21.90s | −69d02m59.0s | 50338 | Matsuura | |

TABLE 5 — *Continued*

| AOR key IRS | RA (J2000) requested | Dec (J2000) requested | Proposal ID | PI | AOR key MIPS SED |
|---|---|---|---|---|---|
| 23886848 | 05h42m33.71s | −71d17m27.8s | 40650 | Looney | |
| 25689344 | 05h42m35.48s | −69d08m48.3s | 50167 | Clayton | |
| 23887360 | 05h42m48.90s | −69d44m46.3s | 40650 | Looney | |
| 33291776 | 05h43m12.86s | −68d33m57.2s | 50092 | Gielen | |
| 11239424 | 05h43m19.70s | −69d26m27.6s | 3591 | Kemper | |
| 23887360 | 05h43m30.33s | −69d24m46.6s | 40650 | Looney | |
| 11239424 | 05h43m30.34s | −69d24m46.7s | 3591 | Kemper | |
| 10970624 | 05h43m36.05s | −70d10m35.0s | 3426 | Kastner | |
| 11239424 | 05h44m13.67s | −69d44m18.4s | 3591 | Kemper | |
| 10970880 | 05h44m13.70s | −66d16m44.8s | 3426 | Kastner | |
| 11196160 | 05h44m30.00s | −67d15m00.0s | 3578 | Misselt | |
| 10999296 | 05h44m46.38s | −65d44m07.9s | 3470 | Bouwman | |
| 23885824 | 05h44m49.63s | −67d19m34.7s | 40650 | Looney | |
| 23894016 | 05h45m20.03s | −69d46m44.8s | 40650 | Looney | |
| 23894016 | 05h45m27.92s | −69d46m22.6s | 40650 | Looney | |
| 23885824 | 05h45m44.78s | −67d09m28.2s | 40650 | Looney | 22459392 |
| 27576576 | 05h45m51.85s | −67d14m25.40s | 485 | Ardila | |
| 23886080 | 05h46m29.32s | −69d35m14.2s | 40650 | Looney | |
| 23883264 | 05h46m56.26s | −67d59m26.4s | 40650 | Looney | |
| 7102208 | 05h47m09.69s | −66d33m04.5s | 654 | Houck | |
| 7102208 | 05h47m09.69s | −66d42m44.5s | 654 | Houck | |
| 7250688 | 05h47m09.69s | −66d33m04.5s | 657 | Houck | |
| 7250688 | 05h47m09.69s | −66d42m44.5s | 657 | Houck | |
| 23886848 | 05h47m12.97s | −70d44m16.9s | 40650 | Looney | |
| 8089600 | 05h47m16.69s | −66d42m43.5s | 668 | Houck | |
| 7292160 | 05h47m24.09s | −66d42m52.24s | 658 | Houck | |
| 7102208 | 05h47m24.69s | −66d33m09.5s | 654 | Houck | |
| 7102208 | 05h47m24.69s | −66d42m39.5s | 654 | Houck | |
| 7250688 | 05h47m24.69s | −66d33m09.5s | 657 | Houck | |
| 7250688 | 05h47m24.69s | −66d42m39.5s | 657 | Houck | |
| 23892480 | 05h48m18.15s | −70d01m09.0s | 40650 | Looney | |
| 7102208 | 05h48m18.69s | −66d37m54.50s | 654 | Houck | |
| 7250688 | 05h48m18.69s | −66d37m54.50s | 657 | Houck | |
| 7292160 | 05h48m18.69s | −66d37m54.5s | 658 | Houck | |
| 7304704 | 05h48m18.69s | −66d37m54.50s | 664 | Houck | |
| 7306752 | 05h48m18.69s | −66d37m54.50s | 664 | Houck | |
| 8089600 | 05h48m18.69s | −66d37m54.5s | 668 | Houck | |
| 9406976 | 05h48m18.69s | −66d37m54.50s | 1405 | Armus | |
| 6726144 | 05h48m18.70s | −66d37m54.50s | 654 | Houck | |
| 23886080 | 05h48m26.21s | −70d08m50.2s | 40650 | Looney | |
| 23894016 | 05h48m38.23s | −70d02m08.1s | 40650 | Looney | |
| 11183872 | 05h49m02.00s | −70d02m36.0s | 3578 | Misselt | |
| 10971136 | 05h49m08.83s | −71d32m7.1s | 3426 | Kastner | |
| 6015232 | 05h49m12.00s | −70d42m39.0s | 200 | Houck | |
| 7102208 | 05h49m12.69s | −66d33m09.5s | 654 | Houck | |
| 7250688 | 05h49m12.69s | −66d33m09.5s | 657 | Houck | |
| 7250688 | 05h49m12.69s | −66d42m39.5s | 657 | Houck | |
| 7292160 | 05h49m16.29s | −66d42m47.6s | 658 | Houck | |
| 23884800 | 05h49m24.34s | −68d02m34.2s | 40650 | Looney | |
| 7102208 | 05h49m27.69s | −66d33m04.5s | 654 | Houck | |
| 7102208 | 05h49m27.69s | −66d42m44.5s | 654 | Houck | |
| 7250688 | 05h49m27.69s | −66d33m04.5s | 657 | Houck | |
| 7250688 | 05h49m27.69s | −66d42m44.5s | 657 | Houck | |
| 19005952 | 05h49m56.52s | −70d53m11.0s | 30788 | Sahai | |
| 10971392 | 05h50m06.72s | −71d46m03.0s | 3426 | Kastner | |
| 23887360 | 05h50m26.08s | −69d56m03.1s | 40650 | Looney | |
| 25991424 | 05h50m26.30s | −69d56m02.0s | 50338 | Matsuura | |
| 19010560 | 05h50m49.91s | −71d23m35.0s | 30788 | Sahai | |
| 6016512 | 05h52m27.80s | −69d14m12.0s | 200 | Houck | |
| 23883520 | 05h52m43.32s | −70d25m20.4s | 40650 | Looney | |
| 23892480 | 05h52m43.32s | −70d25m20.4s | 40650 | Looney | |
| 23894016 | 05h52m43.32s | −70d25m20.4s | 40650 | Looney | |
| 19010816 | 05h53m49.15s | −71d05m27.0s | 30788 | Sahai | |
| 23886848 | 05h54m24.93s | −71d44m18.0s | 40650 | Looney | |
| 25649152 | 05h55m21.03s | −70d00m03.1s | 50147 | Sloan | |
| 25649408 | 05h55m21.03s | −70d00m33.1s | 50147 | Sloan | |
| 10971648 | 05h55m21.05s | −70d00m3.2s | 3426 | Kastner | |
| 6077184 | 05h55m21.08s | −70d00m03.2s | 1094 | Kemper | |
| 23891200 | 05h55m37.79s | −70d44m38.6s | 40650 | Looney | |
| 23886080 | 05h56m08.79s | −68d37m20.5s | 40650 | Looney | |
| 10974208 | 05h56m38.76s | −67d53m34.4s | 3426 | Kastner | |
| 10278656 | 05h56m42.42s | −68d54m34.8s | 2333 | Woodward | |
| 10278656 | 05h56m42.42s | −68d54m34.8s | 2333 | Woodward | |
| 10278912 | 05h56m42.42s | −68d54m34.8s | 2333 | Woodward | |
| 10278912 | 05h56m42.42s | −68d54m34.8s | 2333 | Woodward | |
| 10279424 | 05h56m42.42s | −68d54m34.8s | 2333 | Woodward | |

F. Kemper et al.

TABLE 5 — *Continued*

| AOR key IRS | RA (J2000) requested | Dec (J2000) requested | Proposal ID | PI | AOR key MIPS SED |
|---|---|---|---|---|---|
| 10279424 | 05h56m42.42s | −68d54m34.8s | 2333 | Woodward | |
| 10279680 | 05h56m42.42s | −68d54m34.8s | 2333 | Woodward | |
| 10279680 | 05h56m42.42s | −68d54m34.8s | 2333 | Woodward | |
| 25036288 | 05h56m47.74s | −66d39m05.3s | 472 | Cohen | |
| 23887360 | 05h57m01.49s | −69d34m08.7s | 40650 | Looney | |
| 25035520 | 05h58m12.23s | −66d20m23.7s | 472 | Cohen | |
| 25992960 | 05h58m25.97s | −69d44m25.0s | 50338 | Matsuura | |
| 24324608 | 05h58m31.72s | −69d51m23.0s | 464 | Cohen | |
| 25036800 | 05h59m20.90s | −66d31m58.1s | 472 | Cohen | |
| 25037056 | 06h00m18.61s | −66d13m27.4s | 472 | Cohen | |
| 25035776 | 06h00m51.05s | −66d44m39.5s | 472 | Cohen | |
| 25036544 | 06h00m53.14s | −66d55m48.2s | 472 | Cohen | |
| 25036032 | 06h01m37.48s | −66d35m20.2s | 472 | Cohen | |
| 24326144 | 06h01m44.30s | −70d06m49.0s | 464 | Cohen | |
| 14705152 | 06h01m45.30s | −67d56m07.99s | 20443 | Stanghellini | |
| 10972160 | 06h02m31.03s | −67d12m46.79s | 3426 | Kastner | |
| 6078208 | 06h02m45.08s | −67d22m42.99s | 1094 | Kemper | |
| 6077696 | 06h04m25.50s | −67d23m18.58s | 1094 | Kemper | |
| 10972416 | 06h06m47.81s | −66d48m12.6s | 3426 | Kastner | |
| 7629312 | 06h06m50.55s | −67d16m59.99s | 666 | Houck | |
| 13351168 | 06h06m50.55s | −67d16m59.99s | 1419 | Armus | |
| 14705408 | 06h10m25.50s | −67d56m20.98s | 20443 | Stanghellini | |

TABLE 6
POSITIONS AND MAP SIZES OF EXTENDED REGION OBSERVATIONS IN THE
*SAGE-Spec* PROGRAM.

| region | AOR key IRS | AOR key MIPS SED | RA (J2000) | Dec (J2000) | size |
|---|---|---|---|---|---|
| SSDR[a] 4 | 22461696 | 22465792 | 04h47m40.85s | −67d12m31.0s | $1.0' \times 1.0'$ |
| DEM[b] L 8 | 22469120 | 22474240 | 04h52m06.31s | −66d55m27.1s | $1.0' \times 1.0'$ |
| DEM L 10 | 22469376 | 22474496 | 04h52m11.90s | −69d20m43.1s | $2.3' \times 1.0'$ |
| DEM L 34 | 22469632 | 22474752 | 04h56m50.09s | −66d24m50.0s | $5.4' \times 1.0'$ |
| DEM L 40 | 22469888 | 22475008 | 04h57m41.21s | −67d38m53.9s | $2.1' \times 1.0'$ |
| DEM L 55 | 22470144 | 22475264 | 05h01m41.21s | −70d38m48.8s | $5.4' \times 1.0'$ |
| DEM L 86 | 22470400 | 22475520 | 05h09m55.99s | −68d54m03.2s | $4.6' \times 1.0'$ |
| SSDR 3 | 22461440 | 22465536 | 05h15m43.64s | −68d03m20.3s | $1.0' \times 1.0'$ |
| DEM L 188 | 22470656 | 22475776 | 05h25m04.30s | −71d27m47.2s | $0.5' \times 1.0'$ |
| SSDR 8 | 22462720 | 22466816 | 05h26m25.17s | −67d29m08.1s | $1.0' \times 1.0'$ |
| SSDR 11 | 24242176 | $\cdots$ | 05h31m07.10s | −68d19m12.0s | $1.0' \times 1.0'$ |
| SSDR 1 | 22460928 | 22465024 | 05h32m02.18s | −68d28m13.6s | $1.0' \times 1.0'$ |
| SSDR 9 | 22479360 | 22480384 | 05h32m10.73s | −68d21m10.8s | $1.0' \times 1.0'$ |
| SSDR 10 | 22479872 | 22480896 | 05h32m22.95s | −66d28m41.5s | $1.0' \times 1.0'$ |
| SSDR 7 | 22462464 | 22466560 | 05h35m09.36s | −70d03m24.2s | $1.0' \times 1.0'$ |
| DEM L 243 | 22470912 | 22476032 | 05h35m31.10s | −66d02m38.8s | $5.4' \times 1.0'$ |
| SSDR 12 | 24241664 | 24242432 | 05h43m39.65s | −68d46m18.6s | $1.0' \times 1.0'$ |
| SSDR 2 | 22461184 | 22465280 | 05h43m42.01s | −68d15m07.4s | $1.0' \times 1.0'$ |
| DEM L 308 | 22471168 | 22476288 | 05h44m53.90s | −67d20m54.2s | $5.4' \times 1.0'$ |
| SSDR 6 | 22462208 | 22466304 | 05h47m16.29s | −70d42m55.5s | $1.0' \times 1.0'$ |
| DEM L 323 | 22471424 | 22476544 | 05h48m52.39s | −70d03m51.5s | $3.9' \times 1.0'$ |
| SSDR 5 | 22461952 | 22466048 | 05h55m54.19s | −68d11m57.1s | $1.0' \times 1.0'$ |
| 30 Dor[c] | $\cdots$ | $\cdots$ | $\cdots$ | $\cdots$ | $\sim 7' \times \sim 6'$ |

[a] *SAGE-Spec* diffuse region
[b] Nomenclature according to the catalog by Davies et al. (1976)
[c] This region is covered by a set of 14 IRS and 2 MIPS SED AORs, all part of Spitzer PID 30653 (Indebetouw et al. 2009)